STUDY ON THE SENSING MECHANISM OF CELLULAR IRON FOR IRON HOMEOSTASIS MEDIATED BY HEME IN IRON REGULATORY PROTEIN 1

Mariko Ogura

小倉　麻梨子

Graduate School of Chemical Sciences and Engineering,

Hokkaido University

北海道大学大学院　総合化学院

2018

Acknowledgements

This thesis entitled “Study on the Sensing Mechanism of Cellular Iron for Iron Homeostasis Mediated by Heme in Iron Regulatory Protein 1” was supervised by Professor Koichiro Ishimori (Department of Chemistry, Faculty of Science, Hokkaido University). The work in this thesis has been conducted from April 2012 to March 2018.

First, I would like to express my great gratitude to Professor Koichiro Ishimori. He always gave me continuous guidance, fruitful discussion, and hearty encouragement.

I gratefully appreciate Dr. Takeshi Uchida (Hokkaido University) for his precise indication and technical assistance. I am also grateful to Dr. Hiroshi Takeuchi for his passionate inspiration, Dr. Tomohide Saio for his helpful discussion, and Secretary Maki Tanaka for accepting the troublesome office procedure. I also thank the members of Structural Chemistry Laboratory for helps and assistances, especially Dr. Yuta Watanabe for the productive discussion and contributing to this work.

I was given a lot of cooperation with a number of researchers for conducting the researches. I appreciate Professor Kazuhiro Iwai and Dr. Yukiko Takeda (Kyoto University) for the construction of baculovirus to express IRPs. Professor Genji Kurisu, Dr. Hideaki Tanaka, and Ms. Yuko Misumi (Osaka University) gave me the opportunity for learning many wonderful experiments of X-ray crystallography from the beginning.

At the review of this work, Professor Yota Murakami (Laboratory of Bioorganic Chemistry), Professor Yasuyuki Fujita (Division of Molecular Oncology, Institute for Genetic Medicine), Professor Kazuki Sada (Material Chemistry Laboratory), and Professor Tohru Dairi (Laboratory of Applied BioChemistry) gave me the valuable suggestion and guidance.

Lastly, I would like to appreciate my family, who are Mr. Akihiko Ogura, Ms. Rumi Ogura, Mr. Kazuya Ogura, Ms. Rutsu Hamazaki, Mr. Jun Ogura, and Mr. Kame Ogura, with my whole heart. They have mentally and financially supported me a lot. I’m certain of spending unforgettable times and having invaluable experiences in Hokkaido University for nine years owing to their assistances.

June, 2018

Graduate School of Chemical Sciences and Engineering, Hokkaido University

Mariko Ogura

List of Publications

Chapter II

Mariko Ogura, Ryosuke Endo, Haruto Ishikawa, Yukiko Takeda, Takeshi Uchida, Kazuhiro Iwai, Kazuo Kobayash and Koichiro Ishimori, “Redox-dependent Axial Ligand Replacement and Its Functional Significance in Heme-bound Iron Regulatory Proteins”, *J. Inorg. Biochem*, **182**, 238-248 (2018)

Chapter III

Mariko Ogura, Yuta Watanabe, Hirotaka Okutani, Yukiko Takeda, Takeshi Uchida, Kazuhiro Iwai, and Koichiro Ishimori, “Heme as the Regulatory Molecule for Iron Regulatory Protein 1 (IRP1)”, manuscript in preparation.

Chapter IV

Mariko Ogura, Yuta Watanabe, Hirotaka Okutani, Yukiko Takeda, Takeshi Uchida, Kazuhiro Iwai, and Koichiro Ishimori, “Heme as the Regulatory Molecule for Iron Regulatory Protein 1 (IRP1)”, manuscript in preparation.

List of Presentations

Oral Presentations

1. Mariko Ogura, Yuta Watanabe, Takeshi Uchida, Kazuhiro Iwai, and Koichiro Ishimori
   "Regulation mechanism in Iron Regulatory Proteins by specific heme binding"
   The 93rd CSJ Annual Meeting (Shiga, Japan) March 22-25, 2013

2. Mariko Ogura, Yuta Watanabe, Yukiko Takeda, Takeshi Uchida, Kazuhiro Iwai, and Koichiro Ishimori
   "Structural characterization of heme binding as a signaling molecule for Iron Regulatory Protein 1"
   The 8th Annual Meeting of Japan Society for Molecular Science (Hiroshima, Japan) September 21-24, 2014

3. Mariko Ogura, Yuta Watanabe, Takeshi Uchida, Kazuhiro Iwai, and Koichiro Ishimori
   "Specific heme binding-dependent regulation mechanism in Iron Regulatory Protein"
   The 95th CSJ Annual Meeting (Chiba, Japan) March 26-29, 2015

Poster Presentations

1. Mariko Ogura, Yuta Watanabe, Yukiko Takeda, Takeshi Uchida, Kazuhiro Iwai, and Koichiro Ishimori
   "Structural characterization of heme binding sites in Iron Regulatory Protein1"
   The 24th Symposium on Role of Metals in Biological Reactions, Biology and Medicine (Kyoto, Japan) June 14-15, 2014

2. Mariko Ogura, Yukiko Takeda, Takeshi Uchida, Kazuhiro Iwai, and Koichiro Ishimori
   "Heme as a Signaling Molecule in Iron Regulatory Protein 1"
   Metals in Biology (Saitama, Japan) June 16-17, 2015

3. Mariko Ogura, Takeshi Uchida, Kazuhiro Iwai, and Koichiro Ishimori

   “Spectral Characterization of Heme Binding to IRP, a Sensor Protein for the Iron Homeostasis in Cells”

   The 16th Annual Meeting of the Protein Science Society of Japan (Fukuoka, Japan) June 7-9, 2016

4. Mariko Ogura, Tomohide Saio, Takeshi Uchida, Hideaki Tanaka, Genji Kurisu, Kazuhiro Iwai, and Koichiro Ishimori

   “Structural characterization of heme binding as a signaling molecule for the iron homeostasis”

   The 17th Annual Meeting of the Protein Science Society of Japan (Sendai, Japan) June 20-22, 2017

Contents

CHAPTER I

GENERAL INTRODUCTION

Iron is a transition metal, which is an essential element for many organisms and has the ability to readily accept and donate electrons, allowing it to function as an oxidant or reductant in a large number of biochemical reactions. In mammals, iron is required for oxygen transport as a component of hemoglobin, DNA synthesis as a component of ribonucleotide reductase, and as an electron acceptor/donor in cytochromes and so on (1). Iron deficiency, therefore, causes many health problems, immunological deterioration, and impairing physical and mental development in children (2). On the other hand, once the iron level in cells exceeds the capacity of organisms, iron can be toxic, resulting in oxidation of lipids, proteins, and other cellular components (3, 4). High levels of iron have been supposed to be associated with increased incidence of certain cancers and dysfunction of organs, such as heart, pancreas, or liver. Thus, the intracellular iron metabolism is regulated in mammal. In this chapter, the general information of the heme-regulated mechanism for the iron metabolism and homeostasis is described.

1.1. Iron Metabolism.

Mammalian cells regulate expression of proteins involved in iron uptake and sequestration to ensure that iron supplies are sufficient for metabolic needs. Mammals possess a network of proteins that promote the transport, use, and storage of iron as shown in Figure 1.1 (5). First, iron is released from the intestinal enterocyte to the blood vessel, and binds to an iron-transporting protein, transferrin (Tf). Tf transports iron to tissues and binds to transferrin receptor (TfR) on the cell surface (6). The Tf-TfR complex is internalized to deliver iron to the cytoplasm, and, after the dissociation of iron, TfR and apo-Tf are recycled to the cell surface (6, 7). Iron delivered to the cytoplasm is used for synthesis of iron containing prosthetic group such as heme and iron-sulfur clusters, while an excess of iron is stored in a multi-subunit iron storage protein, ferritin (8). Therefore, TfR and ferritin are crucial proteins and the coordinated

iron-dependent modulation of TfR and ferritin synthesis plays a key role in iron homeostasis (9).

1.2. Coordinate post-transcriptional Regulation of Cellular Iron Metabolism via IRE/IRP Interactions.

The regulation of the ferritin and TfR synthesis is linked to the cellular iron status of cytosolic RNA binding proteins, iron regulatory proteins (IRPs) (5, 9). As shown in Figure 1.2, IRPs are the primary regulators of the iron metabolism through the modulation of the expression level of the genes that are involved in the iron metabolism such as iron uptake, storage, utilization, and export (10). In iron-depleted cells, IRPs bind to the specific mRNA, iron responsive-elements (IREs) sequence. IREs have highly conserved hairpin structures of 25‑30 nucleotides (11). H- and L-ferritin mRNAs contain a single IRE in their 5'-untranslated regions 5' UTR, which is located relatively close to the cap structure at the 5' end, while TfR1 mRNA contains five IREs in its 3' UTR.

The IRE/IRP regulatory system was first described in the late 1980s with the discovery of IREs in the UTRs of the mRNAs encoding the H- and L-subunits of ferritin and TfR1 (12–14). Under conditions of iron deficiency, IRPs bind with high affinity to the IRE in H- and L-ferritin mRNAs, and thereby inhibit their translation by a steric hindrance mechanism (Figure 1.2). On the other hands, IRPs bind to the IREs in TfR1 mRNA to protect them against endonucleolytic degradation. These homeostatic responses prevent storage of cellular iron by Ft and mediate increased cellular iron uptake by Tf. By contrast, in iron-replete cells, the IRE-binding activities of IRPs are diminished, allowing degradation of mRNA coding TfR1 and ferritin mRNA translation. The loss of binding activity for IRP1 inhibits iron uptake and stimulates storage of excessive intracellular iron within ferritin. Therefore, the iron content in cells is regulated by the association/dissociation of IRPs to IRE.

1.3. Sensing of Intracellular Iron by IRP1 and IRP2.

Two IRP homologues, IRP1 and IRP2, are identified, which share the high sequence homology. The IRE binding activity of both IRPs is regulated by cellular iron concentration. However, their regulatory mechanisms definitely differ between the two proteins (Figure 1.3). IRP1 assembles an aconitase-type 4Fe-4S cluster in response to the increased intracellular iron levels. Assembly of the 4Fe-4S cluster alters the conformation of IRP1 and precludes the IRE-binding (15, 16). On the other hand, holo-IRP1 acquires enzymatic activity as cytosolic aconitase, which catalyzes isomerization of citrate to iso-citrate. Thus, IRP1 is a bifunctional protein that is regulated by the 4Fe-4S cluster assembly.

Contrary to IRP1, IRP2 does not assemble the 4Fe-4S and is regulated by iron-induced ubiquitination and degradation. IRP2 is oxidized and ubiquitinated in iron-replete cells, leading to subsequent degradation by proteasomes, along with loss of its IRE binding activity (17–20). For this degradation of IRP2, oxidation of a domain specific to IRP2, the iron-dependent degradation (IDD) domain, which is not found in the sequence of IRP1, is essential (15, 21), and lack of the IDD domain results in no degradation of the protein (19). A previous study revealed that oxidation of the IDD domain is triggered by heme binding to IRP2 and IDD domain-oxidized IRP2 is preferentially recognized by heme-oxidized IRP2 ubiquitin ligase-1 (HOIL-1) for the ubiquitination (22).

1.4. Heme Binding to IRP1 and IRP2 Using Heme as Signaling Molecule.

Although heme-induced oxidation was not observed for IRP1, incubation of IRP1 with heme prevented subsequent repression of ferritin synthesis in a wheat germ extract (23) and heme was found to be crosslinked to the specific region of IRP1 (24). The previous studies suggested that the IRE binding of IRP1 is also regulated by heme, but without the heme-induced

oxidation.

Heme is a prosthetic group best known for essential roles in oxygen transport, oxidative catalysis, and respiratory electron transport. More than 95% of functional (not storage) iron in the human body is in the form of heme (25). Recent years, the roles of heme is further evident from identification of the proteins, called “heme-regulated” proteins, that bind heme reversibly, using it as a signal to regulate gene expression in circadian rhythm pathways and control heme synthesis itself (26, 27). Most of such “heme-regulated” proteins have heme regulatory motifs (HRMs) (28, 29), and the cysteine residue of the HRM in “heme-regulated” proteins often serve as the axial ligand for heme. Two homologues of IRPs, IRP1 and IRP2, also have HRM in their sequence. The heme binding sites in IRP2 was reported to be ^{201}Cys in the IDD domain, and heme binding underpins its iron-sensing mechanism (30). On the other hands, IRP1 shares heme binding sites as HRM (Cys-Pro) in IRP2 (Figure 1.4) and has other HRM (Cys-Ile). However, the specific heme binding has been reported only for IRP2, which is essential for oxidative modification and loss of binding to IRE. The ligation of heme for IRP1 has not yet been confirmed.

In Chapter II, I found that IRP1 also specifically binds two molar equivalents of heme, and the absorption and resonance Raman spectra of heme-bound IRP1 were quite similar to those of heme-bound IRP2, showing that the heme environmental structures in IRP1 are close to those of proteins using heme as a signaling molecule. Using pulse radiolysis, we successfully identified the structural factors differentiating heme binding to HRM in the IDD domain of IRP2 from those of other HRMs outside of the IDD domain. Considering that the oxidative modification is only observed in heme-bound IRP2, but not IRP1, I suggest that functional significance of heme binding to IRP1 is different from that to IRP2, although both IRPs seem to utilize heme as the signaling molecule for sensing cellular iron concentration.

In Chapter III, to examine the functional significance of heme binding to IRP1, I focused

on the affinity of heme for hemoproteins. Typical hemoproteins such as hemoglobin and P450 tightly binds heme as the active center, but “heme-regulated” proteins, which bind heme as the signaling molecule, have decreased heme binding affinity. To estimate the heme binding affinity of IRP1, I followed the association/dissociation kinetics for the heme binding to IRP1. The kinetics data revealed that the affinity of heme for IRP1 was similar to that of “heme-regulated” protein, and the heme binding to IRP1 inhibited the IRE binding to IRP1. The addition of heme to IRP1 resulted in the dissociation of IRE from IRP1, supporting the idea that heme functions as the signaling molecule for IRP1.

In Chapter IV, the crystal structure of IRP1 in the complex with heme was solved to structurally characterize the heme-regulated IRE binding mechanism in IRP1. The crystal structure clarified that IRP1 binds heme to ^{506}Cys, not to HRM, and this cysteine residue located in the IRE recognition site in the cleft formed by domains 3 and 4 in IRP1. The heme binding to ^{506}Cys would induce conformational changes around the IRE recognition site to inhibit the IRE binding to IRP1, which is a different regulation mechanism from that of IRP2.

In Chapter V, based on the results in Chapters II, III and IV, I proposed a mechanism of the heme-regulated IRE binding in IRP1, where IRP1 binds heme as the signaling molecule for the intracellular iron concentration. The results and discussion in this thesis shed new light on molecular mechanisms for iron homeostasis in cells, which will, I believe, provides important clues to new drug design and therapies for various kinds of deceases derived from the defects in iron homeostasis.

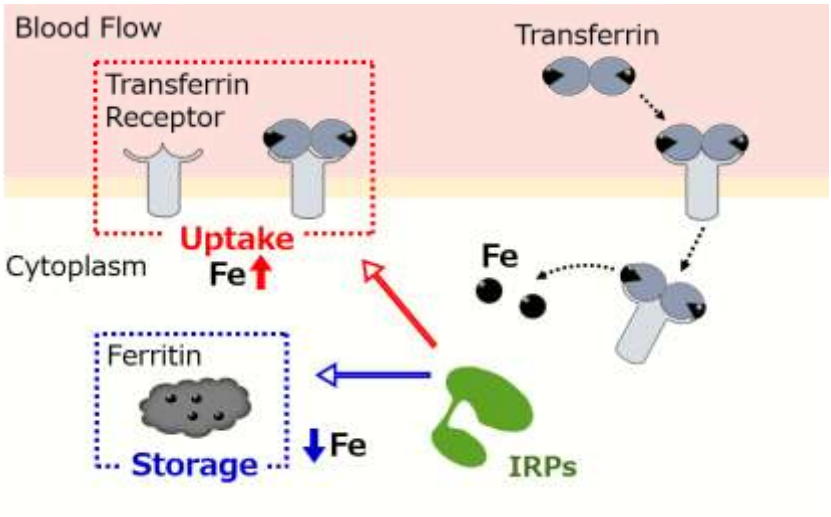

Figure 1.1 Intracellular iron metabolism.

Extracellular iron binds to transferrin (Tf). Tf binds to transferrin receptor (TfR) to be taken in iron into cell. The Tf-TfR complex is internalized by receptor-mediated endocytosis, and iron released from Tf. The iron released Tf-TfR complex is exposed to the cell surface, and Tf is released and reused. Released iron is utilized or stored in ferritin.

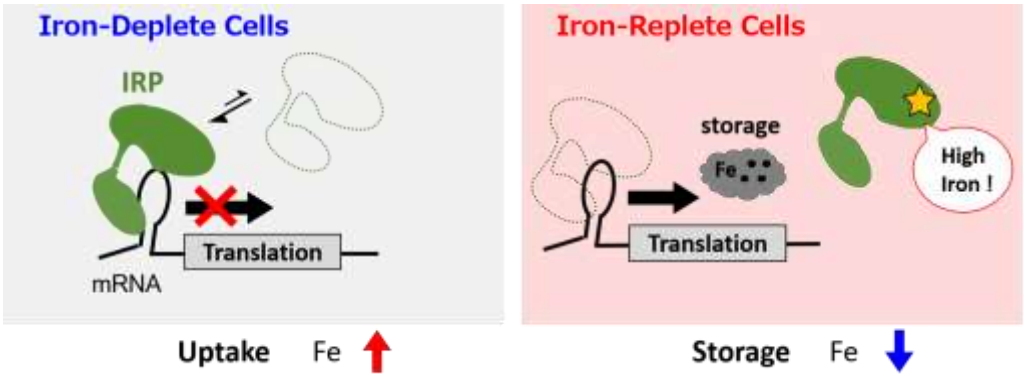

Figure 1.2 A regulation mechanism of cellular iron level by IRP. (Ex. Iron Storage)

Left: IRP binds to IRE in iron-deplete cells. In Ft mRNA, IRP prevents the initiation of the translation by endosome, and its expression is down regulated. As a result, cellular iron level is going to be high. Right: IRP cannot bind to IRE in iron-replete cells and Ft is translated stably. As a result, cellular iron level is going to be low.

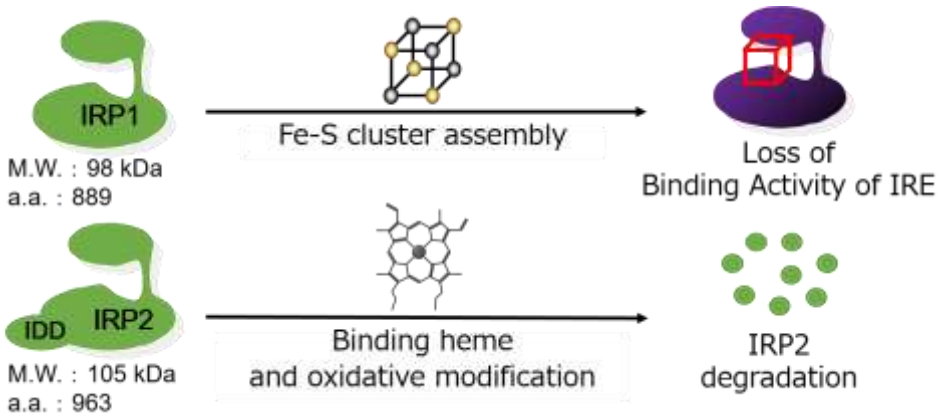

Figure 1.3 The mechanism of regulation of the function in IRPs.

In iron-replete cells, IRP1 assembles a Fe-S cluster and it induces some conformational changes in IRP1, while IRP2 bind to heme and is ubiquitinated to be degraded by proteasome. Both of them lose its activity to binding IRE in iron replete cells.

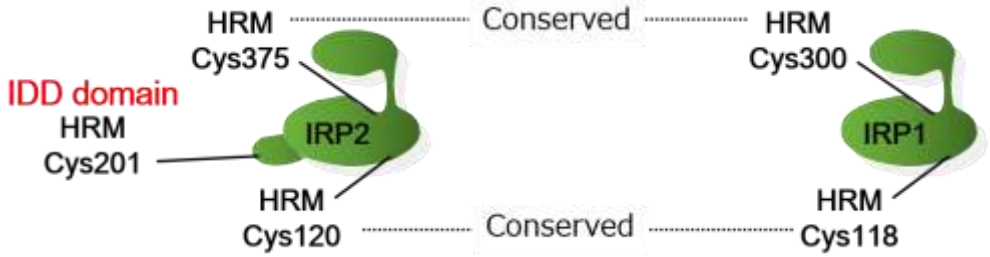

Figure 1.4 Heme binding sites in IRPs.

IRP1 binds two equivalents of heme, and IRP2 binds three equivalents of heme. One of the binding sites, Cys201, in IRP2 is located in the IDD domain. This domain mediates the oxidative modification and subsequently degradation. Other two heme binding sites (Cys118 and Cys300 in IRP1, Cys120 and Cys375 in IRP2) are conserved between IRP1 and IRP2.

References

1. P. Aisen, Chemistry and biology of eukaryotic iron metabolism. *Int. J. Biochem. Cell Biol.* **33**, 940–959 (2001).
2. A.-R. West, P.-S. Oates, Mechanisms of heme iron absorption: current questions and controversies. *World J. Gastroenterol.* **14**, 4101–4110 (2008).
3. B. Halliwell, J. M. C. Gutteridge, Role of free radicals and catalytic metal ions in human disease: An overview. *Methods Enzymol.* **186**, 1–85 (1990).
4. G. Papanikolaou, K. Pantopoulos, Iron metabolism and toxicity. *Toxicol. Appl. Pharmacol.* **202**, 199–211 (2005).
5. K. Pantopoulos, Iron Metabolism and the IRE/IRP Regulatory System: An Update. *Ann. N. Y. Acad. Sci.* **1012**, 1–13 (2004).
6. P. Ponka, C. Beaumont, D. R. Richardson, Function and regulation of transferrin and ferritin. *Semin. Hematol.* **35**, 35–54 (1998).
7. Y. Cheng, O. Zak, P. Aisen, S. C. Harrison, T. Walz, Structure of the human transferrin receptor-transferrin complex. *Cell*. **116**, 565–576 (2004).
8. P. M. Harrison, P. Arosio, The ferritins: molecular properties, iron storage function and cellular regulation. *Biochim. Biophys. Acta - Bioenerg.* **1275**, 161–203 (1996).
9. M. W. Hentze, M. U. Muckenthaler, N. C. Andrews, Balancing Acts: Molecular Control of Mammalian Iron Metabolism. *Cell*. **117**, 285–297 (2004).
10. L. C. Kühn, Iron regulatory proteins and their role in controlling iron metabolism. *Metallomics*. **7**, 232–243 (2015).
11. P. Piccinelli, T. Samuelsson, Evolution of the iron-responsive element. *RNA*. **13**, 952–966 (2007).
12. M. W. Hentze, S. W. Caughman, T. A. Rouault, J. G. Barriocanal, A. Dancis, J. B. Harford, R. D. Klausner, Identification of the iron-responsive element for the translational regulation of human ferritin mRNA. *Science*. **238**, 1570–1573 (1987).
13. W. Casey, D. Jones, B. Kugler, B. Watkins, Integration of down's syndrome children in the primary school: A longitudinal study of cognitive development and academic attainments. *Br. J. Educ. Psychol.* **58**, 279–286 (1988).
14. E. W. Müllner, L. C. Kühn, A stem-loop in the 3′ untranslated region mediates iron-dependent regulation of transferrin receptor mRNA stability in the cytoplasm. *Cell*. **53**, 815–825 (1988).
15. J. Dupuy, A. Volbeda, P. Carpentier, C. Darnault, J.-M. Moulis, J. C. Fontecilla-Camps, Crystal Structure of Human Iron Regulatory Protein 1 as Cytosolic Aconitase. *Structure*. **14**, 129–139 (2006).
16. W. E. Walden, A. I. Selezneva, J. Dupuy, A. Volbeda, J. C. Fontecilla-Camps, E. C. Theil, K. Volz, Structure of dual function iron regulatory protein 1 complexed with ferritin IRE-RNA. *Science*. **314**, 1903–1908 (2006).

17. P. A. DeRusso, C. C. Philpott, K. Iwai, H. S. Mostowski, R. D. Klausner, T. A. Rouault, Expression of a constitutive mutant of iron regulatory protein 1 abolishes iron homeostasis in mammalian cells. *J. Biol. Chem.* **270**, 15451–15454 (1995).
18. E. Menotti, B. R. Henderson, L. C. Kü, Translational Regulation of mRNAs with Distinct IRE Sequences by Iron Regulatory Proteins 1 and 2.
19. K. Iwai, S. K. Drake, N. B. Wehr, A. M. Weissman, T. LaVaute, N. Minato, R. D. Klausner, R. L. Levine, T. A. Rouault, Iron-dependent oxidation, ubiquitination, and degradation of iron regulatory protein 2: implications for degradation of oxidized proteins. *Proc. Natl. Acad. Sci. U. S. A.* **95**, 4924–4928 (1998).
20. E. S. Hanson, L. M. Foot, E. A. Leibold, Hypoxia post-translationally activates iron-regulatory protein 2. *J. Biol. Chem.* **274**, 5047–5052 (1999).
21. K. Iwai, R. D. Klausner, T. A. Rouault1, Requirements for iron-regulated degradation of the RNA binding protein, iron regulatory protein 2. *EMBO J.* **14**, 5350–5357 (1995).
22. K. Yamanaka, H. Ishikawa, Y. Megumi, F. Tokunaga, M. Kanie, T. A. Rouault, I. Morishima, N. Minato, K. Ishimori, K. Iwai, Identification of the ubiquitin–protein ligase that recognizes oxidized IRP2. *Nat. Cell Biol.* **5**, 336–340 (2003).
23. J. J. Lin, S. Daniels-McQueen, M. M. Patino, L. Gaffield, W. E. Walden, R. E. Thach, Derepression of ferritin messenger RNA translation by hemin in vitro. *Science*. **247**, 74–77 (1990).
24. J.-J. Lin, M. M. Patinot, L. Gaffieldt, W. E. Waldent, A. Smithf, R. E. Thach, Crosslinking of hemin to a specific site on the 90-kDa ferritin repressor protein (iron/translational regulation/induction of gene expression). **88**, 6068–6071 (1991).
25. J. Hooda, A. Shah, L. Zhang, Heme, an essential nutrient from dietary proteins, critically impacts diverse physiological and pathological processes. *Nutrients*. **6**, 1080–1102 (2014).
26. T. Shimizu, Binding of cysteine thiolate to the Fe(III) heme complex is critical for the function of heme sensor proteins. *J. Inorg. Biochem.* **108**, 171–177 (2012).
27. H. M. Girvan, A. W. Munro, Heme sensor proteins. *J. Biol. Chem.* **288**, 13194–13203 (2013).
28. L. Zhang, L. Guarente, Heme binds to a short sequence that serves a regulatory function in diverse proteins. *EMBO J.* **14**, 313–320 (1995).
29. T. Kühl, A. Wißbrock, N. Goradia, N. Sahoo, K. Galler, U. Neugebauer, J. Popp, S. H. Heinemann, O. Ohlenschläger, D. Imhof, Analysis of Fe(III) Heme Binding to Cysteine-Containing Heme-Regulatory Motifs in Proteins. *ACS Chem. Biol.* **8**, 1785–1793 (2013).
30. H. Ishikawa, M. Kato, H. Hori, K. Ishimori, T. Kirisako, F. Tokunaga, K. Iwai, Involvement of heme regulatory motif in heme-mediated ubiquitination and degradation of IRP2. *Mol. Cell*. **19**, 171–181 (2005).

CHAPTER II

REDOX-DEPENDENT AXIAL LIGAND REPLACEMENT AND ITS FUNCTIONAL SIGNIFICANCE IN HEME-BOUND IRON REGULATORY PROTEIN

Abstract

IRP1 and IRP2, regulators of iron homeostasis in mammalian cells, control the translation of proteins involved in iron metabolism by binding to IRE. Although two IRPs share the significant homology and have the HRM sequence, a consensus sequence found in “heme-regulated proteins”, specific heme binding has been reported only for IRP2, which is essential for oxidative modification and loss of binding to target mRNAs. In this chapter, I spectroscopically confirmed that IRP1 also specifically binds two molar equivalents of heme, and the absorption and resonance Raman spectra of heme-bound IRP1 were quite similar to those of heme-bound IRP2. While these spectroscopic properties show that the heme environmental structure in heme-bound IRP1 is close to that of IRP2, the heme binding to IRP1 does not induce the oxidative modification as found for heme-bound IRP2. To identify the structural factors to differentiate the functional significance of the heme binding between two IRPs, I focused on the reduction process of heme iron bound to IRPs, which is supposed to be one of the crucial processes for the heme-induced oxidative modification in IRP2. I utilized pulse radiolysis experiments to follow the reduction process, and the time-dependent spectra of heme-bound IRPs after reduction of the heme iron revealed an axial ligand exchange from Cys to His immediately after the reduction of the heme iron to form a 5-coordinate His-ligated heme in heme-bound IRP2. However, the 5-coordinate His-ligated heme was not observed after the reduction of heme-bound IRP1. Considering that the oxidative modification is only observed in heme-bound IRP2, but not IRP1, probably owing to the structural flexibility of IRP2, I propose that the transient 5-coordinate His-ligated heme is a prerequisite for oxidative modification of heme-bound IRP2, which functionally differentiates heme binding of IRP2 from that of IRP1.

2.1. Introduction.

As described in General Introduction, two IRPs, IRP1 and IRP2, have been identified to date, and share the significant homology. However, IRP2 has a specific domain of 73 amino acid residues, the IDD domain, between domains 1 and 2. This domain contains one HRM sequence and heme binding to the HRM in the IDD domain in IRP2 and its functional significance has been examined by spectroscopy methods, including absorption, resonance Raman, and EPR spectra, and biochemical analysis of the oxidative modification (1). The spectroscopic data clearly showed that the IDD domain specifically binds ferric heme via a cysteine residue (^{201}Cys) in the HRM (2). This binding triggers the oxidative modification of the IDD domain. Such heme binding at the cysteine residue in the HRM is also thought to be the first step for the oxidative modification of a heme-dependent transcription factor important for bacterial heme biosynthesis, iron-responsive regulator (Irr), in a nitrogen fixing bacterium, *Bradyhizobium joponicum* (3, 4).

Although heme binding to Cys in the HRM is observed for various "heme-regulated" proteins including IRP2 and Irr (3–5), heme-dependent oxidative modification has only been confirmed in IRP2 and Irr (3–5). Heme-regulated proteins that use heme as a signaling or effector molecule, such as Hap1 (6), ALAS1 (7), ALAS2 (7), HRI kinase (8), and Bach1 (9), can specifically bind heme, but no heme-induced protein oxidation has been reported. Based on a sequence alignment of heme-regulated proteins containing HRMs, both IRP2 and Irr found to have His at the same position in the HRM (Cys-Pro-X-His), unlike other heme-regulated proteins, and positionally shifting of this His (Cys-Pro-X-X-His) in the HRM suppressed protein oxidation (1).

The crucial role of His in the HRM for protein oxidation was also supported by the fact that another homologous protein, IRP1, which has two HRMs lacking histidine residues, was not oxidized in the presence of heme under conditions where IRP2 is oxidized (10). Although heme-induced oxidation was not observed for IRP1, incubation of IRP1 with heme prevented

subsequent repression of ferritin synthesis in a wheat germ extract (11) and heme was found to be crosslinked to the specific region of IRP1 (12), suggesting that the IRE binding of IRP1 is also regulated by the heme binding. As indicated in Figure 2.1, two HRM sequences in IRP1 are conserved in IRP2, which allowed us to speculate that IRP1 specifically binds heme at HRMs to regulate the IRE binding. However, heme binding to these HRMs has not yet been examined.

In this chapter, I found that IRP1 also specifically binds heme, and spectroscopically characterized the heme environments of both heme-bound IRP1 and IRP2. In particular, using pulse radiolysis, I focused on the heme coordination structure of intermediates after reduction of the heme iron, revealing the structural factors differentiating heme binding to HRM in the IDD domain of IRP2 from those of other HRMs located outside of the IDD domain.

```
IRP1    -AVCPADLVIDHSIQVDFNR----------------------------------------  134
IRP2    -PACPTDLTVDHSLQIDFSKCAIQNAPNPGGGDLQKAGKLSPLKVQPKKLPCRGQTTCRGS  177

IRP1     --------------------------------RADSLQKNQDLEFERNRERFEFLKWGSQ- 162
IRP2     CDSGELGRNSGTFSSQIENTPILCPFHLQPVPEPETVLKNQEVEFGRNRERLQFFKWSSR- 237

IRP1     -PGVAQLSIADRATIANMCPEYGATAAFFPVDEVSITYLVQTGRDEEKLKYIKKYLQAVGM 342
IRP2     -SGVSQLSIVDRTTIANMCPEYGAILSFFPVDNVTLKHLEHTGFSKAKLESMETYLKAVKL 417
```

Figure 2.1. Amino acid sequences including the HRM regions in IRP1 and IRP2.
HRMs are shown as bold letters. HRMs in IRP1: ^{118}Cys-^{119}Pro, ^{300}Cys-^{301}Pro, HRMs in IRP2: ^{120}Cys-^{121}Pro, ^{201}Cys-^{202}Pro-X-^{204}His (IDD domain, red), ^{375}Cys-^{376}Pro.

2.2. Experimental Procedures.

2.2.1. Materials.

All chemicals were purchased from Wako Pure Chemical Industries (Osaka, Japan), Nacalai Tesque (Kyoto, Japan), or Sigma-Aldrich (St. Louis, MO, USA) and used without further purification.

2.2.2. Protein Expression and Purification.

Procedures for the protein expression and purification were described by our previous paper (1). High Five cells were cultured at 27 °C in Express Five serum-free medium (Invitrogen) supplemented with 16.5 mM L-glutamine, 100 IU/mL penicillin G and 100 μg/mL streptomycin, and infected with P3 baculovirus to express His_6-tagged IRPs. At 60 hours after infection, the infected cells were harvested and centrifuged. The cells were washed and subsequently suspended in lysis buffer containing 50 mM Tris-HCl (pH 7.4), 10 mM 2-mercaptoethanol, 0.2 mg/mL heat-treated ribonuclease A (Roche Diagnosis, Basel, Switzerland) and 1 tablet/50 mL protease inhibitor cocktail tablet (Complete EDTA-free, Roche Diagnosis). After incubation for 10 minutes on ice, the suspended cells were homogenized with a Dounce homogenizer (WATSON, Tokyo, Japan). The supernatant was applied to Ni-NTA agarose resin (QIAGEN, Hilden, Germany) pre-equilibrated with 50 mM Tris-HCl (pH 7.4), and the mixture was incubated for 2 hours at 4 °C. After extensive washing, the bound protein was eluted with 50 mM Tris-HCl (pH 7.4) buffer containing 300 mM imidazole and 10 mM 2-mercaptoethanol.

For the purification of IRP1, the eluate was dialyzed against 50 mM Tris-HCl (pH 8.0) containing 10 mM 2-mercaptoethanol to remove imidazole. The His_6-tag was cleaved by TEV protease (Accelagen, San Diego, CA, USA) for 16 hours at 4 °C. After cleavage, the reaction mixture was again applied to Ni-NTA agarose pre-equilibrated with 50 mM Tris-HCl (pH 7.4)

containing 10 mM 2-mercaptoethanol. The flow-through was concentrated and applied to a HiLoad 16/600 Superdex 200 pg gel-filtration column (GE Healthcare, Uppsala, Sweden) pre-equilibrated with 50 mM Tris-HCl and 100 mM NaCl (pH 7.4).

The purification procedure for IRP2 was essentially the same as that for IRP1. However, after the eluate was concentrated, buffer was exchanged to 50 mM Tris-HCl, 0.5 mM EDTA, and 1 mM dithiothreitol (DTT) (pH 8.0) using a PD-10 MidiTrap column (GE Healthcare) instead of a HiLoad 16/600 Superdex 200 gel-filtration column to avoid partial aggregation during purification. The collected flow-through was exchanged with 50 mM Tris-HCl, 100 mM NaCl (pH 7.4). The protein concentrations of IRP1 and IRP2 were estimated using the absorbance at 280 nm with extinction coefficients (ε_{280}) calculated in ProtParam (http://web.expasy.org/protparam/) of 84,690 and 77,240 M^{-1} cm^{-1}, respectively.

2.2.3 Absorption Spectroscopy.

All absorption spectra were obtained using a V-660 UV-Vis spectrophotometer (JASCO Corporation, Japan). Heme binding studies were conducted with difference absorption spectroscopy. Hemin was dissolved in 0.1 M NaOH and its concentration was determined based on the absorbance at 385 nm using an extinction coefficient (ε_{385}) of 58.44 mM^{-1} cm^{-1}. Aliquots of a hemin solution (500 μM) were added to both the sample cuvette containing 5 μM apo-IRPs, and the reference cuvette at 4 °C. Spectra were recorded 2 min after the addition of hemin. The absorbance difference at 372 nm for IRP1 and 373 nm for IRP2 was plotted as a function of heme concentration.

2.2.4 Resonance Raman Spectroscopy.

Resonance Raman spectra were recorded with a single monochromator (SPEX500M, Jobin Yvon, Edison, NJ, USA), equipped with a liquid nitrogen-cooled CCD detector (Spec-10:400B/LN, Roper Scientific, Princeton, NJ, USA). The spectra were obtained by excitation

with 363.8 nm light from an argon ion laser (BeamLok 2065, Spectra Physics, Santa Clara, CA), 413.1 nm light from a krypton ion laser (BeamLok 2060, Spectra Physics), or 441.6 nm light from a helium-cadmium laser (IK5651R, Kimmon Electrics, Tokyo, Japan). The laser power at the sample point was adjusted to ~5 mW for the ferric and ferrous forms and to 0.1 mW for the CO-bound form to avoid photodissociation. Raman shifts were calibrated with indene, CCl_4, acetone, and an aqueous solution of ferrocyanide. The accuracy of the peak positions of well-defined Raman bands was ±1 cm^{-1}. Heme-reconstituted protein concentrations for Raman experiments were approximately 40 μM in 50 mM Tris-HCl (pH 7.4), in the presence of two molar equivalents of heme, at room temperature.

2.2.5 Pulse Radiolysis.

Pulse radiolysis experiments were performed with a pulse width of 8 ns and an energy of 27 MeV, using a linear accelerator at the Institute of Scientific and Industrial Research at Osaka University (11). Samples for the pulse radiolysis measurements were solutions of heme-bound IRP1 or IRP2 in 50 mM phosphate (pH 7.4). The sample was placed in a quartz cell with an optical path length of 1 cm, and the temperature of the sample was maintained at 25 °C. The light source for the monitoring light was a 150 W halogen lamp or a 200 W xenon lamp. After passing through the optical path, the transmitted light intensity was monitored using a fast spectrophotometric system composed of a Nikon monochromator and a Hamamatsu R-928 photomultiplier, and then analyzed using a Unisoku (Osaka, Japan) data analysis system. All data points at different wavelengths were obtained in separate measurements.

2.3. Results.

2.3.1 Absorption Spectra of Heme-bound IRP1 and IRP2.

The specific heme binding to IRPs was confirmed by the absorption spectra of IRPs in the presence of heme. The absorption spectrum of IRP1 in the presence of ferric heme (solid line, Figure 3.2A) exhibits a broad Soret peak at 372 nm, with a shoulder at approximately 420 nm. This was also found for IRP2 (solid line, Figure 2.2B), where Cys in the HRM is ligated to the ferric heme iron (1), suggesting heme binding to Cys of the HRM in IRP1. To determine the heme stoichiometry of IRPs, spectrophotometric titration of heme to IRP1 was performed (inset, Figure 2.2A). It is clear that two equivalents of heme bind to IRP1, which corresponds to the number of HRMs in IRP1 (Figure 2.1), and supports the heme binding to Cys in the HRM. In IRP2, the spectrophotometric titration of heme to IRP2 (inset, Figure 2.2B) indicates that three equivalents of heme can bind to IRP2, consistent with the presence of three HRMs in IRP2. One of the HRMs is located in the IRP2-specific domain, the IDD domain, and other two HRMs are conserved in both IRP homologues (Figure 2.1). The close similarity of the absorption spectra between the two IRPs suggest that the heme environments for both IRP1 and IRP2 are quite similar, and characteristic of heme-regulated proteins (12).

Upon reduction of the heme iron with sodium dithionite, the Soret band shifted to 423 and 425 nm for IRP1 and IRP2, respectively (Figure 2.2A, 2.2B). Both peak positions can be categorized into the 6-coordinate ferrous low-spin heme such as observed for cytochrome b_5 (13) and the acidic form of CBS (14), where neutral Cys/His or His/His are ligated to the heme iron. In addition to the peak at approximately 425 nm, however, both spectra showed a broad peak or shoulder at approximately 390 nm, assignable to the Soret band of a neutral Cys-ligated heme (15), implying that the axial cysteine is protonated in a part of ferrous heme-bound IRPs. On the other hand, the absorption peaks in the Soret region of the carbon-monoxide (CO) adducts of heme-bound IRPs appeared at 421 nm (dotted lines, Figure 2.2A and 2.2B), distinctly

different from that of P450cam (450 nm) (16), but similar to that of myoglobin (421 nm) (17) or P420cam (420 nm) (18, 19). The axial ligand for IRP1-CO and IRP2-CO is, therefore, a neutral His or Cys, rather than an anionic Cys. The absorption maxima for typical hemoproteins are summarized in Table 2.1.

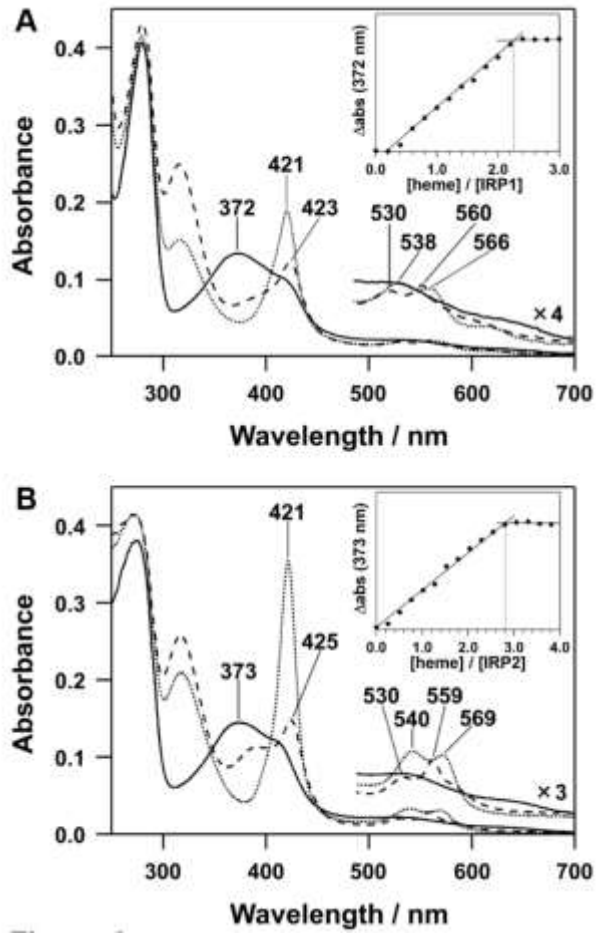

Figure 2.2 Optical absorption spectra of heme-bound IRP 1(A) and IRP2 (B).

Solid, dashed, and dotted lines represent the ferric heme-bound, ferrous heme-bound, and CO adducts of reduced heme-bound IRPs, respectively. (Inset) Heme titration of IRPs was followed by measurement of the absorbance at 372 nm and 373 nm. The protein concentration was approximately 5 μM in 50 mM Tris-HCl buffer, 100 mM NaCl, pH 7.4, in the presence of one molar equivalent of heme.

Table 2.1 Absorption peaks for hemoproteins.

Proteins	Coordination	Soret	Visible	Reference
Fe(III) complexes				
IRP1	Cys, Cys/His	372, 415[1]	broad	This work
IRP2	Cys, Cys/His	373, 415[1]	broad	This work
Irr	Cys, His/His	372, 414	broad	(20)
HRI	Cys/?	418	538	(21)
HRI-NTD	His/His	415	533	(22)
CBS	His/Cys	428	550	(14)
CooA	Cys/Pro	424	541, 566	(23)
P450cam	Cys	391	511, 646	(24)
P450cam(Imidazole)	Cys/Imidazole	425	542, 574	(24)
P420	Cys	422	541, 566	(19)
Aquomet Mb	His/H_2O	409	505, 630	(17)
Cytochrome b_5	His/His	412	530-560[2]	(25)
Fe(II) complexes				
IRP1	His/(Cys or His)	423	532, 559	This work
IRP2	His/(Cys or His)	425	530, 559	This work
Irr	His, His/His	423	broad	(26)
HRI	His/?	426	531, 560	(21)
HRI-NTD	His/His?	428	530, 560	(22)
CBS, pH 8.0	His/Cys	448	540, 571	(14)
CBS, pH 6.0	His/Cys	425	530, 558	(14)
CooA	His/Pro	426	529, 559	(23)
P450cam	Cys	408	543	(16)
P450cam(pyridine)	Cys/pyridine	444	538, 566	(16)
P420cam	Cys	424	530, 558	(19)
Deoxy Mb	His	434	559	(17)
Cytochrome b_5	His/His	423	525, 556	(25)
Fe(II)-CO complexes				
IRP1	His	421	540, 568	This work
IRP2	His	421	540, 569	This work
HRI(CO)	His	421	539, 565	(21)
HRI-N-terminal domain(CO)	His	422	537, 569	(22)
CBS(CO)	His	420	540, 570	(14)
CooA(CO)	His	422	540, 568	(27)
P450cam(CO)	Cys	446	551	(16)
P420cam(CO)	His	420	540, 572	(19)
MbCO	His	420	541, 576	(17)

[1]Shoulder peak

2.3.2 Resonance Raman Spectra of Ferric Heme-bound IRP1 and IRP2.

To further characterize the heme environmental structures of IRPs, I utilized resonance Raman spectroscopy. The resonance Raman spectra can provide valuable information about the heme coordination structure (28). In the high-frequency region, the intense Raman band at approximately 1360–1370 cm^{-1}, ν_4, serves as an oxidation marker band. In the presence of heme, IRP1 and IRP2 displayed the ν_4 band at 1372 cm^{-1}, characteristic of ferric heme (28). The spin-state marker band for the heme iron, ν_3, was also detected in the high-frequency region, and both IRPs displayed two ν_3 bands. In ferric heme-bound IRP1, the Raman band at 1489 cm^{-1} can be assigned to the 5-coordinate high-spin heme, and a shoulder band at 1500 cm^{-1} is derived from the 6-coordinate low-spin heme (Ferric, Figure 2.3A). The high-frequency region of the resonance Raman spectrum for ferric heme-bound IRP2 also has two ν_3 bands at 1490 and 1500 cm^{-1}. Thus, the heme coordination states in ferric heme-bound IRPs were a mixture of 5-coordinate high-spin and 6-coordinate low-spin hemes.

To spectroscopically examine the axial ligand for the heme iron in IRPs, I measured the low-frequency region of the resonance Raman spectra of ferric heme-bound IRPs excited at 363.8 nm, in which the Fe-Cys stretching mode is expected to be detected in the region of 310–350 cm^{-1} (29). The resonance Raman spectra for ferric heme-bound IRP1 and IRP2 showed broad bands at approximately 331 and 333 cm^{-1}, respectively (Figure 2.4). To unambiguously assign the Fe-S stretching mode, I used ^{54}Fe-substituted heme and the Raman bands were fitted by two Gaussian bands. The broad band consisted of two bands at 331 and 345 cm^{-1}, and only the band centered at 331 cm^{-1} for ferric ^{56}Fe-heme-bound IRP1 displayed an ^{54}Fe-isotopic shift to 333 cm^{-1} (Figure 2.4A). In the resonance Raman spectrum of ferric ^{56}Fe-heme-bound IRP2, the band centered at 333 cm^{-1} was also shifted to 335 cm^{-1} after substitution with ^{54}Fe-heme (Figure 2.4B). These isotopic shifts (2 cm^{-1}) were also reported for Irr (20), where Cys in the HRM is ligated to the heme iron, and correspond to the calculated value (2.2 cm^{-1}) (29) that

confirms the ligation of cysteine to the heme iron in ferric heme-bound IRPs.

As found for ferric heme-bound Irr, lower Fe-S stretching frequencies were observed for IRPs and their line-widths were broad (~30 cm^{-1}) when compared with those of the typical Cys-ligated hemoprotein, P450cam (Fe-S frequency: 351 cm^{-1}, line width: ~15 cm^{-1}) (29). These spectral features are also encountered for heme-bound Irr that uses the cysteine residue in the HRM as the axial ligand for the heme iron (20). The marker bands of the resonance Raman spectra for typical hemoproteins are summarized in Table 2.2.

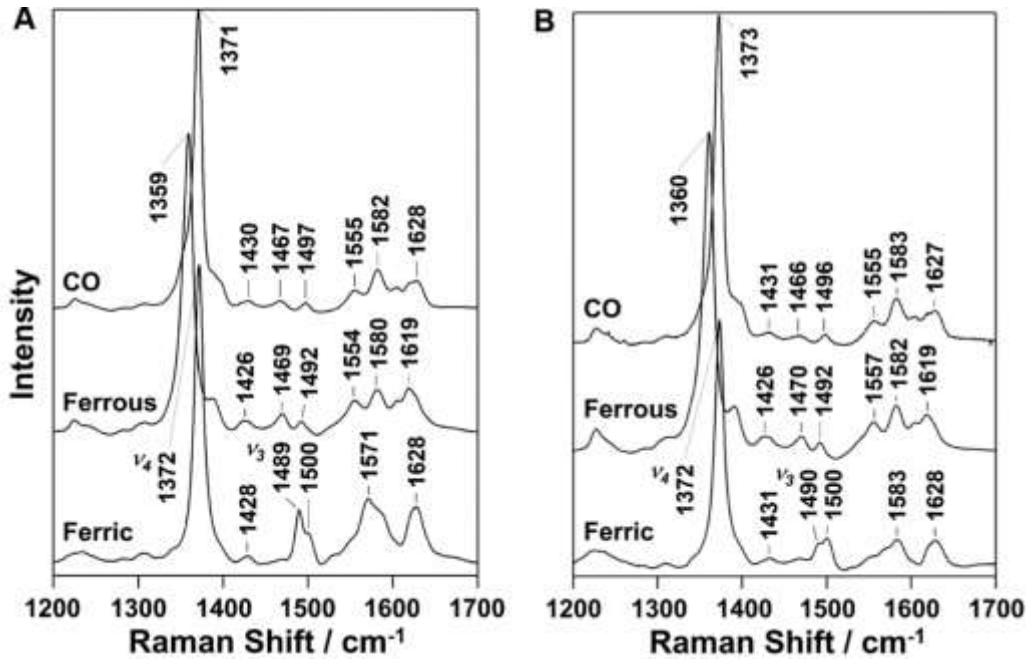

Figure 2.3 Resonance Raman spectra of ferric heme-bound, ferrous heme-bound, and CO adducts of IRPs in the high frequency region.

Resonance Raman spectra of IRP1 (A) and IRP2 (B) are shown. These spectra were obtained by excitation with 413.1 nm. Samples were dissolved in 50 mM Tris-HCl buffer, pH7.4. The protein concentration was approximately 40 μM in the presence of two molar equivalents of heme.

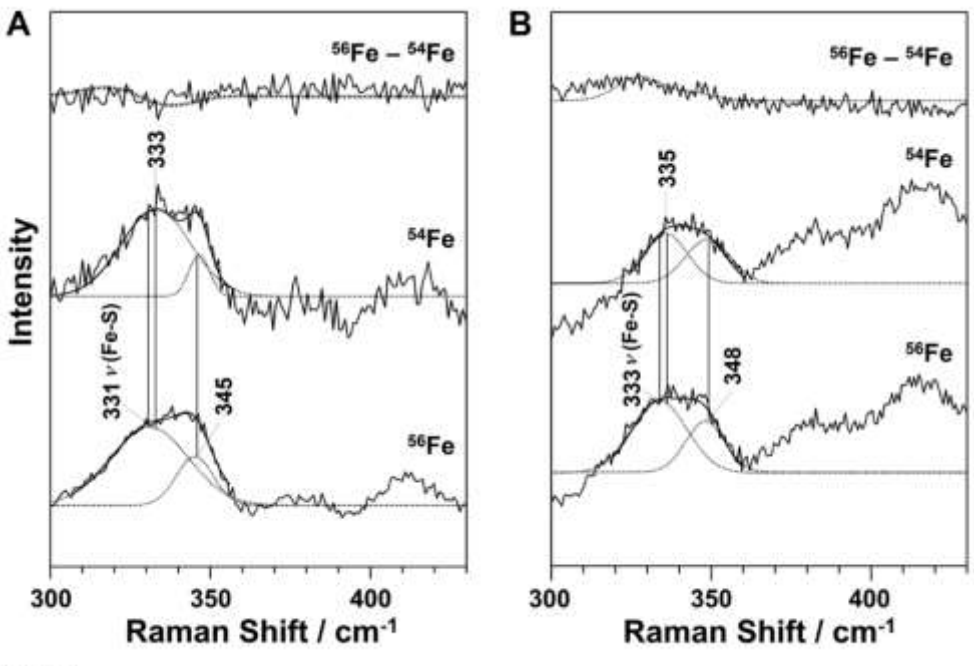

Figure 2.4 Resonance Raman spectra of ferric heme-bound IRPs in the low frequency region.
^{56}Fe and ^{54}Fe heme-bound IRP1 (A), IRP2 (B). The spectra were obtained by excitation with 363.8 nm light from an argon ion laser. Samples were dissolved in 50 mM Tris-HCl buffer, pH 7.4. The protein concentration was approximately 40 μM in the presence of two molar equivalents of heme. The spectra show enlarged Raman lines at approximately 340 cm^{-1} for the ^{54}Fe- and ^{56}Fe-heme-bound IRPs and their difference spectra (^{56}Fe - ^{54}Fe). The Raman lines were fitted by two Gaussian functions (dotted lines).

Table 2.2 Frequencies of spin state markers for hemoproteins.

Proteins	Coordination	ν (Fe-ligand)	ν_4	ν_3	ν_2	Reference
Fe(III) complexes						
IRP1	Cys, Cys/His	331	1372	1489, 1500	1571	This work
IRP2	Cys, Cys/His	333	1372	1490, 1500	1583	This work
CBS	His/Cys	312	1372	1500	1575	(14)
P450cam	Cys	351	1368,1372	1488	1570,1582	(30)
P420cam	Cys	n.d.[1]	1374	1491,1503	1572,1588	(30)
Aquomet Mb	His	n.d.	1373	1503	1584	(31)
Cytochrome b_5	His/His	n.d.	1374	1506	1583	(32)
$Fe^{3+}(PP)Im_2$[2]	Im/Im	n.d.	1374	1503	1582	(32)
Fe(II) complexes						
IRP1	His/(Cys or His)	220	1359	1469,1492	1580	This work
IRP2	His/(Cys or His)	221	1360	1470,1492	1582	This work
CBS, pH 8.0	His/Cys	n.d.	1358	1493	1585	(14)
P450cam	Cys	n.d.	1345	1468	1563	(30)
P420cam	Cys	n.d.	1361	1470,1493	1560,1583	(30)
Deoxy Mb	His	220	1357	1473	1564	(33, 34)
Cytochrome b_5	His/His	n.d.	1360	1492	1582	(32)
$Fe^{2+}(PP)Im_2$	Im/Im	n.d.	1360	1492	1582	(32)
Fe(II)-CO complexes		ν (Fe-CO, FeC-O)				
IRP1(CO)	His	494,1962	1371	1497	1582	This work
IRP2(CO)	His	495,1961	1373	1496	1583	This work
P450cam(CO)	Cys	465	1371	1497	1588	(30)
P420cam(CO)	His	496	1372	1498	1583	(30)
MbCO	His	510,1944	1372	1500	1587	(35, 36)
Mb(^{64}His→Leu)(CO)	His	489,1966	n.d.	n.d.	n.d.	(37, 38)

[1]Not determined, [2]bis-imidazole-ligated porphyrin.

2.3.3 Resonance Raman Spectra for Ferrous Heme-bound IRP1 and IRP2.

In the proposed mechanism for oxidative modification in IRP2 (1) and Irr (3), the reduced state of heme-bound forms binds molecular oxygen, which is one of the crucial steps for the generation of reactive oxygen species (ROS) in the oxidation of the protein moiety. To examine the environmental structures of reduced heme-bound IRPs, I measured the resonance Raman spectra for reduced heme-bound IRPs (Figure 2.3). The ν_4 band appeared at 1359 and 1360 cm^{-1} for IRP1 and IRP2, respectively. As found for ferric heme-bound IRPs, the reduced states of the heme-bound IRPs also gave two spin-state marker bands (1469 and 1492 cm^{-1} for IRP1; 1470 and 1492 cm^{-1} for IRP2), and reduced heme-bound IRPs had two spin states: the 5-coordinate high-spin and 6-coordinate low-spin states.

To get further insights into the heme environmental structures of reduced heme-bound IRPs, the resonance Raman spectra of the CO adducts were measured. In the high-frequency region, the C-O stretching mode of CO ligated to the heme iron is observed at 1920–1980 cm^{-1}, while the Fe-C stretching mode is detected at 470–530 cm^{-1} (39). As shown in Figure 2.5A1, the Raman band at 494 cm^{-1}, which was down-shifted to 484 cm^{-1}, upon ^{13}CO substitution, were assigned to the ν(Fe-CO) bands in the CO adduct of ferrous heme-bound IRP1. Meanwhile, in the high-frequency region (Figure 2.5B1), one isotope-sensitive band appeared at 1962 cm^{-1} in the spectrum of the CO adduct of ferrous heme-bound IRP1 was assignable to the ν(C-O) band. In the CO adduct of heme-bound IRP2 (Figures 2.5A2 and 2.5B2), the isotope-sensitive bands at 495 and 1961 cm^{-1} were assigned to ν(Fe-CO) and ν(C-O), respectively. Based on the inverse correlation of the frequencies between ν(Fe-CO) and ν(FeC-O) (Figure 3.6), the ligand trans to CO was proposed to be a neutral His, but not an anionic Cys. In addition to the ν(Fe-CO) band from His-ligated heme, the isotope-sensitive Raman bands were observed at 525 and 526 cm^{-1} for the CO adducts of ferrous heme-bound IRP1 and IRP2, respectively (Figures 2.5A1 and 2.5A2). These Raman bands can be assigned to ν(Fe-CO) of the 5-coordinate heme, suggesting

the release of the axial ligand upon reduction.

The ligation of His to the ferrous heme iron in heme-bound IRPs was further examined by the low-frequency regions of the resonance Raman spectra for heme-bound IRPs. As previously reported (34), the Fe-His stretching mode was observed at 200–250 cm^{-1} for the 5-coordinated ferrous heme. Because the 6-coordinate heme was dominant for ferrous heme-bound IRP1 and IRP2 (Figure 2.2), I measured resonance Raman spectra of photo-dissociated CO adducts of ferrous heme-bound IRPs to detect the Fe-His stretching mode. In both IRP1 and IRP2, the characteristic Raman bands assignable to the Fe-His stretching mode were observed at 220 and 221 cm^{-1}, respectively (Figure 2.7), as found for deoxymyoglobin (220 cm^{-1}) (34), supporting the idea that a neutral His is the axial ligand for the CO adducts of heme-bound IRPs.

The frequencies for the Fe-CO, and C-O stretching modes also reflect the heme environment, particularly polarity in the exogenous ligand binding sites (40). In the CO adduct of myoglobin, the ν(Fe-CO) and ν(C-O) bands were observed at 510 and 1944 cm^{-1}, respectively (35, 36). Down-shifted ν(Fe-CO) and up-shifted ν(C-O) bands were also encountered for the "distal mutant" of myoglobin (ν(Fe-CO): ~489 cm^{-1}, ν(FeC-O): ~1966 cm^{-1}), where the distal histidine, ^{64}His, was replaced with leucine or alanine (37, 38). The spectral similarity between the distal mutant of myoglobin and reduced heme-bound IRPs implies that the ligand-binding site of heme-bound IRPs is apolar.

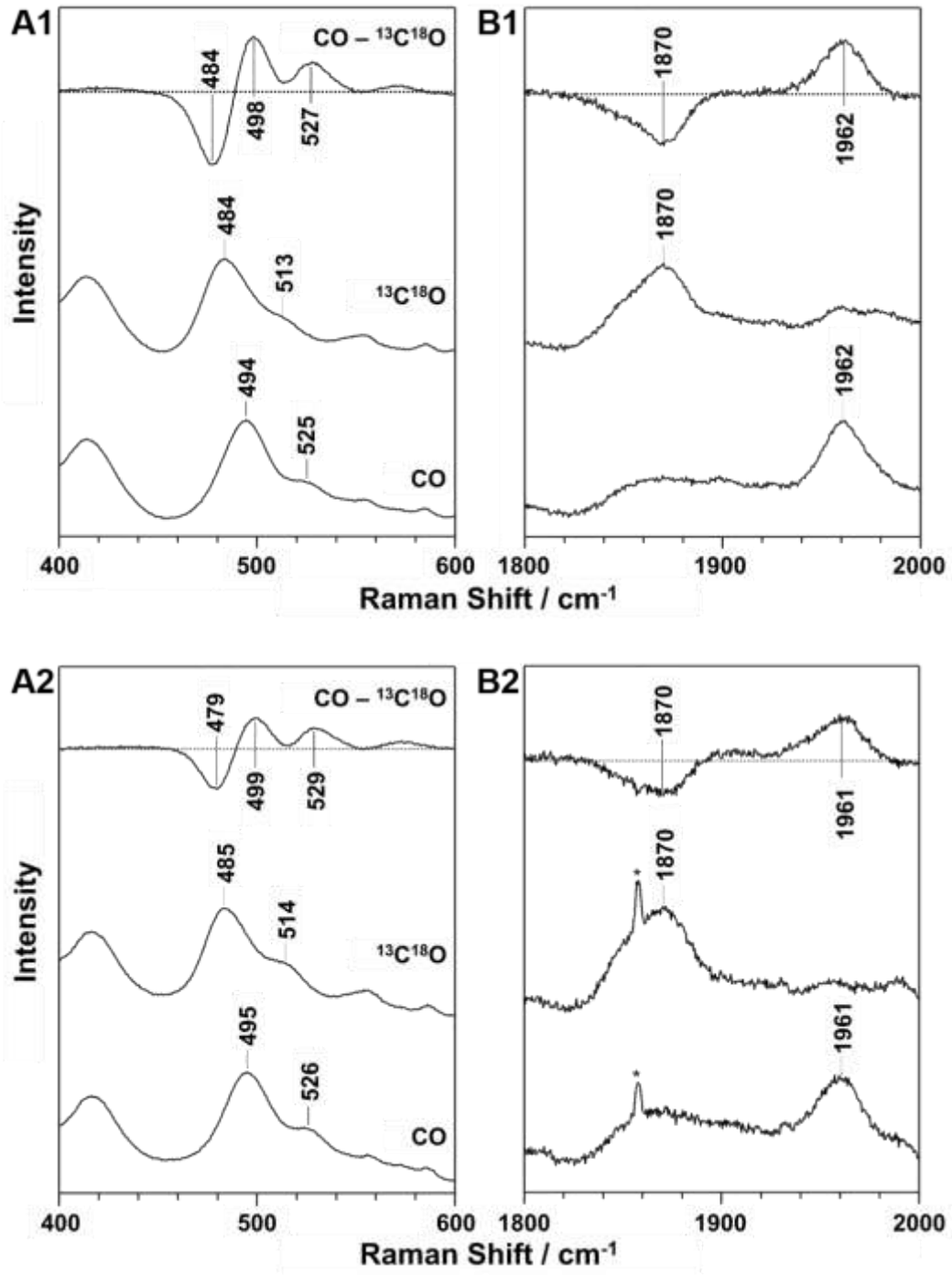

Figure 2.5 Resonance Raman spectra of Fe(II)-CO complexes of IRPs.

The low-frequency (A) and high-frequency (B) regions of the resonance Raman spectra for CO adducts of reduced heme-bound IRP1 (1) and IRP2 (2) excited at 413.1 nm. Asterisks mark the position of laser plasma lines.

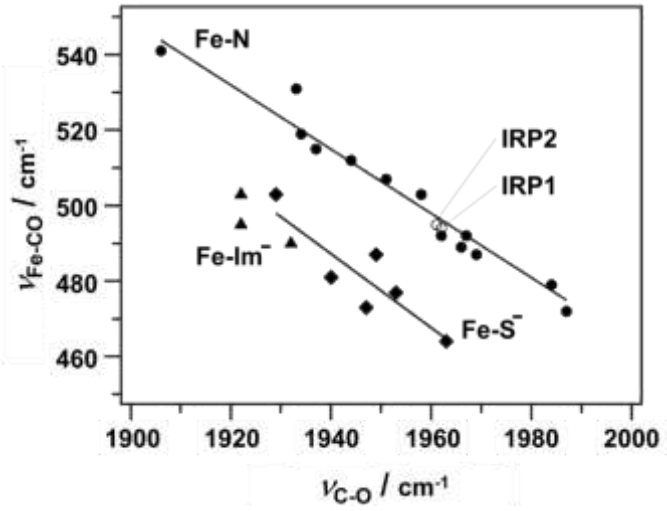

Figure 2.6 Correlation plot between ν_{Fe-CO} and ν_{C-O} of hemoproteins and porphyrin model compounds.

Proteins with an anionic ligand (◆), proteins with a neutral ligand (●), and model complexes with an anionic ligands (▲). Data for IRP1, IRP2 are represented as ○.

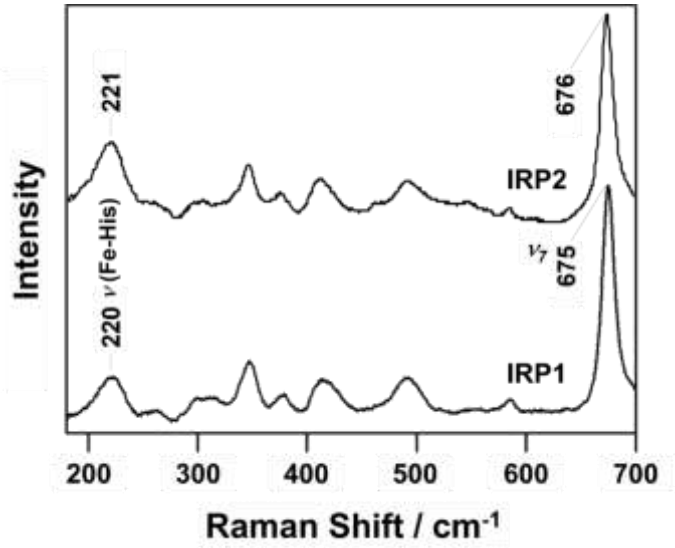

Figure 2.7 Resonance Raman spectra of photodissociated products of CO adducts of IRPs in the low-frequency regions.

Ferrous-CO complexes of IRP1 (A) and IRP2 (B). The protein concentration was approximately 30 μM in 50 mM Tris-HCl buffer, pH 7.4, in the presence of two molar equivalents of heme. Excitation wavelength was 441.6 nm.

2.3.4 Axial Ligand Exchange Evident by Pulse Radiolysis.

As shown in the absorption and resonance Raman spectra, the spectroscopic properties of ferric heme-bound IRPs were quite similar to that of ferric heme-bound Irr (20), a bacterial iron regulatory protein that uses heme as an effector molecule to regulate transcription activity, where Cys in the HRM is ligated to the heme iron. After reduction of the heme iron, however, the spectral features of heme-bound IRPs were significantly different from that of a typical anionic Cys-ligated hemoprotein such as P450cam, which were rather similar to those of the His-ligated hemoproteins including myoglobin and hemoglobin. Using mutations in the HRM region of the IDD domain in IRP2, Ishikawa *et al.* (1) have shown that the axial ligand for ferric heme-bound IRP2 is ^{201}Cys in the HRM and one of the axial ligands for reduced heme-bound IRP2 is ^{204}His, allowing them to propose a redox-dependent axial ligand exchange. Similar axial ligand replacement was also found for Irr (11). In Irr, the axial ligand replacement of Cys in the HRM with His is induced immediately after the reduction of the heme iron to transiently form a 5-coordinate His-ligated heme, which is one of the intermediates for the oxidative modification and successive loss of the ability of Irr to bind to target DNA (11).

Formation of the 5-coordinate His-ligated intermediate in heme-bound IRPs was examined by the spectral changes after reduction of the heme using pulse radiolysis (Figure 2.8). The kinetic difference spectrum for heme-bound IRP1 (Figure 2.8A) exhibited a broad positive absorption band in the region between 410 and 450 nm, whereas in the kinetic difference spectrum at 100 μs for heme-bound IRP2 (Figure 2.8B), an absorption maximum at 435 nm was detected, indicating formation of 5-coordinate His-ligated heme, as found for heme-bound Irr (11). The absorption maximum at 435 nm remained 2 ms after the reduction (dashed line, Figure 2.8B), while the difference spectrum between ferric heme- and ferrous heme-bound IRP2 showed an absorption maximum at 425 nm, not at 435 nm (solid line, Figure 2.8B), which corresponds to the Soret peak of ferrous heme-bound IRP2 (425 nm) (Figure 2.2B). Because

our previous mutational study reported that ferrous heme-bound IRP2 has a 6-coordinate His-ligated heme (1), the 6-coordinate His-ligated heme would, therefore, be formed more than 2 ms after the reduction of the heme.

On the other hand, the difference spectra at 100 μs and 2 ms after heme reduction showed no distinct absorption minimum at approximately 425 nm, where the absorption peak for the 6-coordinate neutral Cys/His-ligated heme appears, suggesting that the 6-coordinate neutral Cys/His-ligated heme is insensitive to the reduction of the heme iron. However, considering that the 6-coordinate His/His-ligated ferrous heme exhibits a Soret band similar to that of the 6-coordinate neutral Cys/His-ligated ferric heme (Table 2.1) and that axial ligand replacement from Cys to His is induced for the 5-coordinate Cys-ligated heme, the axial cysteine residue for the 6-coordinate neutral Cys/His-ligated heme might be also replaced by His to form the 6-coordinate His/His-ligated heme after the reduction. Together with the results from the mutational study of IRP2 (1), immediately after the reduction, the axial cysteine residue, ^{201}Cys, in the 5-coordinate heme is dissociated from the heme iron, and the adjacent histidine, ^{204}His, is then rapidly ligated to the ferrous heme iron to form the 5-coordinate His-ligated heme. In the 6-coordinate heme, I could not unambiguously determine the axial ligands immediately after the reduction of ferric heme-bound IRP2.

After more than 2 ms, the 5-coordinate His-ligated heme is further converted into a 6-coordinate His-ligated heme as shown in the difference spectrum between dithionite-reduced and oxidized IRP2. The amino acid residue ligated to the heme iron more than 2 ms after the reduction has not yet been identified, but the IDD domain has only one histidine residue, ^{204}His, and we speculate that a histidine residue from a region outside of the IDD domain coordinates to the heme iron, as suggested in our previous study (1).

In contrast to the difference spectrum for IRP2, the intermediate species with the absorption maximum at 435 nm was not observed for ferric heme-bound IRP1 (Figure 2.8A).

Instead of the absorption maximum at 435 nm, a broad positive absorption band in the region between 410 and 450 nm appeared in the difference spectrum at 100 μs after the reduction. It is likely that the absorption maximum at approximately 430–450 nm is derived from a 6-coordinate Cys/His-ligated heme, as found for pyridine-ligated P450cam (444 nm) (16). In addition, another absorption maximum at approximately 410 nm was detected both 100 μs and 2 ms after the pulse radiolysis. The increased absorbance intensity at approximately 410 nm can be assigned to the formation of a ferrous 5-coordinate Cys-ligated heme, similar to ferrous P450cam (409 nm) (41). The appearance of the absorption maxima at approximately 410 and 440 nm suggests that the axial ligand for heme-bound IRP1 immediately after the reduction is the cysteine residue, and reduction of the heme iron in ferric heme-bound IRP1 does not result in the rapid replacement of the axial cysteine, which is distinctly different from the case of ferric heme-bound IRP2.

Although IRP2 has two HRMs outside of the IDD domain, absorption maxima at approximately 410 and 440 nm were not detected. We cannot completely exclude the possibility that all of the heme binding sites in IRP2 form the transient 5-coordinate His-ligated heme after the reduction. As previously reported (1), the intensities of the absorption bands in the Soret and visible regions of the heme-bound IRP mutant lacking the IDD domain were more substantially decreased after gel filtration column, compared to those of intact heme-bound IRP2, suggesting that the heme binding affinities of the HRMs outside of the IDD domain is lower than that of the HRM in the IDD domain. After gel filtration during sample preparation for the pulse radiolysis experiments, some amounts of heme might be released from the HRMs outside of the IDD domain. In addition, the absorption bands for the 5-coordinate and 6-coordinate Cys-ligated heme in the difference spectra were broad and rather featureless, which would make their detection in the difference spectra more difficult in the presence of the 5-coordinate His-ligated heme. The contribution of the heme binding spectral characteristics

located outside of the IDD domain would be much less than those of the IDD domain to the difference spectra of heme-bound IRP2.

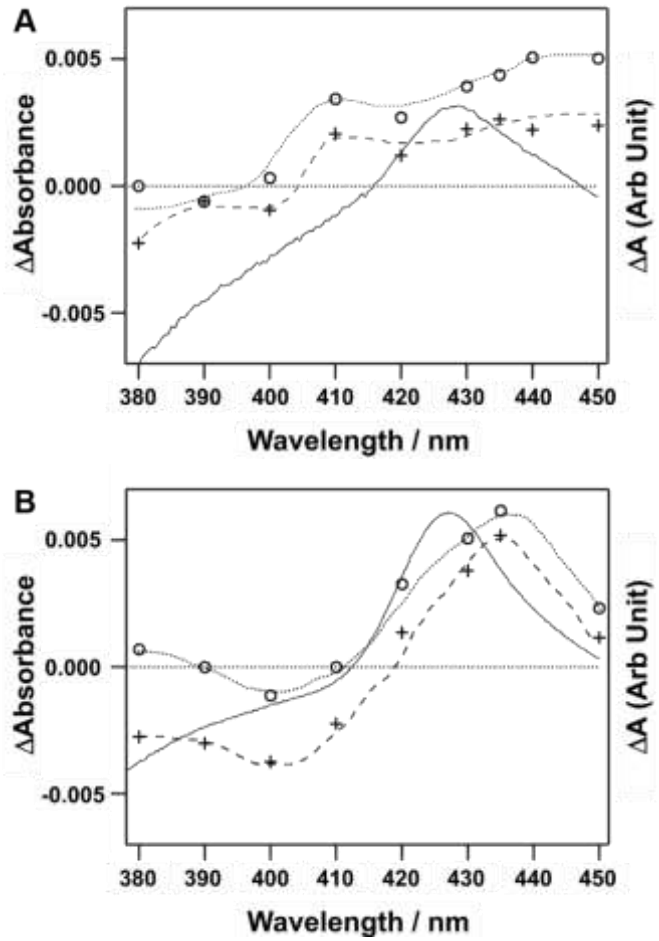

Figure 2.8 Comparison of kinetic difference spectra for IRPs after pulse radiolysis.
Spectra were measured at 100 μs (circle and dotted line) and 2 ms (plus and dashed line) after pulse radiolysis of IRP1 (A), IRP2 (B). The difference spectrum between dithionite-reduced and oxidized IRPs is shown as a solid line. The left axis shows the change in absorbance (ΔA) for the kinetic difference spectrum, and the right axis shows the change in absorbance for the static difference spectrum.

2.4. Discussion.

As we previously reported (20) and reviewed (12), "heme-regulated" proteins that use HRMs as their heme binding sites have some unique spectral characteristics. In IRP2, the heme environmental structures of both of the ferric heme- and ferrous heme-bound forms have been already examined, revealing that the heme environment is significantly different from that of the conventional Cys-ligated hemoprotein such as P450cam (1). In this paper, I successfully identified the Raman band for the Fe-Cys stretching mode in the ferric heme-bound form, and this band was broad and down-shifted to approximately 330 cm^{-1}, compared to those of a typical Cys-ligated hemoprotein, such as P450cam, and more closely resembles those of ferric heme-bound Irr (20). The lower frequency for the Fe-S stretching mode has also been reported for nitric oxide synthase (338 cm^{-1}), where the axial cysteine has only one hydrogen bond to stabilize ligation to the heme iron (42) (two hydrogen bonds are formed in P450cam (43)), and for heme-bound Bach1, which is also a HRM-containing heme-regulated protein using heme as the regulatory molecule (44). The lower frequency of the Fe-S stretching mode in ferric heme-bound IRP2, therefore, means weak interactions between the axial ligand and surrounding amino acid residues and supports a role for heme as the signaling molecule for IRP2 (1).

Although spectral characteristics observed for heme-bound IRP2 were also found for heme-bound IRP1, the spectral changes after the reduction of the heme iron in heme-bound IRP1 were significantly different from those of IRP2 and Irr, as shown by our pulse radiolysis experiments (Figure 2.8). The spectral changes immediately after the reduction of heme-bound IRP2 indicates formation of a 5-coordinate His-ligated ferrous heme, whereas 5-coordinate Cys-ligated and 6-coordinate Cys/His-ligated ferrous hemes were transiently formed in IRP1. Taking into account that the two HRMs outside of the IDD domain are conserved in both IRP1 and IRP2, the intermediate species with the 5-coordinate His-ligated ferrous heme is formed in the HRM of the IDD domain in IRP2, and hemes in the other HRM regions, outside of the IDD

domain, are a mixture of 5-coordinate Cys-ligated and 6-coordinate Cys/His-ligated ferrous hemes. Together with the results from the present spectroscopic measurements, I can propose model structures of hemes in ferric heme- and ferrous heme-bound IRPs schematically represented in Figure 2.9.

In the presence of heme, both IRP1 and IRP2 can specifically bind heme in their HRMs, and the coordination structures of these ferric heme-bound IRPs are a mixture of 5-coordinate Cys-ligated and 6-coordinate Cys/His-ligated hemes (Ferric State, Figure 2.9). In heme-bound IRP1, the ligated cysteines are ^{118}Cys and ^{300}Cys in the HRMs, while in IRP2, three cysteine residues (^{201}Cys in the HRM of the IDD domain, ^{120}Cys, and ^{375}Cys in the HRMs outside of the IDD domain) are ligated to the heme iron. All of the heme environments including the heme-binding site in the IDD domain of IRP2 are quite similar and almost indistinguishable.

After the reduction of the heme ion (Reduction of Heme Iron, Figure 2.9), the heme in IRP1 is reduced to maintain axial ligands to form the reduced 5-coordinate Cys-ligated and the 6-coordinate Cys/His-ligated hemes, as indicated by the absorption at approximately 410 and 440 nm, respectively, in the difference spectra of the pulse radiolysis experiments (Figure 2.8A). These complexes are relatively stable, since they are detected at 2 ms after the reduction (dashed line, Figure 2.8A). After the transient formation of reduced Cys-ligated hemes, the axial cysteine would easily dissociate from the heme iron, due to the decreased relative affinity for ferrous heme iron compared to ferric heme. Once the axial cysteine is dissociated, a histidine residue will be coordinated to the ferrous heme iron to form the 5-coordinate His-ligated and 6-coordinate His/His-ligated heme (Ferrous State, Figure 2.9). Due to the similar spectral pattern of the absorbance spectra between the His/His-ligated and Cys/His-ligated heme, we could not confirm the axial ligand replacement in the Cys/His-ligated heme and some amount of ferrous-heme bound IRP1 would maintain the Cys/His heme after reduction. The resonance Raman spectrum for reduced heme-bound IRP1 indicates two spin state markers arising from

5-coordinate high spin and 6-coordinate low spin hemes, but the absorption spectrum has no distinct absorption maximum at approximately 430 nm, which is characteristic of a 5-coordinate His-ligated heme. Therefore, the 5-coordinate His-ligated heme population is rather small, compared to that of the 6-coordinate heme. Upon addition of CO (CO Adduct, Figure 2.9), the CO adduct of the His-ligated heme is formed in heme-bound IRP1.

The coordination structures of hemes in the HRM outside of the IDD domain in IRP2 ("HRM outside of IDD domain" in Figure 2.9) would be identical to that of IRP1. However, the appearance of the absorption maximum at 435 nm in the difference spectra of the pulse radiolysis experiments (Reduction of Heme Iron, Figure 2.9) and our previous mutational study (1) clearly indicates that the reduction of the heme iron in the HRM of the IDD domain in IRP2 induces dissociation of ^{201}Cys from the heme iron and ligation of the adjacent histidine, ^{204}His, to form the 5-coordinate His-ligated heme. In the 6-coordinate Cys/His-ligated heme in the HRM of the IDD domain, similar axial ligand replacement of ^{201}Cys by ^{204}His might occur to form the 6-coordinate His/His-ligated heme, but we cannot exclude the possibility that protonated ^{201}Cys is ligated to the 6-coordinate heme after the reduction.

Although ^{204}His is located near ^{201}Cys on the amino acid sequence, such ligand replacement requires a large structural change in the heme binding site. In CooA, one of the heme-containing transcription factors, the axial ligand of the ferric heme, ^{75}Cys, is replaced by ^{77}His upon the reduction of the heme iron (45), and the distance between the heme iron and sulfur atom of ^{75}Cys is 4.8 Å in ferrous CooA (46). The x-ray structure of CooA indicates that only one hydrogen bond exists within 10 Å from the heme iron in the proximal pocket, and a smaller number of the hydrogen bond in the heme binding site will reflect the flexibility of the polypeptide around heme binding site in CooA (45). The rapid dissociation of ^{201}Cys from the heme iron and ligation of ^{204}His in heme-bound IRP2 would, therefore, be due to the flexibility of the polypeptide in the IDD domain as suggested for CooA. The lower frequency of the Fe-S stretching mode in ferric heme-bound IRP2 also supports less number of the hydrogen bonds

around the axial ligand. In addition, NMR measurements for the isolated IDD domain suggest that the structure of the IDD domain is disordered (47), and the heme binding site in the HRM of Bach2 is also disordered (48). Such structural flexibility in the IDD domain would promote the axial ligand replacement from ^{201}Cys to ^{204}His.

In the HRM of the IDD domain, more than 2 ms after the reduction, the 6-coordinate His/His-ligated or Cys/His-ligated heme is dominated by the ligation of the histidine residue from the region outside of the IDD domain (Ferrous State, Figure 2.9). By addition of CO, replacement of one of the ligands, possibly ^{204}His (1) or protonated ^{201}Cys, in the 6-coordinate heme and the ligation of CO to the 5-coordonate His-ligated heme are induced to form the CO adduct, in which the histidine serves as the trans ligand (CO adduct, Figure 2.9).

Our spectroscopic characterization of heme-bound IRPs immediately after reduction of the heme iron revealed that the 5-coordinate His-ligated heme is specifically formed in the HRM of the IDD domain in IRP2, although both ferrous heme-bound IRP1 and IRP2 showed the 6-coordinated His-ligated heme. Considering that IRP1 was not oxidized in the presence of heme under the conditions where IRP2 was oxidized (49), the 6-coordinate His-ligated heme after the reduction of the heme iron in IRPs would not effectively generate ROS to oxidize the protein moiety or the amino acid residues in the binding site of the 6-coordinate His-ligated heme would not be susceptible to oxidation by ROS. This allows us to speculate that molecular oxygen can bind to the 5-coordinate His-ligated heme and the amino acid residues constituting the oxygen binding site for the 5-coordinate His-ligated heme in the IDD domain of IRP2 are sensitive to the oxidation of ROS, leading to oxidative modification that is recognized by the ubiquitin ligase and results in proteasomal degradation.

In conclusion, I revealed the heme environmental structures of ferric heme- and ferrous heme-bound IRPs, including the intermediate species after reduction of the heme iron. Although ferric heme bound IRPs have the axial cysteine residues in the HRMs, the heme coordination structures were significantly different from those of typical Cys-ligated proteins

such as P450. In the IDD domain of IRP2, ^{201}Cys in the HRM is ligated to the ferric heme iron, while, upon reduction of the heme iron, ^{201}Cys is dissociated and ^{204}His will be ligated. Despite similar spectral characteristics in ferric heme- and ferrous heme-bound IRPs, the 5-coordinate His-ligated heme is specifically formed in the HRM of the IDD domain in IRP2, probably due to the structural flexibility of the IDD domain. The specific formation of this 5-coordinate His-ligated heme would be essential for oxidative modification of IRP2, which differentiates the functions of heme between these two IRPs.

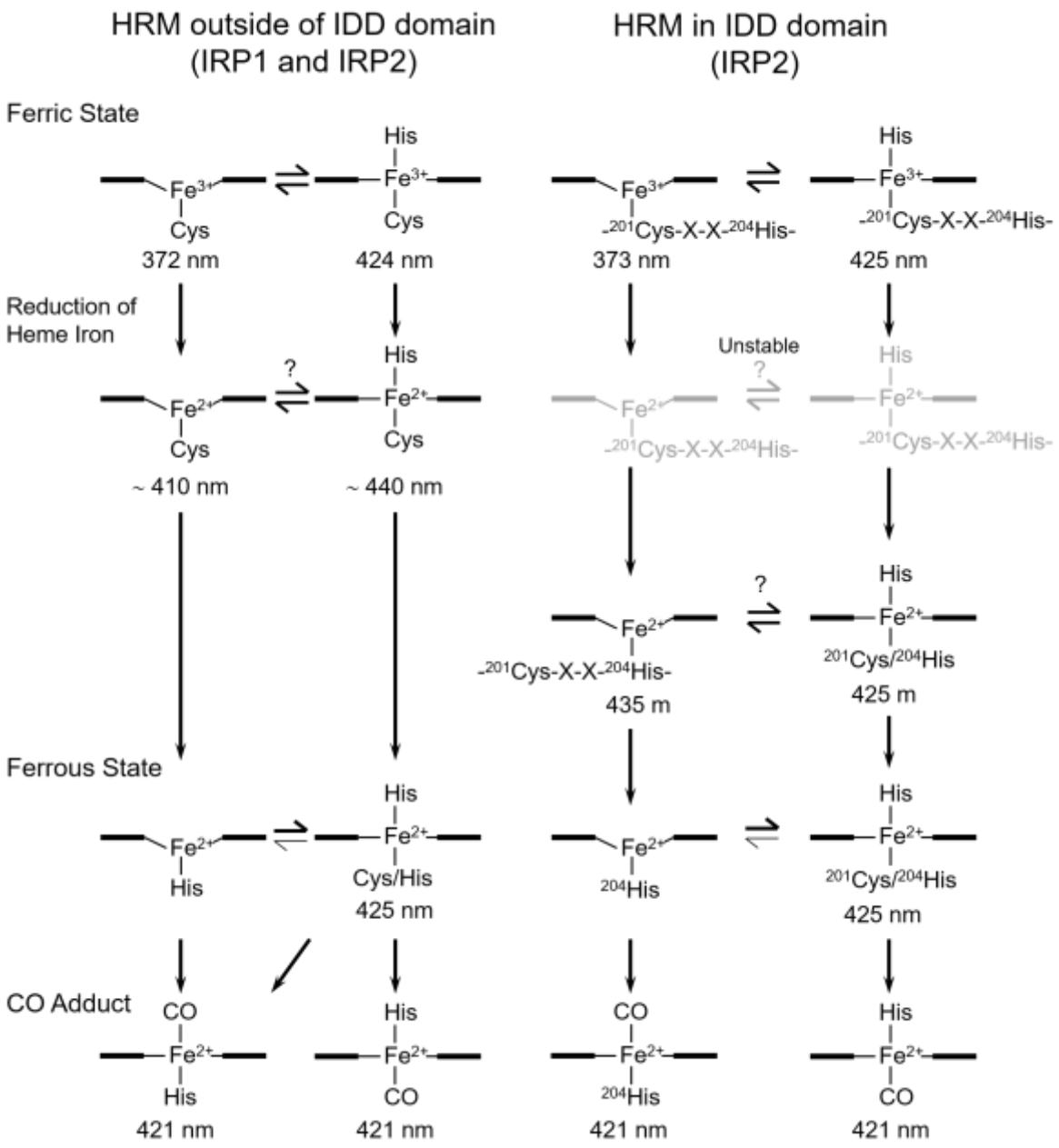

Figure 2.9 Model structures of heme coordination at the HRM region outside of (left) and in (right) the IDD domain.

The species not confirmed by spectroscopy are gray. The wavelengths of the peak in the Soret region are shown below.

References.

1. H. Ishikawa, M. Kato, H. Hori, K. Ishimori, T. Kirisako, F. Tokunaga, K. Iwai, Involvement of heme regulatory motif in heme-mediated ubiquitination and degradation of IRP2. *Mol. Cell*. **19**, 171–181 (2005).

2. L. Zhang, L. Guarente, Heme binds to a short sequence that serves a regulatory function in diverse proteins. *EMBO J.* **14**, 313–320 (1995).

3. C. Kitatsuji, K. Izumi, S. Nambu, M. Kurogochi, T. Uchida, S.-I. Nishimura, K. Iwai, M. R. O'Brian, M. Ikeda-Saito, K. Ishimori, Protein oxidation mediated by heme-induced active site conversion specific for heme-regulated transcription factor, iron response regulator. *Sci Rep.* **6**,18703 (2016)

4. Z. Qi, I. Hamza, M. R. O'Brian, Heme is an effector molecule for iron-dependent degradation of the bacterial iron response regulator (Irr) protein. *Proc. Natl. Acad. Sci. U. S. A.* **96**, 13056–13061 (1999).

5. K. Iwai, R. D. Klausner, T. A. Rouault1, Requirements for iron-regulated degradation of the RNA binding protein, iron regulatory protein 2. *EMBO J.* **14**, 5350–5357 (1995).

6. K. Pfeifer, K.-S. Kim, S. Kogan, L. Guarente, Functional dissection and sequence of yeast HAP1 activator. *Cell*. **56**, 291–301 (1989).

7. J. T. Lathrop, M. P. Timko, Regulation by heme of mitochondrial protein transport through a conserved amino acid motif. *Science*. **259**, 522–525 (1993).

8. J.-J. Chen, J. K. Pal, R. Petryshynt, I. Kuo, J. M. Yang, M. S. Throop, L. Gehrke, I. M. London, Amino acid microsequencing of internal tryptic peptides of heme- regulated eukaryotic initiation factor 2a subunit kinase: Homology to protein kinases. *Biochemistry*. **88**, 315–319 (1991).

9. K. Ogawa, J. Sun, S. Taketani, O. Nakajima, C. Nishitani, S. Sassa, N. Hayashi, M. Yamamoto, S. Shibahara, H. Fujita, K. Igarashi, Heme mediates derepression of Maf recognition element through direct binding to transcription repressor Bach1. *EMBO J.* **20**, 2835–2843 (2001).

10. K. Yamanaka, H. Ishikawa, Y. Megumi, F. Tokunaga, M. Kanie, T. A. Rouault, I. Morishima, N. Minato, K. Ishimori, K. Iwai, Identification of the ubiquitin–protein ligase that recognizes oxidized IRP2. *Nat. Cell Biol.* **5**, 336–340 (2003).

11. K. Kobayashi, M. Nakagaki, H. Ishikawa, K. Iwai, M. R. O'Brian, K. Ishimori, Redox-dependent dynamics in heme-bound bacterial iron response regulator (Irr) protein. *Biochemistry*. **55**, 4047–4054 (2016).

12. K. Ishimori, Y. Watanabe, Unique heme environmental structures in heme-regulated

proteins using heme as the signaling molecule. *Chem. Lett.* **43**, 1680–1689 (2014).

13. S. Beck von Bodman, M. A. Schuler, D. R. Jollie, S. G. Sligar, Synthesis, bacterial expression, and mutagenesis of the gene coding for mammalian cytochrome b_5. *Proc. Natl. Acad. Sci. U. S. A.* **83**, 9443–9447 (1986).

14. T. Omura, H. Sadano, T. Hasegawa, Y. Yoshida, S. Kominami, Hemoprotein H-450 identified as a form of cytochrome P-450 having an endogenous ligand at the 6th coordination position of the heme. *J. Biochem*. **96**, 1491–1500 (1984).

15. Yi Liu, Pierre Moënne-Loccoz, Dean P. Hildebrand, Angela Wilks, Thomas M. Loehr, and A. Grant Mauk, Paul R. Ortiz de Montellano, Replacement of the proximal histidine iron ligand by a cysteine or tyrosine converts heme oxygenase to an oxidase (1999)

16. J. H. Dawsons, L. A. Anderssons, M. Sono, The diverse spectroscopic properties of ferrous cytochrome P-450-cam ligand complexes. *J. Biol. Chem.* **258**, 13637–13645.

17. E. Antonini, M. Brunori, Hemoglobin and myoglobin in their reactions with ligands. Sience. **178**, 296-297 (1972)

18. Y. Sun, W. Zeng, A. Benabbas, X. Ye, I. Denisov, S. G. Sligar, J. Du, J. H. Dawson, P. M. Champion, Investigations of Heme Ligation and Ligand Switching in Cytochromes P450 and P420. *Biochemistry*. **52**, 5941–5951 (2013).

19. Susan A. Martinis, Steven R. Blanke, A. Lowell P. Hager, S. G. Sligar, G. H. B. Hoa, J. J. R. And, J. H. Dawson, Probing the heme iron coordination structure of pressure-induced cytochrome P420cam (1996)

20. H. Ishikawa, M. Nakagaki, A. Bamba, T. Uchida, H. Hori, M. R. Oâbrian, K. Iwai, K. Ishimori, Unusual heme binding in the bacterial iron response regulator protein: Spectral characterization of heme binding to the heme regulatory motif. *Biochemistry*. **50**, 1016–1022 (2011).

21. J. Igarashi, A. Sato, T. Kitagawa, T. Yoshimura, S. Yamauchi, I. Sagami, T. Shimizu, Activation of heme-regulated eukaryotic initiation factor 2alpha kinase by nitric oxide is induced by the formation of a five-coordinate NO-heme complex: optical absorption, electron spin resonance, and resonance raman spectral studies. *J. Biol. Chem.* **279**, 15752–15762 (2004).

22. J. Igarashi, A. Sato, T. Kitagawa, I. Sagami, T. Shimizu, CO binding study of mouse heme-regulated eIF-2α kinase: kinetics and resonance Raman spectra. *Biochim. Biophys. Acta - Proteins Proteomics*. **1650**, 99–104 (2003).

23. D. Shelver, R. L. Kerby, Y. He, G. P. Roberts, CooA, a CO-sensing transcription factor from Rhodospirillum rubrum, is a CO-binding heme protein. *Biochemistry*. **94**, 11216–11220 (1997).

24. J. H. Dawson, L. A. Anderssons, M. Sono, Spectroscopic investigations of ferric cytochrome P-450-cam ligand complexes identification of the ligand trans to cysteinate in the native enzyme. *J. Biol. Chem.* **257** (1982)

25. Y. Yoshida, H. Kumaoka, R. Sato, Studies on the Microsomal Electron-transport System of Anaerobically Grown Yeast II Purification and Characterization of cytochrome b_5. *J. Biochem*. **75**, 1211–1219 (1974).

26. J. Yang, K. Ishimori, M. R. O'Brian, Two heme binding sites are involved in the regulated degradation of the bacterial iron response regulator (Irr) protein. *J. Biol. Chem.* **280**, 7671–7676 (2005).

27. S. Aono, K. Ohkubo, T. Matsuo, H. Nakajima, Redox-controlled ligand exchange of the heme in the CO-sensing transcriptional activator CooA. *J. Biol. Chem.* **273**, 25757–25764 (1998).

28. T. G. Spiro, X.-Y. Li, Resonance Raman Spectroscopy of Metalloporphyrins. *Biol. Appl. Raman Spectrosc.* **3**, 1–37 (1988).

29. P. M. Champion, B. R. Stallard, G. C. Wagner, I. C. Gunsalus, Resonance Raman detection of an iron-sulfur bond in cytochrome P 450cam. *J. Am. Chem. Soc.* **104**, 5469–5472 (1982).

30. A. V. Wells, P. Li, P. M. Champion, S. A. Martinis, S. G. Sligar, Resonance Raman investigations of *Escherichia coli*-expressed Pseudomonas putida cytochrome P450 and P420. *Biochemistry*. **31**, 4384–4393 (1992).

31. A. Feis, M. P. Marzocchi, M. Paoli, G. Smulevich, Spin state and axial ligand bonding in the hydroxide complexes of metmyoglobin, methemoglobin, and horseradish peroxidase at room and low temperatures. *Biochemistry*. **33**, 4577–4583 (1994).

32. T. Kitagawa, T. Sugiyama, T. Yamano, Differences in stability against thermal unfolding between trypsin- and detergent-solubilized cytochrome b_5 and structural changes in the heme vicinity upon the transition: resonance Raman and absorption study. *Biochemistry*. **21**, 1680–1686 (1982).

33. S. D. Carson, I. Constantinidis, J. Mintorovitch, J. D. Satterlee, M. R. Ondrias, The structural bases for the unique ligand binding properties of *Glycera dibranchiata* hemoglobins. A resonance Raman study. *J. Biol. Chem.* **261**, 2246–2255 (1986).

34. T. Kitagawa, K. Nagai, M. Tsubaki, Assignment of the Fe-Nε (His F8) stretching band in the resonance Raman spectra of deoxy myoglobin. *FEBS Lett.* **104**, 376–378 (1979).

35. M. W. Makinen, R. A. Houtchens, W. S. Caughey, Structure of carboxymyoglobin in crystals and in solution. *Proc. Natl. Acad. Sci. U. S. A.* **76**, 6042–6046 (1979).

36. M. Tsubaki, R. B. Srivastava, N. T. Yu, Resonance Raman investigation of carbon monoxide bonding in (carbon monoxy)hemoglobin and -myoglobin: detection of Fe-CO stretching and Fe-C-O bending vibrations and influence of the quaternary structure change. *Biochemistry*. **21**, 1132–1140 (1982).

37. C. L. Anderton, R. E. Hester, J. N. Moore, A chemometric analysis of the resonance Raman spectra of mutant carbonmonoxy-myoglobins reveals the effects of polarity. *Biochim. Biophys. Acta - Protein Struct. Mol. Enzymol.* **1338**, 107–120 (1997).

38. T. Li, M. L. Quillin, G. N. Phillips, J. S. Olson, Structural determinants of the stretching frequency of CO bound to myoglobin. *Biochemistry*. **33**, 1433–1446 (1994).

39. K. E. Yu N-T, Vibrational modes of coordianted CO, CN and NO. *Biol. Appl. Raman Spectrosc.* **3**, 39–95 (1988).

40. H. Cao, S. L. Suib, Highly efficient heterogeneous photooxidation of 2-propanol to acetone with amorphous manganese oxide catalysts. *J. Am. Chem. Soc.* **116**, 5334–5342 (1994).

41. T. Egawa, T. Hishiki, Y. Ichikawa, Y. Kanamori, H. Shimada, S. Takahashi, T. Kitagawa, Y. Ishimura, Refolding processes of cytochrome P450cam from ferric and ferrous acid forms to the native conformation. Formations of folding intermediates with non-native heme coordination state. *J. Biol. Chem.* **279**, 32008–32017 (2004).

42. J. P. M. Schelvis, V. Berka, G. T. Babcock, A. L. Tsai, Resonance Raman detection of the Fe-S bond in endothelial nitric oxide synthase. *Biochemistry*. **41**, 5695–5701 (2002).

43. C. M. Krest, A. Silakov, J. Rittle, T. H. Yosca, E. L. Onderko, J. C. Calixto, M. T. Green, Significantly shorter Fe–S bond in cytochrome P450-I is consistent with greater reactivity relative to chloroperoxidase. *Nat. Chem.* **7**, 696–702 (2015).

44. S. Hira, T. Tomita, T. Matsui, K. Igarashi, M. Ikeda-Saito, Bach1, a heme-dependent transcription factor, reveals presence of multiple heme binding sites with distinct coordination structure. *IUBMB Life*. **59**, 542–551 (2007).

45. H. Nakajima, E. Nakagawa, K. Kobayashi, S. I. Tagawa, S. Aono, Ligand-switching Intermediates for the CO-sensing Transcriptional Activator CooA Measured by Pulse Radiolysis. *J. Biol. Chem.* **276**, 37895–37899 (2001).

46. T. L. Poulos, W. N. Lanzilotta, D. J. Schuller, M. V. Thorsteinsson, R. L. Kerby, G. P. Roberts, Structure of the CO sensing transcription activator CooA. *Nat. Struct. Biol.* **7**, 876–880 (2000).

47. C. Dycke, C. Bougault, J. Gaillard, J.-P. Andrieu, K. Pantopoulos, J.-M. Moulis, Human iron regulatory protein 2 is easily cleaved in its specific domain: consequences for the haem binding properties of the protein. *Biochem. J.* **408**, 429–439 (2007).

48. M. Watanabe-Matsui, T. Matsumoto, T. Matsui, M. Ikeda-Saito, A. Muto, K. Murayama, K. Igarashi, Heme binds to an intrinsically disordered region of Bach2 and alters its conformation. *Arch. Biochem. Biophys.* **565**, 25–31 (2015).

49. K. Iwai, S. K. Drake, N. B. Wehr, A. M. Weissman, T. Lavaute, N. Minato, R. D. Klausner, R. L. Levine, T. A. Rouault, Iron-dependent oxidation, ubiquitination, and degradation of iron regulatory protein 2: Implications for degradation of oxidized proteins. *Biochemistry*. **95**, 4924–4928 (1998).

CHAPTER III

FUNCTIONAL SIGNIFICANCE OF HEME BINDING IN IRON RESPONSE ELEMENT BINDING OF IRON REGULATORY PROTEINS

Abstract

In Chapter II, I clarified that IRP1 specifically binds heme as observed for IRP2, and the characteristic of heme environments of heme-bound IRP1 showed that the heme binding site was HRM (Cys-Pro), suggesting that heme binds to IRP1 as the signaling molecule for sensing the intracellular iron concentration status. Although the heme binding to IRP2 induces the oxidative modification and ubiquitin-mediated protein degradation to lose the IRE binding affinity, heme-bound IRP1 showed no oxidative modification and functional significance of heme binding to IRP1 is still unknown.

In Chapter III, to examine the functional significance of the heme binding in IRP1, I focused on the affinity of heme in IRP1. As previously reported, typical hemoproteins using heme as the active center, such as hemoglobin and P450, tightly bind heme to the protein, while "heme-regulated" proteins have relatively low heme binding affinity, which is supposed to facilitate the reversible heme binding in cells. Using various kinds of spectroscopies, I successfully determined the heme binding affinity of IRP1, showing that the affinity of heme in IRP1 is much lower than that of the prevalent hemoproteins, and rather close to that of the "heme-regulated" protein. To further confirm the heme binding as the signaling molecule for the IRE binding in IRP1, I followed the dissociation of IRE from the IRP1-IRE complex by the addition of heme using fluorescence anisotropy of the fluorescent-labelled IRE. As I expected, the addition of heme dissociated IRE from the IRP1 complex, but a large excess amount of heme was required for the dissociation, and it is highly unlikely that intracellular heme concentration, particularly free heme, would be so high to promote the dissociation. Although mechanisms for the heme-induced dissociation of IRE from the IRP1 complex are still controversial, it is clear that the heme binding to IRP1 facilitates the dissociation of IRE from the IRP1 complex, and I suppose that some specific heme carrier or heme chaperone proteins would transfer heme to IRP1 to dissociate IRE from the IRP1 complex.

3.1. Introduction.

In Chapter II, I clarified that IRP1 binds heme at the cysteine residue in the HRM as observed for IRP2, suggesting that IRP1 also utilize heme as the signaling molecule for sensing intracellular iron concentration. In IRP2, the heme binding is the trigger for the oxidation modification of the protein moiety of IRP2 and oxidized IRP2 is degraded by the ubiquitin-proteasome protein degradation system to lose the IRE binding affinity (1). Such heme-mediated oxidative modification was not reported in IRP1 and heme-mediated regulation of the IRE binding in IRP1 has not yet been confirmed. The functional significance of heme binding to IRP1 is, therefore, still unknown, although IRP1 can specifically bind heme at the cysteine residue in the HRM.

One of the characteristics of the heme binding in "heme-regulated" proteins is lower heme binding affinity (2). In conventional hemoproteins using heme as the active center, such as hemoglobin and P450 (3), they show very high heme binding affinity with smaller dissociation constant (K_d) for heme of less than 10^{12} M, while the heme binding affinity of the "heme-regulated" proteins such as HRI and Bach2 is much lower (K_d: ~10^7 M) to facilitate the reversible heme binding in cells (4–6). However, the heme binding affinity of IRP1 and heme-induced inhibition of the IRE binding in IRP1 have not yet been reported.

In Chapter III, to examine the functional significance of the heme binding to IRP1, I measured the heme binding affinity of IRP1 by using spectroscopies, and found that K_d for the heme binding in IRP1 was the range of 10^7 M, which was much lower than that of the typical hemoproteins, and rather close to that of the "heme-regulated" protein, supporting the heme binding as the signaling molecule in IRP1. I also successfully observed the dissociation of IRE from the IRP1-IRE complex by the addition of heme, suggesting a heme-mediated regulation of the IRE binding in IRP1. As previously reported, heme did not induce the oxidative modification of IRP1, which allows us to speculate a heme-mediated regulation mechanism for

the IRE binding without oxidative modification, but a large excess amount of heme was required for the dissociation. Based on the heme binding affinity of IRP1 and the heme-mediated IRE dissociation, I discus the functional significance of heme binding to IRP1 to dissociate IRE from the IRP1 complex and possibility that heme binds to IRP1 in cells.

3.2. Experimental Procedures.

3.2.1. Materials.

All chemicals were purchased from Wako Pure Chemical Industries (Osaka, Japan), Nacalai Tesque (Kyoto, Japan) or Sigma-Aldrich (St. Louis, MO, USA) were used without further purification.

3.2.2. Protein Expression and Purification.

The expression and purification of IRP1 and IRP2 are described in Chapter II. The purified IRP1 was concentrated to 5~10 μM using Vivaspin concentrators with 50 000 molecular-weight cutoff (Sartorius, Goettingen, Germany).

3.2.3. Fluorescence Anisotropy Measurements.

Human ferritin IRE (Figure 3.1A) (7–9), whose 5'-end is covalently bound to 6-FAM (Figure 3.1B), was purchased from Eurofins Genomics as HPLC grade. In this chapter, 6-FAM-labeled IRE is simply depicted as IRE. IRE was dissolved in 50 mM HEPES-NaOH and 100 mM NaCl (pH 7.4). After dissolving in the buffer, IRE was annealed by heating to 94 °C for 3 minutes with slow cooling to 25°C over 6 hours in a water bath. The prepared IRE was stored at -20 °C until use. Fluorescence anisotropy was recorded with a fluorometer FP-8500 (Jasco, Tokyo, Japan). The configuration for fluorescence anisotropy measurement is illustrated in Figure 3.1C. Fluorescence anisotropy *r* is defined as follows:

$$r = \frac{I_{VV} - G \cdot I_{VH}}{I_{VV} + 2G \cdot I_{VH}} \tag{3.1}$$

$$G = \frac{I_{HV}}{I_{HH}} \tag{3.2}$$

where *I* is the intensity of fluorescence with two letters of subscript indicating the directions of excitation and emission polarized lights. "V" and "H" in the eqations represent vertical and

horizontal, respectively. For example, I_{VH} is depicted for the fluorescence intensities by passing through vertical-polarized excitation and horizontal-polarized emission light. The instrumental function, *G*, is used to calibrate the detector sensitivity between the vertical and horizontal light. The *G* value was calculated using Equation 3.2 by the measurement for a buffer containing 1 nM IRE. The concentrations of IRE for titration by IRP1 and IRP2 were 1 nM. To examine the effect of heme on the IRE-binding, IRPs were mixed with heme for approximately 15 minutes prior to the addition of IRE. The excitation and emission wavelengths were 495 and 515 nm, respectively. Each data point represented the integration of five consecutive measurements. A plot of fluorescence anisotropy, *r*, versus protein concentrations, *x*, was analyzed using the Hill equation as follows:

$$r = a + \frac{b - a}{1 + (K_d / x)^n} \tag{3.3}$$

where *a* is the minimum anisotropy difference, *b* is the maximum anisotropy difference, *n* is Hill coefficient and K_d is the dissociation constant. All instruments were treated with RNase remover (RNase ZAP, Ambion, TX, USA) to remove the contamination of RNase, and all buffers were sterilized by 0.2 μm filter.

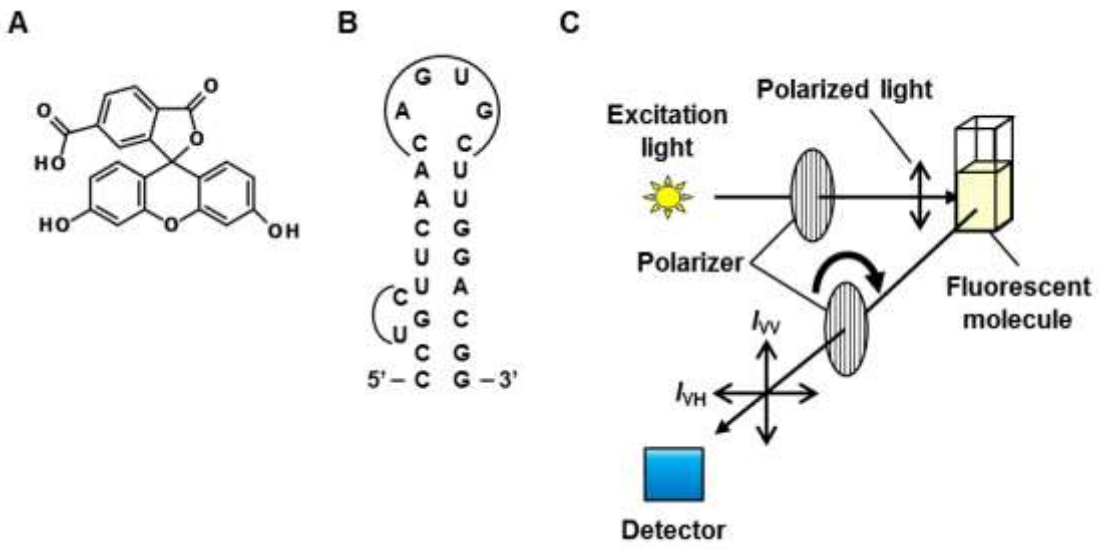

Figure 3.1 Outline of fluorescence anisotropy measurement.

(A) Structure of fluorescent molecule, 6-carboxyfluorescein, termed 6-FAM, conjugated to the 5'-end of IRE. (B) Schematic secondary structure of human ferritin IRE. IRE was composed of a hairpin hexaloop (CAGUGC), stems, and internal loop/bulge (CGU). (C) Schematic representation of apparatus of fluorescence anisotropy. Both excited and emission lights pass through the polarizer.

3.2.4. Dissociation Rate Constant of IRP1.

The dissociation rate constant measurements were made in a 0.5-mL reaction mixture containing 2 μM heme-IRP1 and 20 μM apo-myoglobin in 50 mM Tris-HCl and 100 mM NaCl (pH 7.4) at 5 °C. Apo-myoglobin was prepared by extracting heme from equine skeletal muscle myoglobin using the acid/methylethylketone method (12). The Soret peak of myoglobin (408 nm) was traced using a JASCO V-660 UV-vis absorption spectrophotometer. The dissociation rate (k_{off}) of heme was calculated by fitting the data to a double-exponential (Equation 3.4) equation using Igor Pro (WaveMetrics, Portland, OR, USA) as follows:

$$A_t = A_0 + A_1 \exp(-k_{off,1}t) + A_2 \exp(-k_{off,2}t) \quad (3.4)$$

where A_0 is the initial absorbance, A_1 and A_2 are the proportional constants and k_{off} is the dissociation rate constants (s^{-1}).

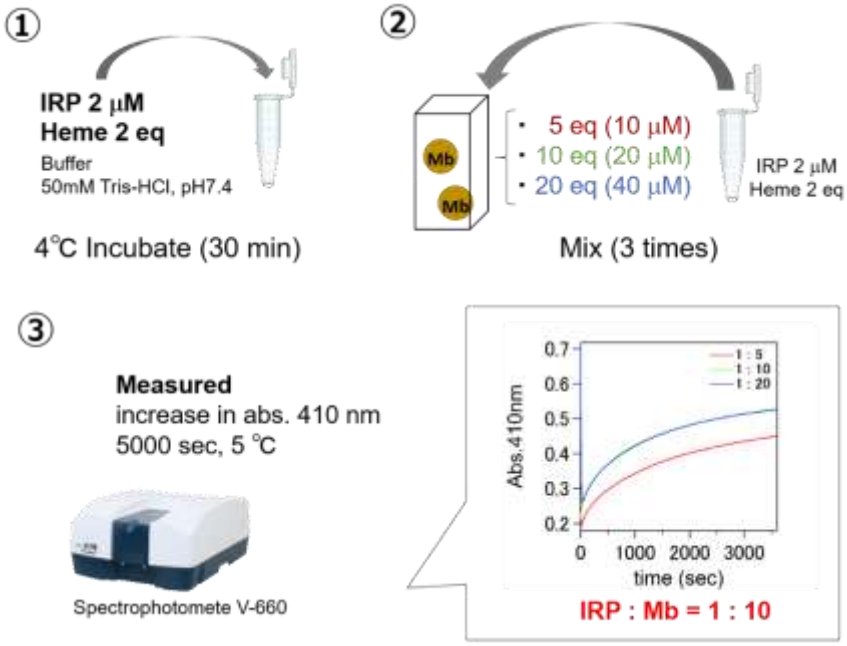

Figure 3.2 Determined of the dissociation rate constants of IRP1 using apo-myoglobin.
The dissociation rate constants measurements were made in a 0.5-mL reaction mixture containing 2 μM heme-IRP1 and 20 μM apo-myoglobin in 50 mM Tris-HCl and 100 mM NaCl (pH 7.4) at 5 °C. The Soret peak of myoglobin (408 nm) was traced, and the increase in the absorbance at 408 nm was plotted against time.

3.2.5. Measurements of the Heme Binding Affinity of IRP1 Using SPR.

The interaction between IRP1 and heme was examined by surface plasmon resonance measurements using a Biacore T200 (GE Healthcare). In Figure 3.3, GST-tagged IRP1 was immobilized on a sensor chip CM5. The sensor chip was activated by injection of 15 μM EDC and NHS buffer for 3 min, and then IRP1 (1 μM) in HBS-P buffer (10 mM Hepes, 150 mM NaCl, 0.005% (v/v) Surfactant P20, pH 7.4) was passed over the chip at flow rate of 10 μL/min for 26 min. The solution of heme was prepared in 0.1M NaOH. Heme of 0.0137–1.11 μM were passed over the sensor chip for a 700 sec association, followed by a 1000 sec dissociation at 4 °C. The chip was regenerated with 10 mM glycine-HCl (pH 2.1) for 2 min. Data were fit to a 1:1 binding model, produced a less random residual contribution than the other binding models, using the BIAevaluation software provided by Biacore.

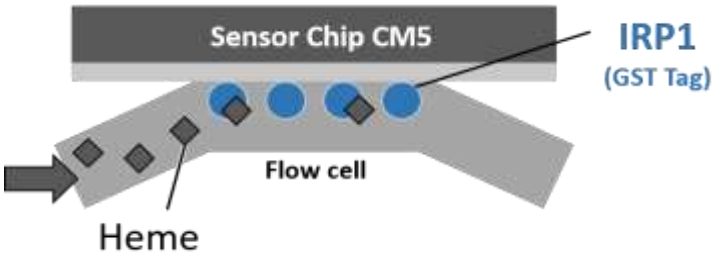

Figure 3.3 Outline of Surface Plasmon Resonance.
GST-tagged IRP1 was immobilized on a sensor chip CM5. The sensor chip was activated by injection of 15 μM EDC and NHS buffer for 3 min, and then IRP1 (1000 nM) in HBS-P buffer (10 mM Hepes, 150 mM NaCl, 0.005% (v/v) Surfactant P20, pH 7.4) was passed over the chip at flow rate of 10 μL/min for 26 min. The solution of heme was prepared in 0.1 M NaOH. Heme was passed over the sensor chip at 4°C.

3.3. Results.

3.3.1. Heme-Binding Kinetics of IRP1.

To determine the heme binding affinity of IRP1, surface plasmon resonance (SPR) analysis was utilized. Surface plasmon resonance (SPR) allows real-time, label-free detection of biomolecular interactions (Figure 3.3) to estimate the association and dissociation rates for the complex formation (5). The change of molecular weight due to the heme binding and the dissociation of heme from the IRP1-IRE complex was recorded in real time. In Chapter II, IRP1 binds to heme with a stoichiometry of 1:2, but, as shown in Figure 3.4, the heme association/dissociation kinetics fits well to a 1:1 binding model, suggesting that two binding site were similar to the heme environmental structures. I calculated association (k_{on}) and dissociation (k_{off}) rate constants from the SPR data and the K_d value was estimated by these rate constants, as summarized in Table 3.1. The association and dissociation rate constants are 2.8×10^3 $M^{-1}s^{-1}$ and 1.3×10^{-3} s^{-1}, respectively, and K_d of the heme binding to IRP1 was determined as 4.7×10^{-7} M, which are close to that of HRI and Bach2 rather than hemoglobin (Table 3.1). Hemoglobin using heme as the active center tightly binds heme to transport oxygen, while "heme-regulated" proteins such as HRI and Bach2 have relatively low heme binding affinity to sense the heme as the signaling molecule in the cells. The heme binding affinity of IRP1 supports the idea that the heme functions as the signaling molecule for IRP1.

I measured the heme dissociation rate using the heme transfer reaction from heme-bound IRP1 to apo-myoglobin with very high heme binding affinity. I mixed the IRP1-heme complex with a 10-fold excess of apo-myoglobin and then monitored changes in the absorption spectra. The increase in the absorbance at 408 nm, indicating the formation of myoglobin, was plotted against time (Figure 3.5). The heme dissociation kinetics fit best to a double exponential equation, yielding dissociation rate constants for IRP1 of $k_{off\text{-}slow,1} = 3.4 \times 10^{-4}$ s^{-1} (about 66%) and $k_{off\text{-}fast,2} = 3.3 \times 10^{-3}$ s^{-1} (about 34%) (Table 3.2). The fast phase makes up 34% of the total

absorbance change, indicating that the second slower phase is the major component for the heme dissociation from heme-bound IRP1. $k_{off\text{-}slow}$ of IRP1 was also comparable to that of HRI and Bach2, suggesting that IRP1 binds heme as the signaling molecule.

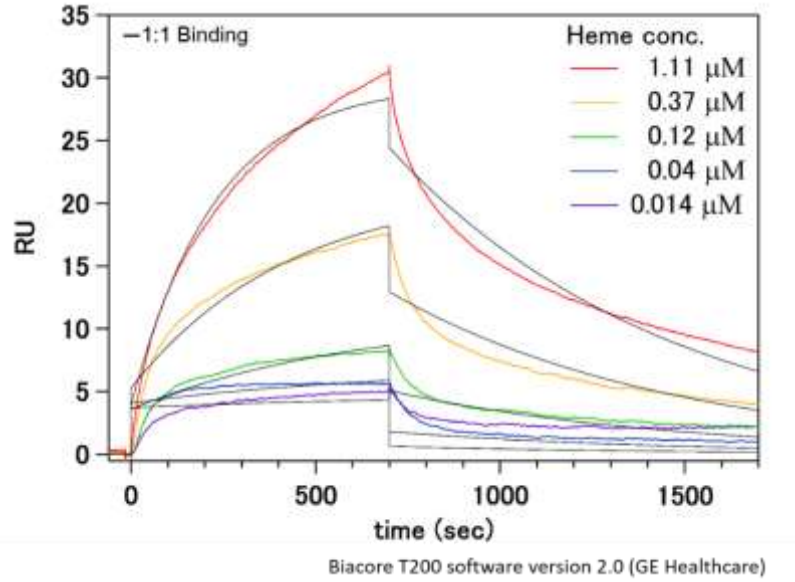

Figure 3.4 Kinetic analysis of IRP1 interactions with heme examined by surface plasmon resonance.

Heme samples were injected over GST immobilized apo-IRP1 at five concentrations (0.014, 0.04, 0.12, 0.37, and 1.11 μM). The heme concentration was adjusted below 1.11 μM to suppress the nonspecific heme binding.

Table 3.1 Comparison of the dissociation constants (K_d) with other hemoproteins.

Protein	K_d (M)	k_{on} ($M^{-1}s^{-1}$)	k_{off} (s^{-1})	Reference
IRP1	4.7×10^{-7}	2.8×10^{3}	1.3×10^{-3}	This study
hemoglobin	2.5×10^{-13}	2.9×10^{7}	7.1×10^{-6}	(3)
HRI	1.4×10^{-10}	1.1×10^{7}	1.5×10^{-3}	(4)
Bach2	1.7×10^{-7}	2.8×10^{4}	4.6×10^{-3}	(5)

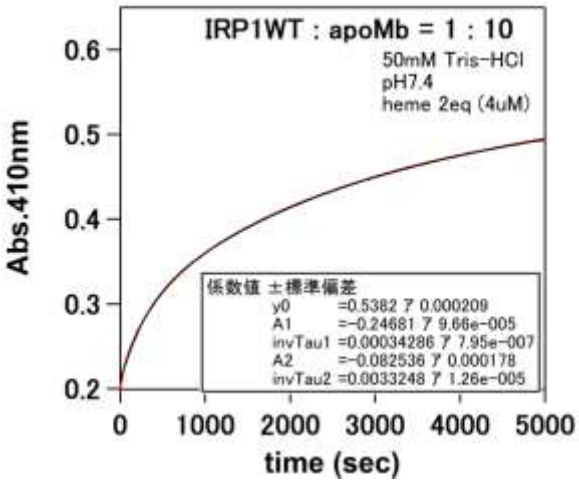

Figure 3.5 Time course of the displacement of hemin from heme-IRP1 to apo-myoglobin.

Time course of the transfer of hemin from heme-IRP1 to apo-myoglobin, measured as the change in the absorption at 408 nm. Dissociation rate constants were calculated by both double-exponential (red line) equations. Spectra were measured at 5-minutes intervals over a period of 5000 sec.

Table 3.2 Heme dissociation rates for IRP1 using apo-myoglobin.

Protein	$k_{off,slow}$ (s^{-1})	$k_{off,fast}$ (s^{-1})	Reference
IRP1	3.4×10^{-4}	3.3×10^{-3}	This study

Rate constants calculated assuming a double-exponential equation (Eq. 3.4)

3.3.2. Detection of Complex Formation by Fluorescence Anisotropy.

To investigate the heme-mediated regulation of the IRE binding in IRP1, I followed the change of the fluorescence anisotropy of the IRP1- fluorescent-labelled IRE complex by the addition of heme. The differences of anisotropy (Δr) were obtained by the comparison of the anisotropy between free IRE and the IRP1-IRE complex as shown in Figure 3.6. The value of Δr is related to the remaining polarization of the fluorescence shown in Equation 3.4, reflecting speed of the Brownian motion of IRE. When the Brownian motion of the fluorescent-labelled IRE becomes fast associated with the dissociation of a complex, the polarization in the fluorescence intensity is reduced, leading to the decreased value of Δr. Thus, the decrease in Δr corresponds to the dissociation of IRE from the IRP1-IRE complex.

In Figure 3.6, the addition of heme dissociated IRE from the IRP1-IRE complex, but a large excess amount of heme was required for the dissociation. Although a large excess amount of heme was required for the dissociation, it was clear that the IRP2-IRE complex was dissociated, as the heme concentration in the solution was increased (Figure 3.7). The results indicate that the heme binding to IRP1 facilitates the dissociation of IRE from the IRP1 complex.

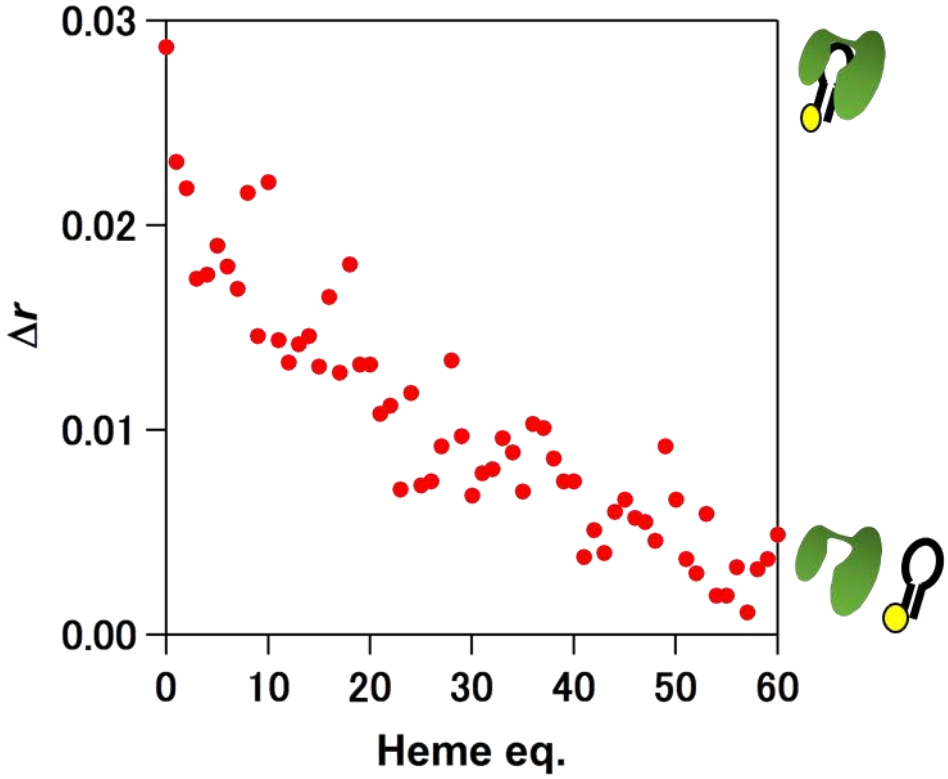

Figure 3.6 Fluorescence anisotropy measurement following titration of heme to IRP1-IRE complex.

Fluorescence anisotropy (Δr) measurements for the detection of interactions between IRP1 and IRE with heme. The fluorescence was measured following the titration of heme to the IRP1-IRE complex in 50 mM HEPES-NaOH and 100 mM NaCl (pH 7.4). The excitation and emission wavelength were 495 and 515 nm, respectively.

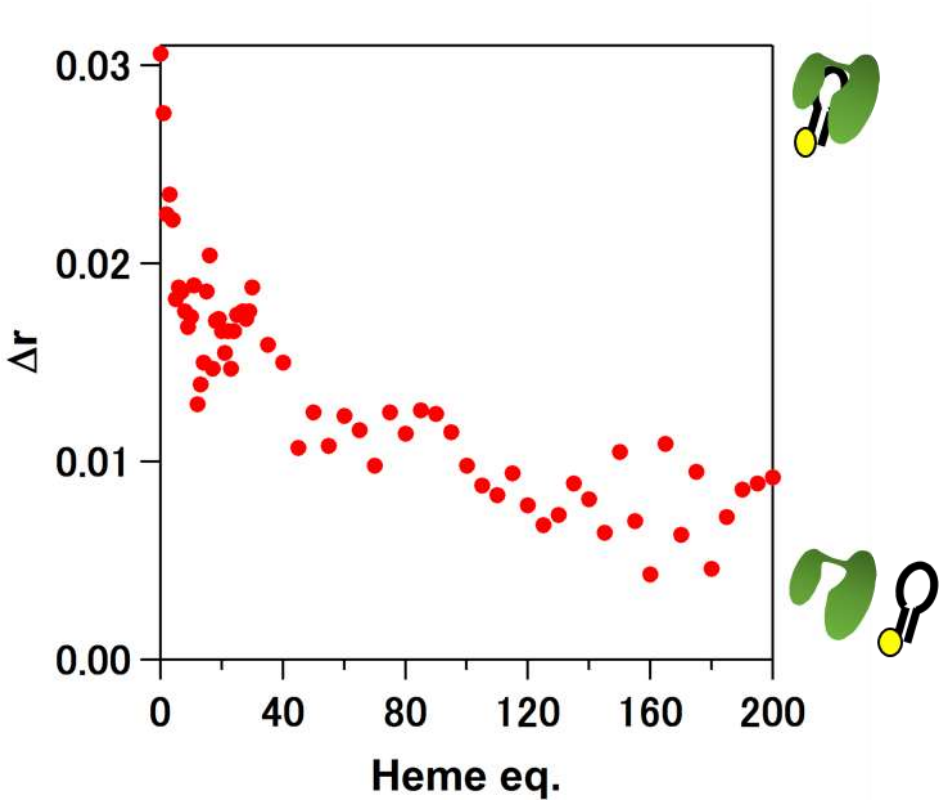

Figure 3.7 Fluorescence anisotropy measurement following titration of heme to IRP2-IRE complex.

Fluorescence anisotropy (Δr) measurements for the detection of interactions between IRP2 and IRE with heme. The fluorescence was measured following the titration of heme to the IRP2-IRE complex in 50 mM HEPES-NaOH and 100 mM NaCl (pH 7.4). The excitation and emission wavelength were 495 and 515 nm, respectively.

3.4. Discussion

3.4.1. Heme-Induced Complex Dissociation in the IRP-IRE Complex.

In this chapter, to clarify the functional significance of the heme binding to IRP1, I measured the heme binding affinity of IRP1, and dissociation of IRE from the IRP1-IRE complex by the addition of heme. The heme binding affinity of IRP1 (K_d = 4.7 ×10^{-7} M) was lower about 10^6 than that of hemoglobin, and close to that of HRI and Bach2 (~10^{-7}) (Table 3.1), due to the large k_{off} value for IRP1 close to that of HRI and Bach2. These results suggest that IRP1 can reversibly binds heme in responses to the heme concentration in cells, since relatively weak binding of heme is important to act as a trigger for "heme regulated" proteins (10). The k_{on} value for IRP1 was different from that of HRI, and the heme association rate with IRP1 was slower about 10^4, compared with those of HRI and hemoglobin. However, the k_{on} value for IRP1 was close to that of the other "heme regulated" protein, Bach2. Although it is not clear the localization and concentration of heme in cells, different k_{on} may be due to the heterogeneity of the heme concentration and these "heme regulated" proteins in cells.

In the dissociation measurements of IRE from the IRP1-IRE complex by the heme binding, the apparent dissociation constant of heme for IRP1-IRE complex was estimated to be approximately 1.5 × 10^{-5} M, which is ~ 30-fold higher than that for IRP1 (Table 3.1), indicating that the heme binding affinity is lower than that in the absence of IRE. The IRE-binding activity for IRP1 is inhibited by the heme binding competitively, and IRE-binding activity of IRP1 was suppressed in a heme-dependent manner. However, a large excess amount of heme was required for the dissociation. Although the intracellular heme concentration is not yet been determined, the heme concentration, particularly free heme, would not be so high to promote such dissociation of IRE from the complex (11). I, therefore, suspect that IRP1 dissociates IRE from the IRP1-IRE complex by transferring heme from some specific heme carrier or heme chaperone proteins, which are still unidentified.

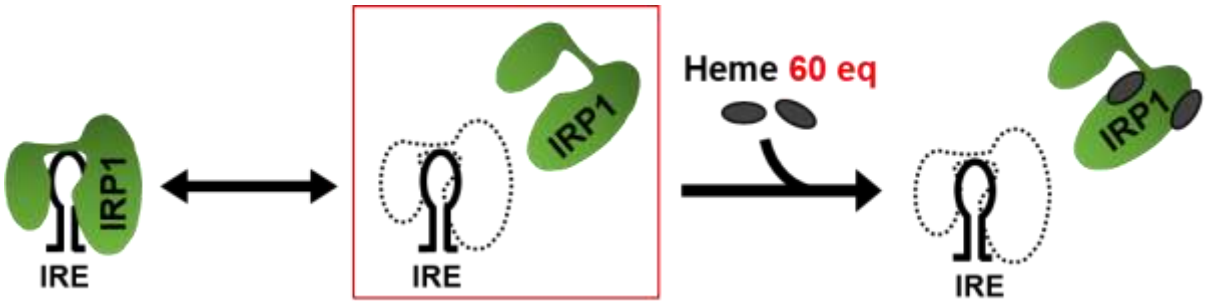

Figure 3.8 The heme-induced IRP1-IRE complex dissociation.

The heme-induced complex dissociation was clearly observed. However large excess amount of heme was required for the dissociation.

References.

1. K. Yamanaka, H. Ishikawa, Y. Megumi, F. Tokunaga, M. Kanie, T. A. Rouault, I. Morishima, N. Minato, K. Ishimori, K. Iwai, Identification of the ubiquitin–protein ligase that recognizes oxidized IRP2. *Nat. Cell Biol.* **5**, 336–340 (2003).
2. H. M. Girvan, A. W. Munro, Heme sensor proteins. *J. Biol. Chem.* **288**, 13194–13203 (2013).
3. M. S. Hargrove, D. Barrick, J. S. Olson, The association rate constant for heme binding to globin is independent of protein structure. *Biochemistry*. **35**, 11293–11299 (1996).
4. M. Miksanova, J. Igarashi, M. Minami, I. Sagami, S. Yamauchi, H. Kurokawa, T. Shimizu, Characterization of heme-regulated eIF2α kinase: Roles of the N-terminal domain in the oligomeric state, heme binding, catalysis, and inhibition. *Biochemistry*. **45**, 9894–9905 (2006).
5. T. Suenaga, M. Watanabe-Matsui, T. Uejima, H. Shima, T. Matsui, M. Ikeda-Saito, M. Shirouzu, K. Igarashi, K. Murayama, Charge-state-distribution analysis of Bach2 intrinsically disordered heme binding region. *J. Biochem.* **160**, 291–298 (2016).
6. M. Watanabe-Matsui, T. Matsumoto, T. Matsui, M. Ikeda-Saito, A. Muto, K. Murayama, K. Igarashi, Heme binds to an intrinsically disordered region of Bach2 and alters its conformation. *Arch. Biochem. Biophys.* **565**, 25–31 (2015).
7. N. Aziz, H. N. Munro, Iron regulates ferritin mRNA translation through a segment of its 5’ untranslated region. *Proc. Natl. Acad. Sci. U. S. A.* **84**, 8478–8482 (1987).
8. M. W. Hentze, S. W. Caughman, T. A. Rouault, J. G. Barriocanal, A. Dancis, J. B. Harford, R. D. Klausner, Identification of the iron-responsive element for the translational regulation of human ferritin mRNA. *Science*. **238**, 1570–1573 (1987).
9. M. W. Hentze, T. A. Rouault, S. W. Caughman, A. Dancis, J. B. Harford, R. D. Klausner, A cis-acting element is necessary and sufficient for translational regulation of human ferritin expression in response to iron. *Proc. Natl. Acad. Sci. U. S. A.* **84**, 6730–6734 (1987).
10. T. Shimizu, Binding of cysteine thiolate to the Fe(III) heme complex is critical for the function of heme sensor proteins. *J. Inorg. Biochem.* **108**, 171–177 (2012).
11. A. A. Khan, J. G. Quigley, Control of intracellular heme levels: Heme transporters and heme oxygenases. *Biochim. Biophys. Acta - Mol. Cell Res.* **1813**, 668–682 (2011).

CHAPTER IV

STRUCTURAL CHARACTERIZATION OF HEME-DEPENDENT REGULATION MECHANISM OF IRON RESPONSE ELEMENT BINDING IN IRON REGULATORY PROTEIN 1.

Abstract

In Chapters II and III, I structurally and functionally characterized the heme binding in IRP1 and revealed that the heme environmental structures of heme-bound IRP1 are quite similar to that of heme-bound IRP2 and other "heme-regulated" proteins such as Irr, suggesting that IRP1 binds heme as the signaling molecule for the intracellular iron concentration. The heme binding affinity of IRP1 was significantly lower than those of the conventional hemoproteins using heme as the active center, but close to those of the "heme-regulated" proteins, supporting the function of heme as the signaling molecule for IRP1. Further experimental evidence for the heme binding as the signaling molecule in IRP1 was the heme-induced dissociation of IRE from the IRP1-IRE complex. However, heme-induced dissociation of IRE from the IRP complex required a large excess amount of heme, which is much higher concentration than that we expect in cells. The heme-dependent regulation for the IRE binding in IRP1 is, therefore, still unclear.

In this chapter, to structurally examine the heme-dependent regulation mechanism for the IRE binding in IRP1, I solved the crystal structure of IRP1 in the complex with heme. Diffraction data of the IRP1-heme complex was 2.3 Å resolution. Unexpectedly, the crystal structure clarified that IRP1 binds heme to ^{506}Cys in HRM (Cys-Ile), not a cysteine residue in HRM (Cys-Pro). However, ^{506}Cys is located in the cleft region in IRP1, where IRE binds to form the IRP1-IRE complex, and the crystal structure of the IRP1-heme complex was in a "closed" conformation that does not allow access of IRE to the IRE binding site. The conformational changes by heme binding to IRP1, therefore, inhibit the IRE binding to IRP1. Based on the structural information from the crystal structure, I proposed a mechanism of the heme-regulated IRE binding regulation in IRP1, which would be one of the crucial steps for sensing cellular iron concentration to maintain iron homeostasis in cells.

4.1. Introduction.

In Chapter II, I structurally characterized the heme binding to IRP1 and spectroscopically confirmed that IRP1 specifically binds heme, and the heme environments structure was characteristic of the ligation of the cysteine residue in HRM, as observed for other "heme-regulated" protein, suggesting that the heme binds to IRP1 as the signaling molecule for sensing iron concentration in cells. In Chapter III, I functionally characterized the heme binding in IRP1 by estimating the heme binding affinity of IRPs. The heme binding affinity of IRP1 was much lower than those of the conventional hemoproteins binding heme as the active center, but it was rather close to those of "heme-regulated" proteins, supporting the binding of heme as the signaling molecule for IRP. I also confirmed the heme-induced dissociation of heme from the IRP1-IRE complex in the presence of high concentration of heme. However, the dissociation of IRE from the IRP-IRE complex required a large excess amount of heme, which is much higher concentration than that we expect in cells. The regulation of the heme-induced association/dissociation between IRP1 and IRE is, therefore, still unclear.

In this Chapter IV, to structurally characterize the heme binding in IRP1 and get structural insight into the heme-regulated IRE binding in IRP1, I solved the crystal structure of the complex of IRP1 with heme and compare with the structure of the IRP1-IRE complex in the absence of heme. I successfully crystallized the complex of IRP1 with heme and the crystal structure was obtained. The crystal structure of the IRP1-heme complex and the comparison with the structure of the IRP1-IRE complex in the absence of heme showed that the heme binding to IRP1 drastically changed relative positions of the domains to form a "closed" conformation that does not allow access of IRE to the binding site of IRE. Based on the structural information from the structure of heme-bound IRP1 and other structural data discussed in the previous chapters, I will propose a mechanism for the heme-regulated IRE binding in IRP1, which is definitely different from that in IRP2 and a novel mechanism utilizing

heme as the signaling molecule for sensing intracellular iron concentration essential to maintain iron homeostasis in cells.

4.2. Experimental Procedures.

4.2.1. Materials.

All chemicals were purchased from Thermo Scientific (Waltham, MA, USA), Nacalai Tesque (Kyoto, Japan), or Sigma-Aldrich (St. Louis, MO, USA) and used without further purification, Hampton research (Aliso Viejo, CA, USA).

4.2.2. Protein Expression and Purification.

The protein expression and purification of IRP1 are described in Chapter II. The sample was applied to a HiLoad 16/600 Superdex 200 preparatory grade gel-filtration column (GE Healthcare) pre-equilibrated with 50 mM Tris-HCl and 100 mM NaCl/10% Glycerol (pH 7.4). The purified IRP1 was concentrated to 80~170 μM using Vivaspin concentrators with 50 kDa molecular-weight cutoff (Sartorius).

4.2.3. Absorption Spectroscopy.

The procedures for the sample preparations and spectroscopic measurements are followed by those described in Chapter II.

4.3. Results.

4.3.1. Expression, Purification and Construction of IRP1.

The purified IRP1 protein was estimated to be ~95% pure by SDS-PAGE (Figure 4.1). An apparent molecular mass of 98 kDa for purified IRP1, which contains 889 amino acid residues, was consistent with a calculated molecular mass of 98,399 Da. A major peak on the size-exclusion chromatogram was detected at the elution volume of 70.2 mL (Figure 4.2), indicating that IRP1 was purified as monomer.

Size-exclusion chromatography showed a broad peak, suggesting that wild type IRP1 (IRP1 WT) was not homogeneous (Figure 4.2) and, aggregation might be induced at higher concentrations, while a sharp peak in the chromatography was observed for purified His-tag attached IRP1, compared to that for the intact protein without His-tag, and the attachment of the His-tag improved the homogeneity of the protein (Figure 4.3). However, the Soret absorption maximum of ferric heme-bound His-tagged IRP1 appeared at 418 nm, not at 372 nm, which was significantly different from that of the intact protein. The heme environmental structures of His-tagged IRP1 are, therefore, substantially perturbed by the addition of the His-tag at the N-terminal (Figure 4.5).

To increase the amount of homogeneous IRP1, I introduced the mutations which did not affect the heme binding of IRP to suppress the protein oxidation and improve the homogeneity as previously reported, enabling single crystal growth of the IRP1-IRE complex (8). The IRP mutant having the mutations at ^{437}Cys and ^{503}Cys were mutated Ser (IRP1C437S/C503S) retained the heme binding activity as found for IRP WT (Figure 4.6), and IRP1C437S/C503S showed no heterogeneity (Figure 4.7 B). In addition, Flag tag used for the Baculoviruses expression system was not so bulky to interrupt the protein packing in the crystals (Figures 4.4, 4.7 C, D). The constructs of the proteins for the crystallization are shown in Figure 4.8-9.

The IRP1C437S/C503S and IRP1 with Flag-tag were expressed in a soluble form in the baculovirus-infected insect cell system and was purified to homogeneity by Ni affinity and gel filtration chromatography. The pattern of SDS–PAGE showed a single band and the molecular weight was approximately 100 kDa, which is in agreement with the predicted molecular weight of IRP1, 98 kDa. The purified IRP1 protein was estimated to be ~95% pure by SDS-PAGE. The yield of purified IRP1 was 16.0~17.0 mg from 600 mL of High Five culture.

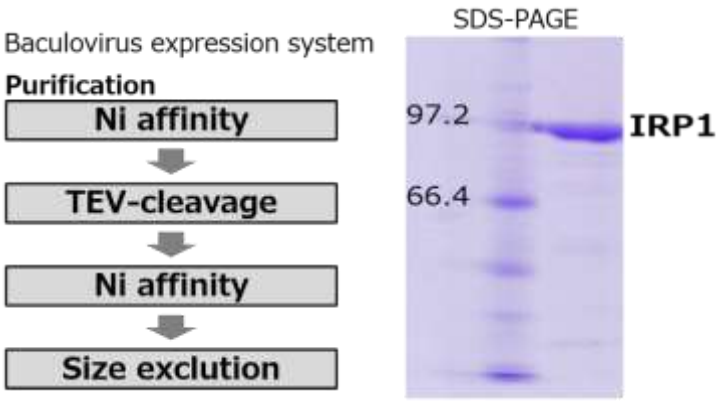

Figure 4.1 SDS-PAGE of IRP1.
SDS-PAGE of IRP1 stained with CBB Stain One. Lane 1: molecular mass marker, Lane 2: IRP1 purified by size-exclusion chromatography

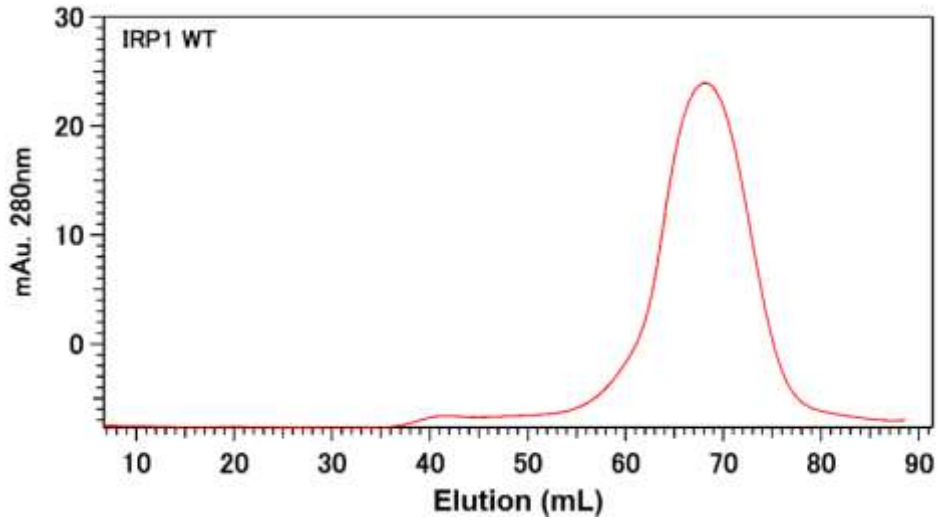

Figure 4.2 Size-exclusion chromatography of IRP1 WT.

Profile of IRP1 on a gel-filtration column (HiLoad 10/600 Superdex 200 pg) pre-equilibrated with 50 mM HEPES-NaOH/100 mM NaCl (pH 7.4). Analytical gel filtration was performed using a Superdex 200 pg column with a flow rate of 1 mL/min.

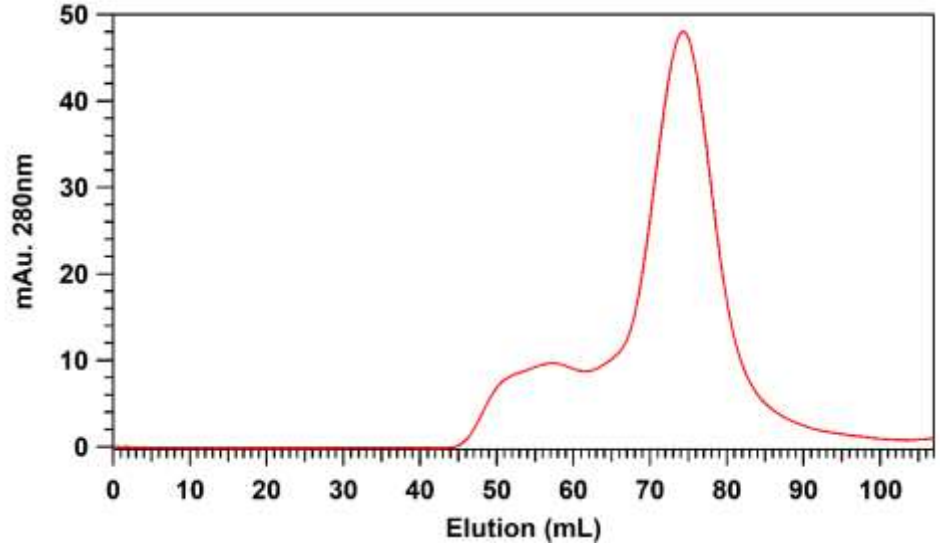

Figure 4.3 Size-exclusion chromatography of His Tag-IRP1 WT.

Profile of His Tag-IRP1 on a gel-filtration column (HiLoad 10/600 Superdex 200 pg) pre-equilibrated with 50 mM HEPES-NaOH/100 mM NaCl (pH 7.4). Analytical gel filtration was performed using a Superdex 200 pg column with a flow rate of 1 mL/min.

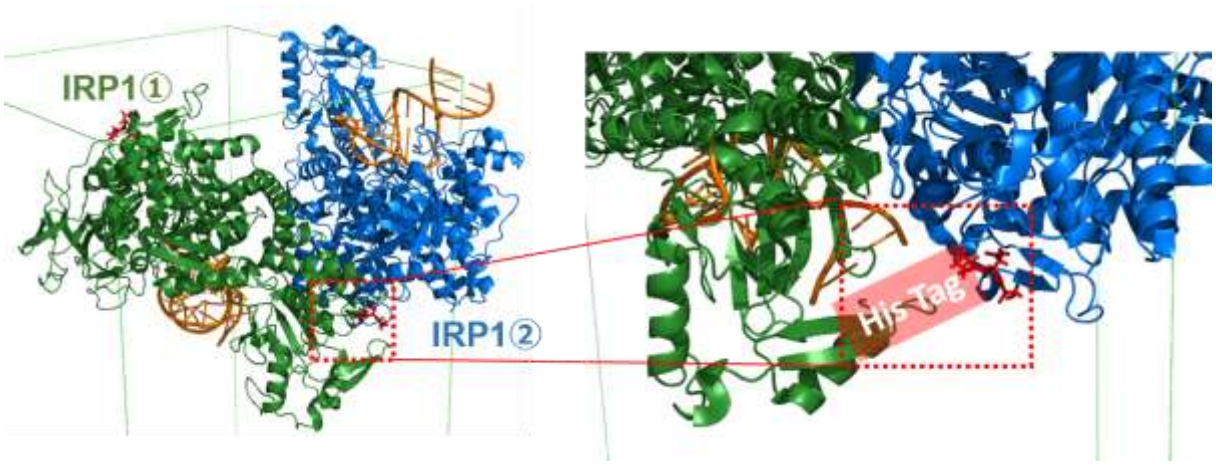

Figure 4.4 Crystal structure of IRP1-IRE complex with His-tag (PDB : 3NSP).

The length of His-tag (red) may be involved in the crystal packing of the IRP1-IRE complex.

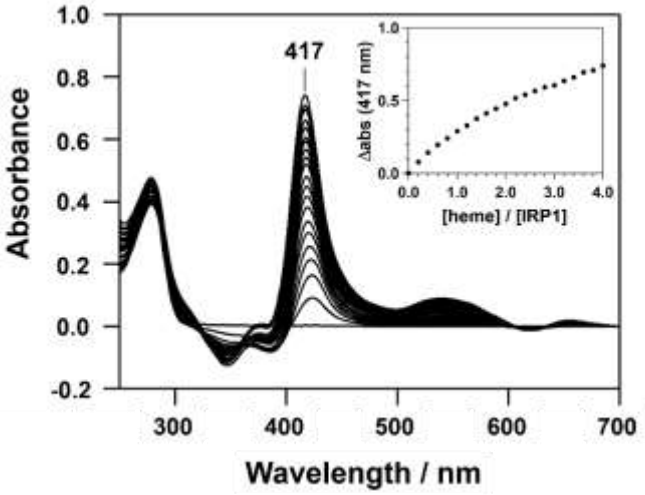

Figure 4.5 Absorption spectrum and titration curve of His Tag-IRP1 WT.

Absorption difference spectra of the heme binding to IRP1. Absorption difference spectra of heme binding to IRP1 were measure by following stepwise addition of heme (1 – 20 μM) to IRP1 (5 μM) versus buffer blank in 50 mM Tris-HCl and 100 mM NaCl at pH 7.4. Inset: Absorbance difference at 417 nm as a function of heme concentrations.

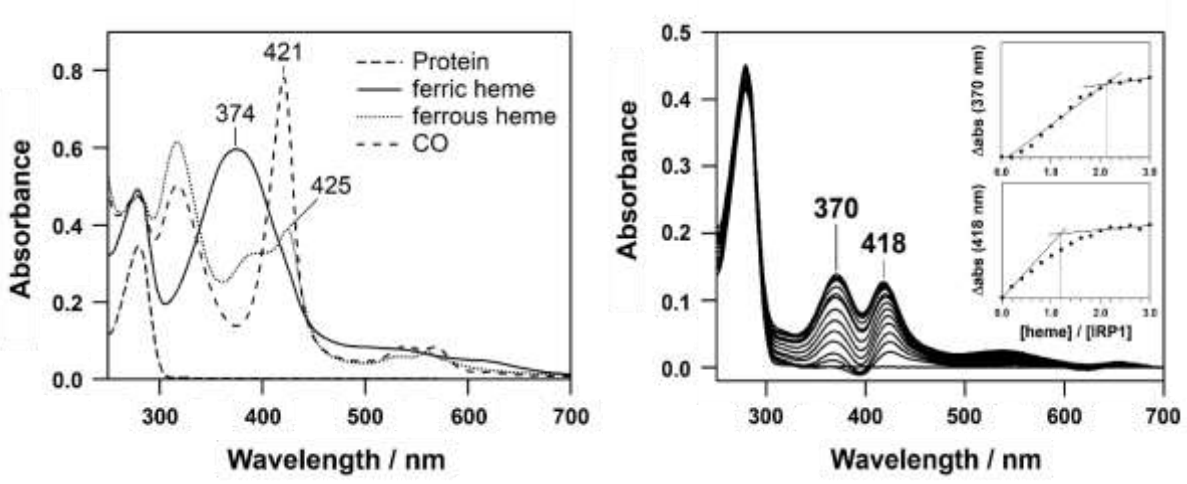

Figure 4.6 Absorption spectra and titration curves of IRP1 C437S/C503S.

Left: Solid, dotted and dashed lines represent the ferric heme-bound, ferrous heme-bound, and CO adducts of reduced heme-bound IRP1, respectively. Right: Absorption difference spectra of the heme binding to IRP1. Absorption difference spectra of the heme binding to IRP1 following stepwise addition of heme (1 – 15 μM) to PRX1 (5 μM) versus buffer blank in 50 mM Tris-HCl and 100 mM NaCl at pH 7.4. (Inset): Heme titration of IRPs was followed by measurements of the absorbance at 370 nm and 418 nm.

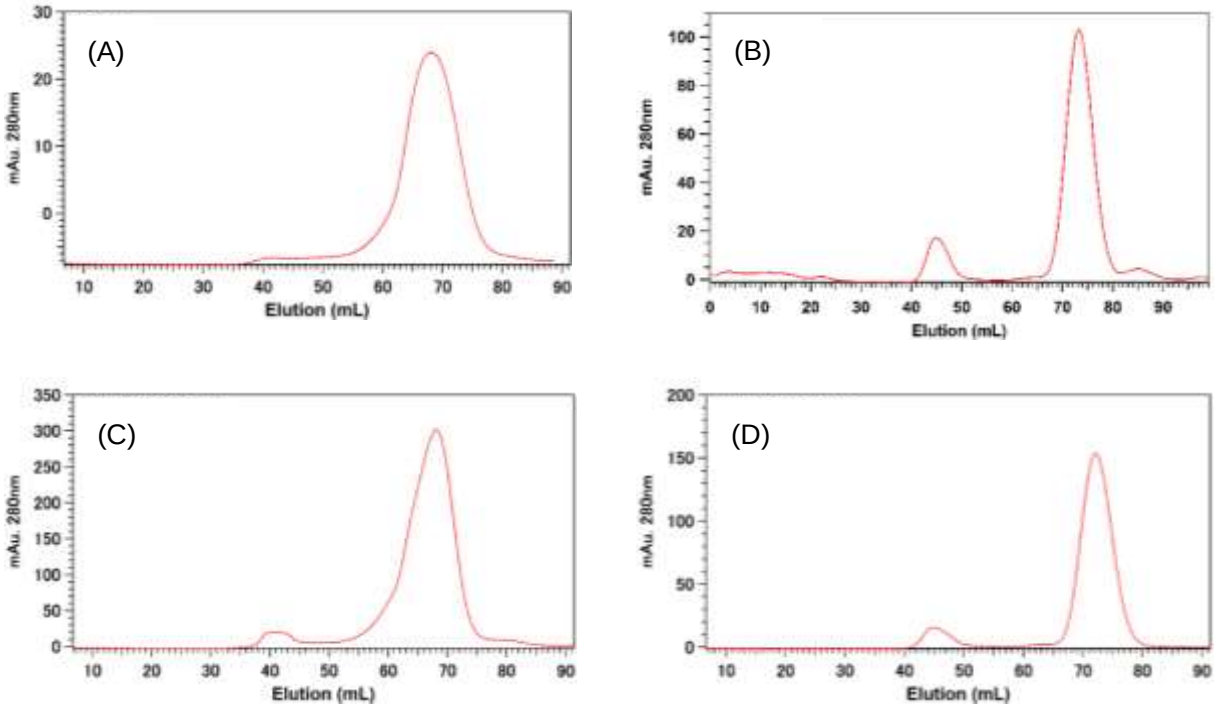

Figure 4.7 Size-exclusion chromatography of IRP1.

Profile of IRP1 WT (A), IRP1 C437S/C503S (B), IRP1 N-terminal Flag tag (C) and IRP1 C437S/C503S N-terminal Flag tag (D) on a gel-filtration column (HiLoad 10/600 Superdex 200 pg) pre-equilibrated with 50 mM Tris-HCl and 100 mM NaCl at pH 7.4. Analytical gel filtration was performed using a Superdex 200 pg 16/60 column with a flow rate of 1 mL/min.

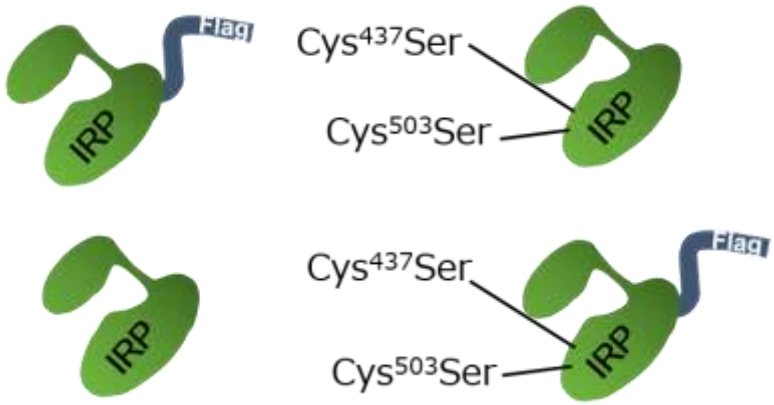

Figure 4.8 Constructs of IRP1 for Crystallization.

N-terminal Flag Tag IRP1: Constructs of IRP1 with Flag-tag at the N-terminus. IRP1 C437S/C503S: Cys/Ser double mutant. IRP1 WT: Wild type. N-terminal Flag Tag IRP1 C437S/C503S: Constructs of IRP1 with Flag-tag at the N-terminus and Cys/Ser double mutant.

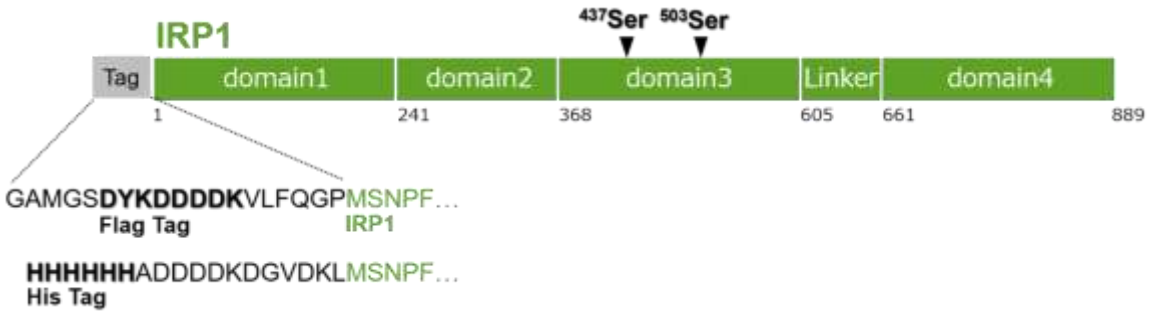

Figure 4.9 The position of construct design for Crystallization for IRP1.

Designs of IRP1 constructs with Flag-tag at the N-terminus and/or Cys/Ser double mutant.

4.3.2. Screening of Crystallization Conditions.

Initial attempts to crystallize the IRP1-heme complex were performed with wild-type IRP1 fused with Flag-Tag and its mutant (Figure 4.10). IRP1 and heme (2.68 mM of heme was dissolved in 0.1 M NaOH) were combined in 1:2.4 molar ratios and incubated on ice for 30 minutes ~1 hour. Crystallization conditions of the proteins were screened by sitting-drop vapor diffusion method. 0.4 μL crystallization drops composed of 0.2 μL protein solution and 0.2 μL reservoir solution were made on siliconized cover slide glass (HR8-090, Hampton reseach) and vapor equilibrated to 150 μL reservoir solutions on 48 well plate (HR3-275, Hampton research). Initial screening of crystallization conditions was carried out with several commercially available screening kits (Crystal Screen 1 and 2, PEG/Ion Screen [Hampton research], Wizard 1, 2, 3 and 4 [Emerald BioSystems]) at 277 K or 293 K. As a result, protein crystals of IRP1 C437S/C503S was obtained (Figure 4.11). The IRP1 C437S/C503S-heme complex formed clusters of needles after two weeks in the following two conditions, (a) Crystal screen Ⅰ No. 38 : 0.1 M HEPES sodium pH 7.5, 1.4 M sodium citrate tribasic dehydrate, and (b) Crystal screen II No. 28 : 1.6 M sodium citrate tribasic dehydrate pH 6.5. Other construction of IRP1 failed to give crystals under the same conditions, as well as under any conditions attempted (Figures 4.12-13).

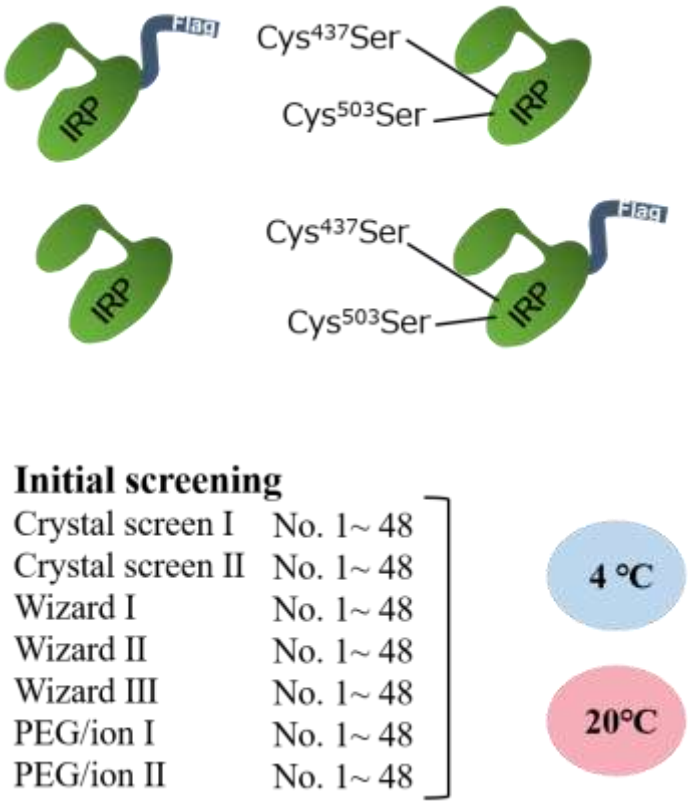

Figure 4.10 Initial screening condition.

Initial screening of crystallization conditions against four constructs were carried out with several commercially available screening kits (Crystal Screen 1 and 2, PEG/Ion Screen [Hampton research], Wizard 1, 2, 3 and 4 [Emerald BioSystems] at 277 K or 293 K.

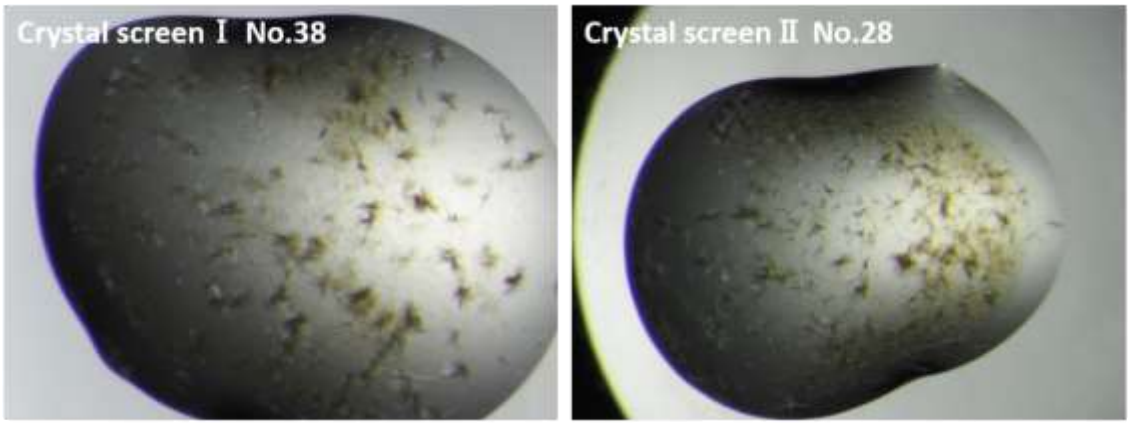

Figure 4.11 Crystals of IRP1 C437S/C503S at initial screening.

Photographs of crystals obtained by (a) Crystal screen I No.38 : 0.1 M HEPES sodium pH 7.5, 1.4 M sodium citrate tribasic dehydrate, and (b) Crystal screen II No.28 : 1.6 M sodium citrate tribasic dehydrate pH 6.5.

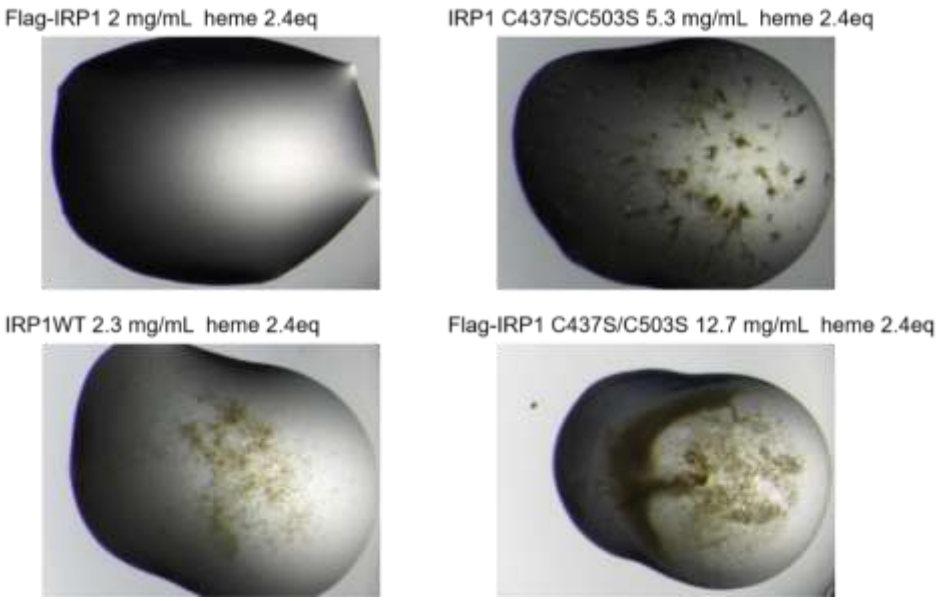

Figure 4.12 Crystals of IRP1 at initial screening.

Photographs of crystals obtained by 0.1 M HEPES sodium pH 7.5, 1.4 M sodium citrate tribasic dehydrate.

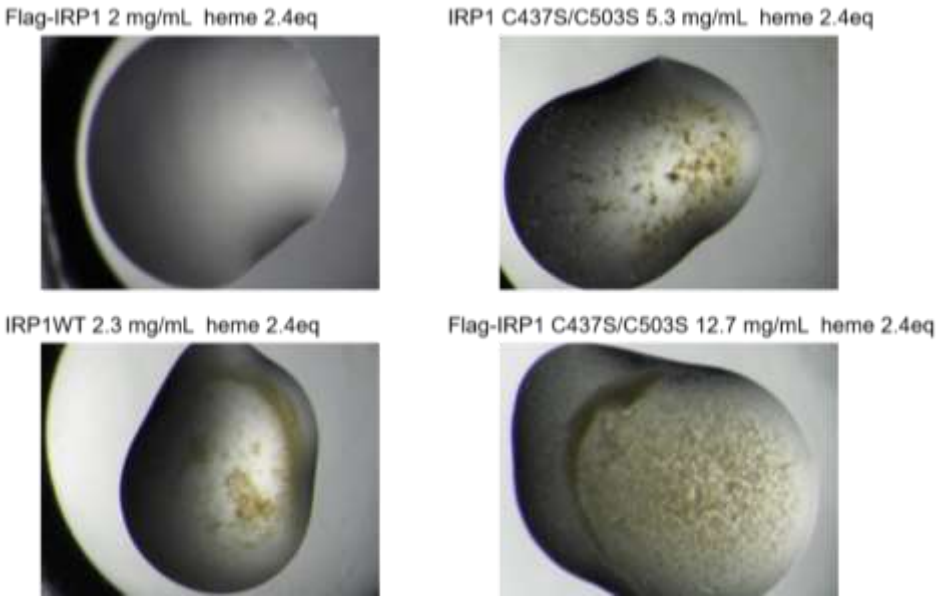

Figure 4.13 Crystals of IRP1 at initial screening.

Photographs of crystals obtained by 1.6 M sodium citrate tribasic dehydrate pH 6.5.

4.3.3 Optimization of Crystallization and Post Crystallization Treatments.

The crystallization conditions of IRP1 C437S/C503S (Figure 4.11), was used as a starting point to determine the optimal conditions for crystal growth at a constant temperature of 277 K. Sample preparation of the complex of IRP1C437S/C503S with heme was followed by the same procedure described above (Figure 4.14 right). To optimize the crystallization conditions, IRP1 C437S/C503S was crystallized by the hanging-drop vapor diffusion method at 277 K (Figure 4.14, left). The 2 μL crystallization drops composed of the 1 μL protein and 1 μL reservoir solutions were vapor-equilibrated to the 150 μL reservoir solutions for 2 weeks.

Crystallizations were improved by varying pH and concentrations of the precipitants and additive screening. After the optimization, crystals suitable for X-ray diffraction were obtained after 2 weeks under the following three conditions, (a) 0.1 M HEPES sodium pH 6.5, 1.4 M sodium citrate tribasic dehydrate, (b) 1.6 M sodium citrate tribasic dehydrate pH 6.0, and (c) 0.1 M HEPES sodium pH 6.5, 1.4 M sodium citrate tribasic dehydrate, 0.01 M TCEP (Figure 4.15). Under the conditions of (a) and (c), IRP1 C437S/C503S with heme produced clusters of needles. Under another condition (b), the mutant IRP1 with heme produced small hexagonal crystals. The obtained crystals were soaked into the reservoir solutions including 20 % glycerol, and picked up from crystallization drops and flash-cooled by liquid nitrogen.

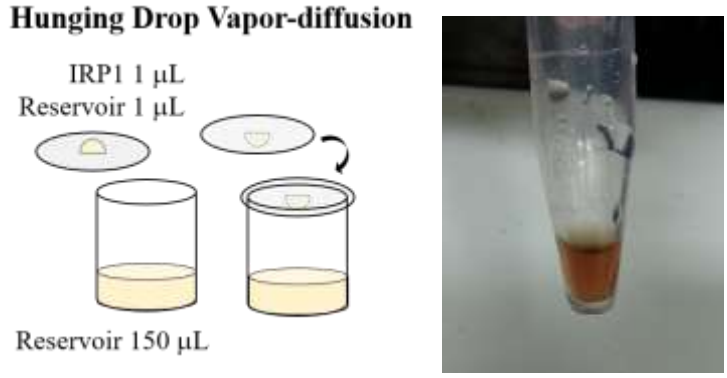

Figure 4.14 IRP1 C437S/C503S was crystallized by hanging-drop vapor diffusion method.
Left: Hanging-drop vapor diffusion method at 277K. The 2 µL crystallization drops composed of the 1 µL protein and 1 µL reservoir solutions were vapor-equilibrated to the 150 µL reservoir solutions for 2 weeks. Right: IRP1C437S/C503S and heme were mixed in 1:2.4 molar ratios and incubated on ice for 30 min ~ 1 h.

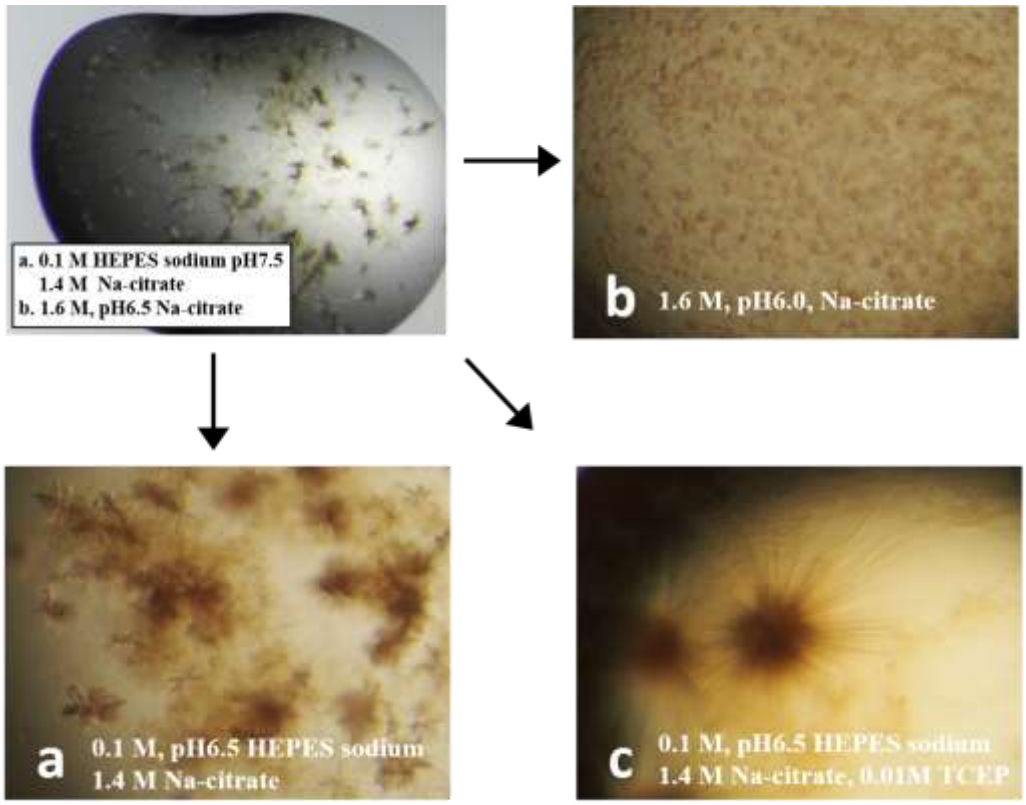

Figure 4.15 Crystals of IRP1 C437S/C503S after optimization.
Photographs of crystals obtained by (a) 0.1 M HEPES sodium pH 6.5, 1.4 M sodium citrate tribasic dehydrate, (b) 1.6 M sodium citrate tribasic dehydrate pH 6.0 and (c) 0.1 M HEPES sodium pH 6.5, 1.4 M sodium citrate tribasic dehydrate, 0.01 M TCEP.

4.3.4 X-ray Data Collection.

Diffraction data were obtained from three crystals (Figure 4.15 a, b, c) at liquid nitrogen temperature using X-ray of 1.0000 Å wavelength at the synchrotron beamlines; BL44XU, SPring-8. The diffraction limit of the crystals of IRP1 C437S/C503S with 1.6 M sodium citrate tribasic dehydrate pH 6.0 and 20% glycerol reached ~1.89 Å (Figure 4.16 and Table 4.1). In other crystals, the complete data set was not collected because of the low resolution of the X-ray diffraction.

Molecular replacement using the previously reported aconitase form (PDB ID: 2B3X) or IRE-binding form (PDB ID: 3SNP) of IRP1 as a search model was tested to obtain the initial phase angles. The IRP1-heme complex structure was solved by the molecular replacement using the aconitase form (PDB 2B3X), and has been refined to an R_{free} = 22.3% and R_{work} = 17.8% at 2.3 Å resolution. Only the data set of 2.3 Å resolution from a glycerol treated crystal provided an interpretable electron density map for the model building. Collected data are listed in Table 4.1-2.

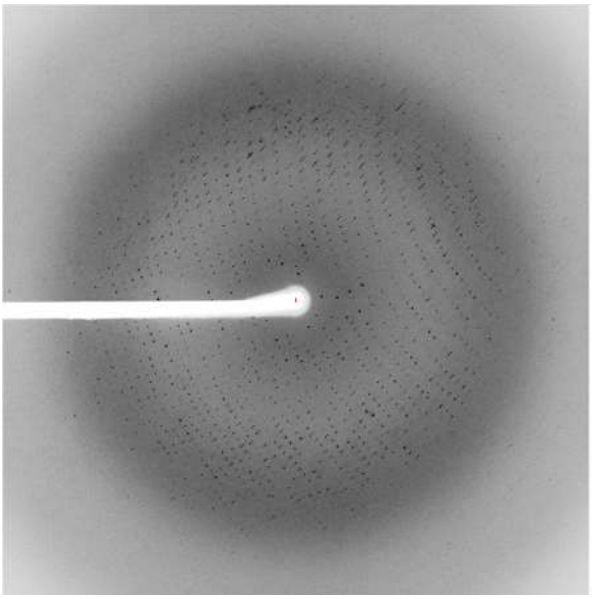

Figure 4.16 X-ray diffraction pattern from IRP1 C437S/C503S crystal.
The X-ray diffraction pattern of the crystal of IRP1 C437S/C503S collected at the synchrotron beamline BL44XU in SPring-8 is shown.

Data collection	
Beamline	SPring-8 BL44XU
Wavelength (Å)	0.98
Resolution range (Å)	86.9 - 2.30 (2.42 - 2.30)
Space group	$P3_1$ 2 1
Cell dimensions	
a, *b*, *c* (Å)	100.45, 100.45, 204.18
α, β, γ (°)	90, 90, 120
Total reflections	272865 (39512)
Unique reflections	53865 (7749)
Multiplicity	5.1 (5.1)
Completeness (%)	100.0 (100.0)
$\langle I/\sigma(I) \rangle$	7.9 (2.0)
R_{sym} (%)	15.3 (75.9)

Table 4.1 Crystallographic statistics of IRP1 C437S/C503S crystals.

Values in parentheses are for the highest resolution shells. a *R* merge(I) $= \Sigma hkl \Sigma i |\mathrm{I}i(hkl)| / \Sigma hkl \Sigma i \mathrm{I}i(hk\mathrm{l})$, where I*i* (*hkl*) is the value of the *i* th measurement of the intensity of reflection *hkl*, is the mean value of the intensity of the reflection *hkl* and the summation is the overall measurements.

Refinement	
R_{work}	0.1750
R_{free}	0.2356
Number of atoms	7497
Protein residues	862
RMS (bonds) (Å)	0.0141
RMS (angles) (°)	1.7615

Table 4.2 Crystallographic statistics of the final model.

[b] R facter $= \Sigma \big| |\mathrm{Fobs}(hkl)| - |\mathrm{Fcalc}(hkl)| \big| / \Sigma |\mathrm{Fobs}(hkl)|$. [c] R_{free} is the R-factor computed for the test set of reflections that were omitted from the refinement process.

4.3.5 Structure Determination of IRP1 C437S/C503S.

All diffraction images were processed by HKL-2000 software (9). Structure solution and refinement were performed by CCP4 software suite, which is a collection of disparate programs covering most of the computations required for macromolecular crystallography (10). The phase angles were initially determined from 2.3 Å resolution dataset using the molecular replacement method. The interpretable electron density map to build the structural model was provided by the calculation with CCP4 (10). This calculation confirmed that the protein was packed into a space group of $P3_121$ with one molecule per asymmetric unit. The Matthews coefficient (VM) of the crystal was estimated as 3.03 $Å^3$ Da^{-1} and its solvent content was 59.49% (11). The model was built using COOT software (12) along with the experimental electron density map. We fitted the aconitase form structure (PDB ID: 2B3X (13)) to the electron density map and extended the N-terminal and C-terminal helices from the fitted aconitase form structure. CCP4i.refine was used for the model refinement of the native structure at 1.89 Å resolution (14). The model was refined to the values of R_{work} = 0.17 and R_{free} = 0.22. The final structure was validated using MOLPROBITY (15). The resolution achieved was 2.3 Å. This analysis showed that 100.0% of the residues were in Ramachandran favored, with no residues as outliers. The final structure contained 100% of all possible atoms of the complexes, plus 490 solvent molecules. All atoms of one heme and one citric acid were present, as well as all residues of one IRP1 molecules. The final statistics of the crystallographic refinement are shown in Table 4.2.

4.3.6. Structure of the IRP1-Heme Complex and Functional Significance.

4.3.6.1. Overall Structure of IRP1-Heme Complex.

The crystal structure of IRP1 in the complex with heme is shown in Figure 4.17. Each asymmetric unit contains a single IRP1 monomer. Except for several amino acid residues in the N- and C-terminus, the residues have good electron density, because the complete native data set has been collected to the high resolution, 2.3 Å.

IRP1 consists of four globular domains, domain 1 (residue 2- 240), domain 2 (241-367), domain 3 (368-604), and domain 4 (661-888), where domains 3 and 4 are connected via an extended linker (605-660) (Figure 4.17). Previous crystallographic studies have unveiled the structures of IRP1 in the complex with IRE (3) as well as in the complex with the Fe-S cluster (13). Comparison of the two structures of IRP1 in the complexes with different ligands highlighted drastic conformational changes of IRP1 upon the binding of IRE. In the IRE-bound state, an 'L-shape' conformation having a large cavity between domains 3 and 4 to bind to IRE (Figure 4.19) was formed, while overall conformation of IRP1 in the complex with the Fe-S cluster is 'U-shape', where domains 3 and 4 are in a "closed" conformation. It should be noted here that ^{506}Cys is involved in cysteine residues constructing the Fe-S cluster (Figure 4.18) (6), which allowed us to speculate that structural effects on the overall structure of IRP1 is quite similar to those induced by the formation of the Fe-S cluster in IRP1. Consequently, the overall conformation of IRP1 in the complex with heme resembles that of the complex with the Fe-S cluster (r.m.s.d., 0.808 Å for 889 residues, core domains 1–2 were fixed (3)) rather than that of the IRE-binding form (r.m.s.d., 5.125 Å for 889 residues core domains 1–2 were fixed (3)) (Figure 4.18).

By binding of heme to ^{506}Cys, domain 3 displayed the largest conformational difference in the IRP1-heme complex, with a rotation of 52° resulting in a translation of ~13 Å , whereas domain 4 rotates by 32° and translates ~14 Å. As a result of the largest conformational change,

the residues used for the recognition of IRE are widespread to domains 2 - 4 (Figure 4.19A), and buried in the cleft between domains 3 and 4 in the IRP1-heme complex (Figure 4.19.B). Thus, the crystal structure of the IRP1-heme complex does not allow access of IRE to binding site of IRE.

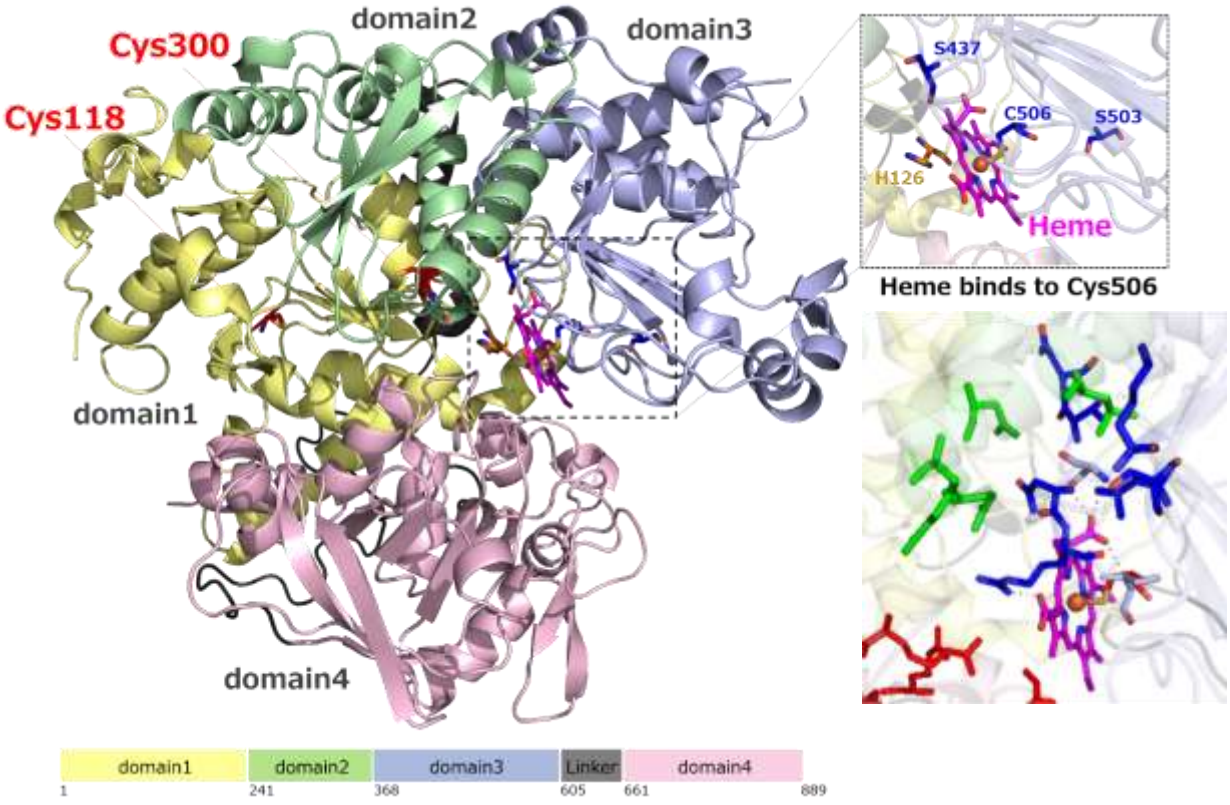

Figure 4.17 The determined X-ray structure of IRP1 with heme.

IRP1-heme complex showing the central core domains 1 (yellow) and 2 (green), domain 3 (blue), linker (black), and domain 4 (red). The heme is colored magenta. Heme is located in the cavity formed between domains 3 and 4, and binds to ^{506}Cys. Schematic diagram of IRP1 domains. Numbers at lower represent amino acids at domain borders (13).

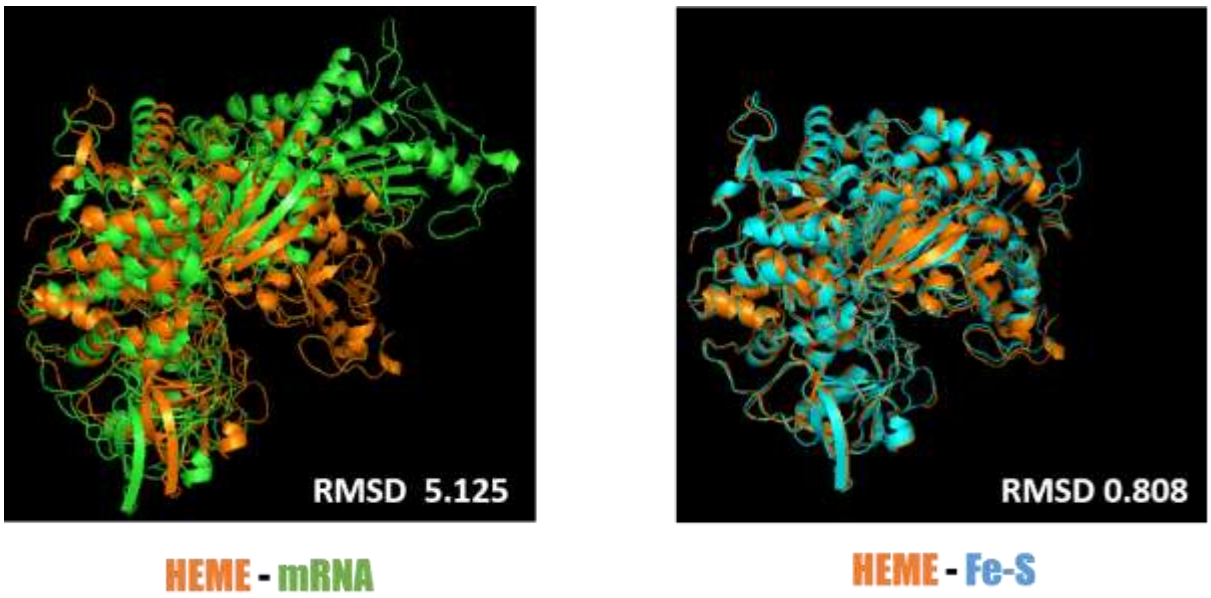

Figure 4.18. Superposition of IRP1-Ligand complex.

Left: Superposition of the IRP1-IRE complex and the IRP1-heme complex. The root-mean-square deviation (*RMSD*) between two structures is 5.125. Right: Superposition of IRP1-Fe-S cluster complex and IRP1-heme complex. *RMSD* between two structures is 0.808.

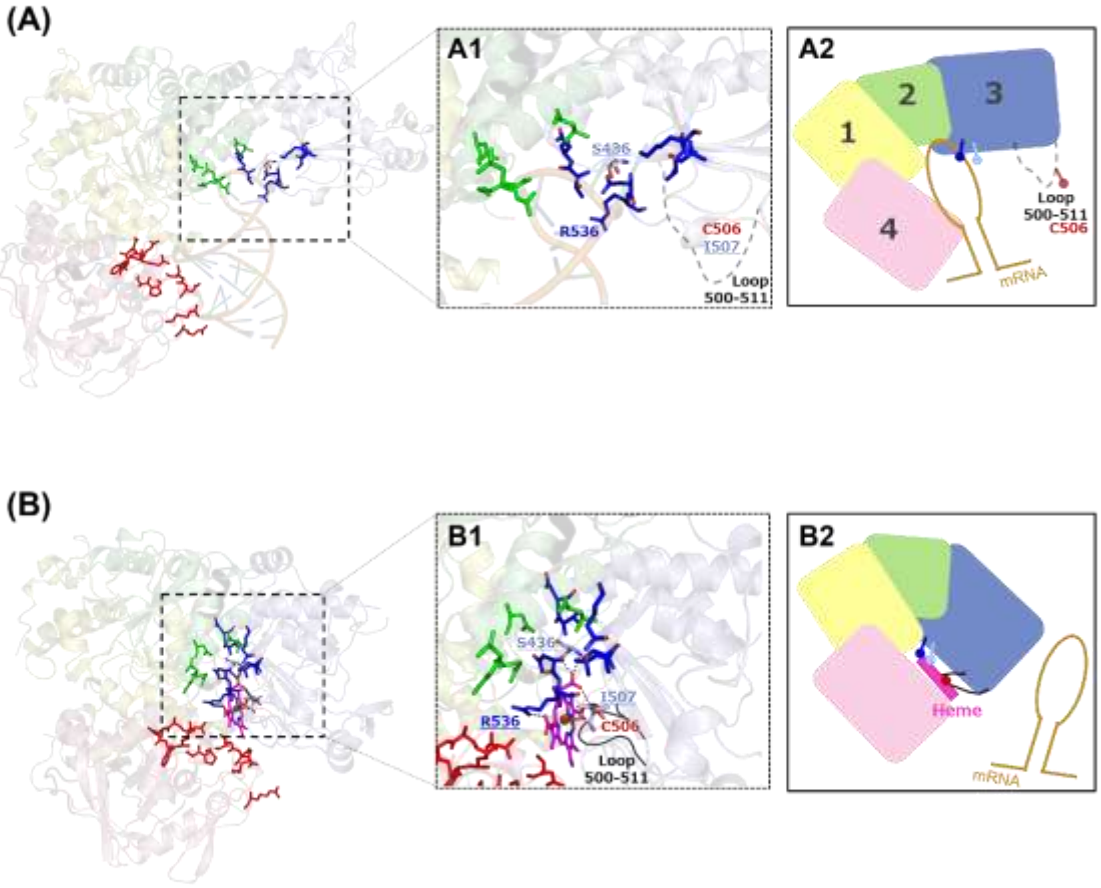

Figure 4.19. The conformational change of IRP1 by binding IRE, heme.

The crystal structure of the IRP1-IRE complex (A). The residues involved in the interaction sites spread over the concave opening of IRP1 (bold). Loop region (500-511) including ^{506}Cys is disordered. IRP1-heme complex (B). IRP1 adopts a "closed" conformation. Heme (pink) binds to ^{506}Cys in the loop region (500-511). Heme interacts with ^{436}Ser, ^{507}Ile, ^{536}Arg (blue). Domain 3 moves with domain 2 and the residues for the mRNA binding are located inside of the cavity between domains 3 and 4.

4.3.6.2. Heme Binding Site of the IRP1-Heme Complex.

The crystal structure of the IRP1-heme complex shows that the protein binds a single heme molecule (Figure 4.20), which is located in the cavity formed between domains 3 and 4. The ligand for the heme iron is ^{506}Cys in the loop region (500-511) disordered in the IRP1-IRE complex (3) and interacted with ^{436}Ser, ^{507}Ile, and ^{536}Arg. In Chapters II, the spectral characteristics of the heme binding in IRP1 suggested that heme binds to the cysteine residue in the HRM (Cys-Pro), but the crystal structure of the IRP-heme complex clearly showed the heme binding to ^{506}Cys in the HRM (Cys-Ile), one of the three iron-binding residues for the Fe-S cluster in c-aconitase (13). In Figure 4.6. (right), the absorption spectra of the heme-bound IRP1 contained two Soret peaks at 370 and 418 nm, and the Soret peak at 370 nm was derived from been the heme binding to the HRM, while the absorbance at 418 nm was typical of the six-coordinate Cys-Fe-H_2O structure as shown in *d*-camphor-bound cytochrome P450 (16). The spectroscopic heme titration for IRP1 C437S/C503S was monitored by the Soret band at 418 nm (Figure 4.6 Inset, Lower), showing that IRP1 C437S/C503S can bind 1 equivalent of six-coordinate heme, which might correspond to the ^{506}Cys-ligated heme.

I also found that the electron density above the heme was similar to that of water, although the electron density around heme was unresolved (Figure 4.22, left). As previously reported, a water molecule can be a ligand for the heme iron, which is stabilized by a hydrogen bond as observed for the deoxy form of myoglobin, in which adjacent ^{64}His forms the hydrogen bond with the iron-bound water molecule (Figure 4.22, Right) (17). Although the electron density of water molecule above heme was unresolved in the IRP1-heme complex, the crystal structure revealed that ^{126}His was located near ^{506}Cys (Figure 4.22, Left), suggesting that ^{126}His stabilizes the water ligand of heme bound to ^{506}Cys.

These observations suggest that IRP1 binds a single heme molecule and has the six-coordinate ^{506}Cys-Fe-H_2O. To further characterize the environmental structure of the heme

binding site, ^{506}Cys, I compared the absorption spectra of wild type and ^{506}Cys-mutated IRP1 (C506S). The Soret peak at 418 nm was shifted to 414 nm by the mutation of ^{506}Cys to Ser (Figure 4.21). Such a peak shift supports the ligation of ^{506}Cys to the heme iron bound in IRP1.

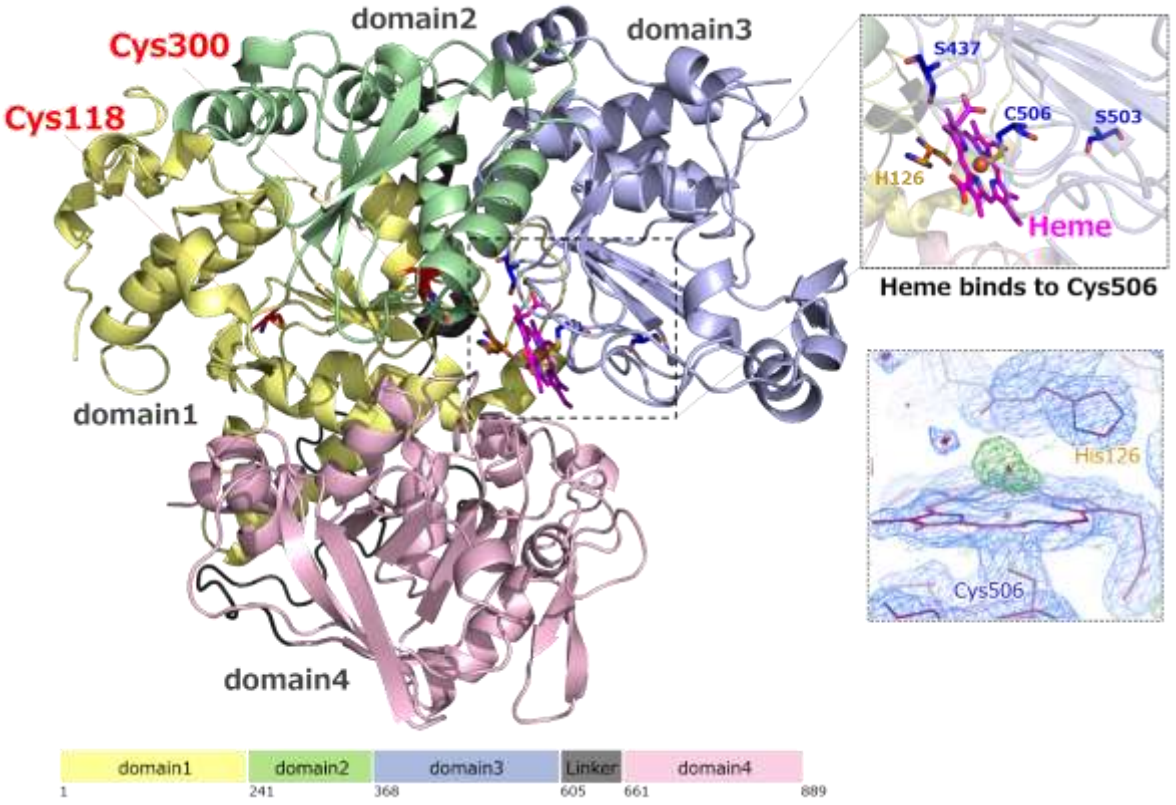

Figure 4.20. Structure of human IRP1 in the complex with heme.

The IRP1-heme complex showing the central core domains 1 (yellow) and 2 (green), domain 3 (blue), linker (black), and domain 4 (red). Heme is colored magenta, and located in the cavity formed between domains 3 and 4 with binding to ^{506}Cys. Lower: Schematic diagram of IRP1 domains. Numbers at lower represent amino acids at domain borders (13).

.

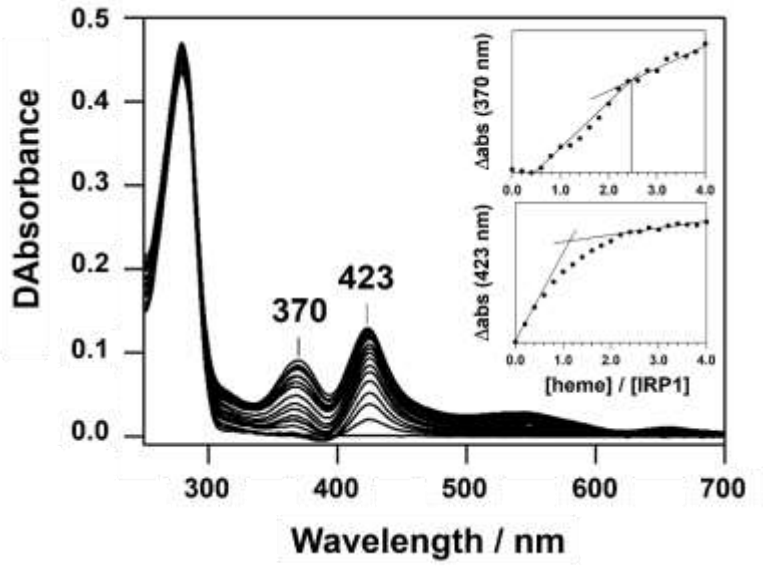

Figure 4.21 Absorption spectra and titration curves of IRP1 C506S.

Absorption difference spectra of heme binding to IRP1 followed by the stepwise addition of heme (1 – 20 μM) to IRP1 (5 μM) versus buffer blank in 50 mM Tris-HCl and 100 mM NaCl at pH 7.4. Inset: Absorbance difference at 370 nm and 423 nm.

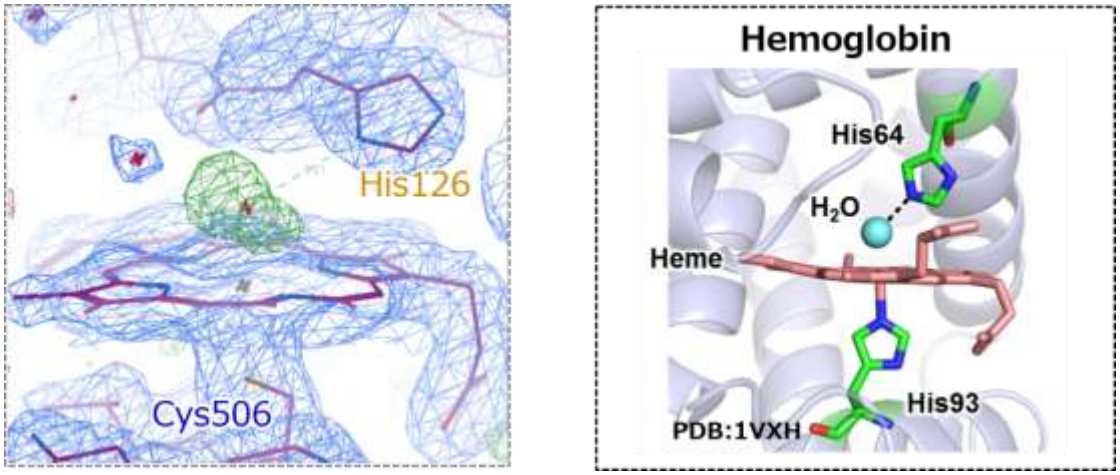

Figure 4.22. The electron density around heme of the IRP1-heme complex.

Left: The electron density around heme of the IRP1-heme complex. The candidate for hydrogen-bonding partner for water ligand with neighbor ^{126}His. Right: The heme pocket of deoxy myoglobin (PDB ID: 1VXH). The water molecule is hydrogen-bonded with ^{64}His.

Table 4.3 Absorption maxima of the heme-IRP1 complex and other heme proteins.

Protein	Ligand	Soret (nm)	Reference
IRP1	Cys, Cys/H_2O	372, 418	This study
[a]Irr	Cys	372	(18)
[b]$P450_{cam}$ (H_2O)	Cys/H_2O	417	(16)
HrtR	His/His	413	(19)

[a]Iron response regulator protein; [b]*d*-camphor-bound $P450_{cam}$

4.4. Discussion.

4.4.1. The Functional Features for Heme Binding to ^{506}Cys.

In the crystal structure of the IRP1-heme complex, heme binds to ^{506}Cys in HRM (Cys-Ile), not in HRM (Cys-Pro), and the structure of the IRP1-heme complex was in a ”closed” conformation that does not allow access of IRE to binding site of IRP1. From the previous studies in my laboratory, the native-PAGE showed that the heme binding to ^{300}Cys, not to ^{118}Cys, in IRP1 inhibits the association of IRE with IRP1. The structure of the IRP1-heme complex showed that ^{118}Cys is far from the IRE-binding site and exposed to the protein surface of IRP1, but ^{300}Cys is closer to the IRE-binding site, and the residues around ^{300}Cys participates in the interaction with IRE (Figure 4.23). Although the experiments of several mutant IRP1 having the mutation at one of the cysteine residues in the HRM and the Fe-S cluster regions are required, it is plausible that the two heme binding sites of IRP1 in Chapter II would be ^{118}Cys and ^{506}Cys. Although ^{506}Cys is not in the HRM (Cys-Pro), the amide group of the main chain at ^{507}Ile in the IRP1-heme complex seems to interact with heme as well as the indie group of Pro in HRM, and the similar structural environment in HRM (Cys-Pro) might be formed around ^{506}Cys in HRM (Cys-Ile) (Figure 4.19.B), suggesting that the heme binding affinity with ^{506}Cys in HRM (Cys-Ile) may be the same as that with HRM (Cys-Pro).

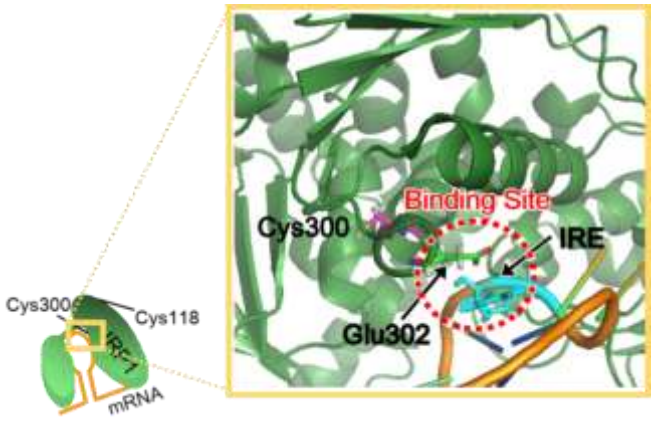

Figure 4.23 The location of HRM on the crystal structure of the IRP1-IRE complex (PDB: 3SNP). ^{118}Cys is far from the IRE-binding site and exposed to the protein surface of IRP1, but ^{300}Cys is close to the IRE-binding site, and the residues around ^{300}Cys participates in the interaction with IRE.

4.4.2. The Conformational Change of IRP1.

In the IRP1-heme complex, three residues, ^{437}Ser, ^{503}Ser and ^{506}Cys, involved in the Fe-S cluster, lie close to the space taken by the Fe-S cluster in c-aconitase (Figure 4.24). In iron-replete cells, IRP1 dissociates from IRE, and, by the complicated protein machinery, the Fe-S cluster is assembled (21). The overall reaction can be dissected into two major steps. First, a transiently bound [4Fe–4S] cluster is assembled on the scaffold protein complex (21). In the second step, the transiently bound [4Fe–4S] cluster on the scaffold protein is transferred to IRP1, and, then, IRP1 becomes c-aconitase. Although the detailed mechanism to transfer the 4Fe–4S cluster to IRP1 remains to be elucidated (21), it may be reasonable for transferring the transiently bound [4Fe–4S] cluster that the residues involved with the Fe-S cluster lie close to the space taken by the Fe-S cluster.

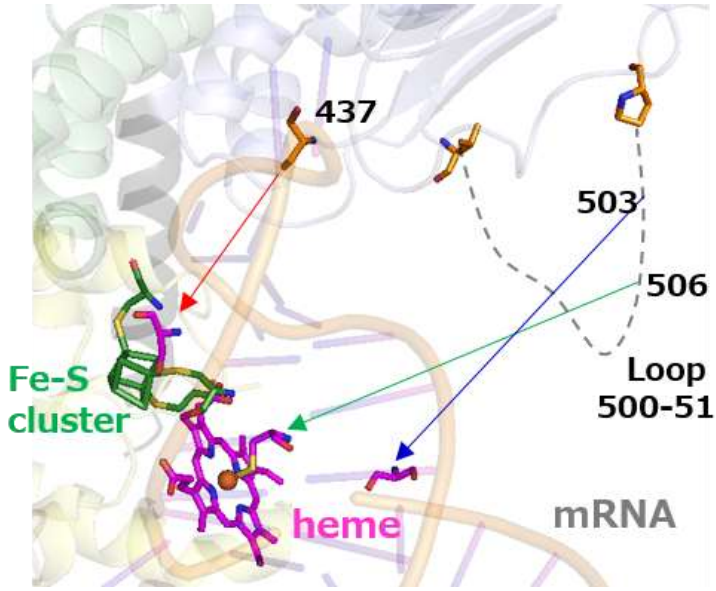

Figure 4.24. Superposition of the models of three IRP1 crystal forms.
Structural differences between ligand binding regions in the IRP1-Fe-S cluster (green), –IRE (orange) and –heme (magenta) complex. The unresolved loops spanning residues 500 to 511 are drawn as dotted lines.

4.4.3. The Heme-Induced Regulation Mechanism of IRE Binding in IRP1-IRE Complex.

Based on the structural information from the IRP1-heme complex, I propose a novel mechanism of the heme-induced regulation of the IRE binding in IRP1 as follows (Figure 4.25). In the first step, heme binds to ^{506}Cys in the loop region (500-511), and interacts with ^{436}Ser, ^{507}Ile, and ^{536}Arg. Domain 3 is close to domain 2 in the IRP1-IRE complex, thus the structure of IRP1 becomes a “closed” conformation that does not allow access of IRE to binding site of IRE. Although the functional significance of the heme binding to ^{118}Cys has not yet been clarified, the mechanism would be one of the crucial steps for sensing cellular iron concentration to maintain iron homeostasis in cells.

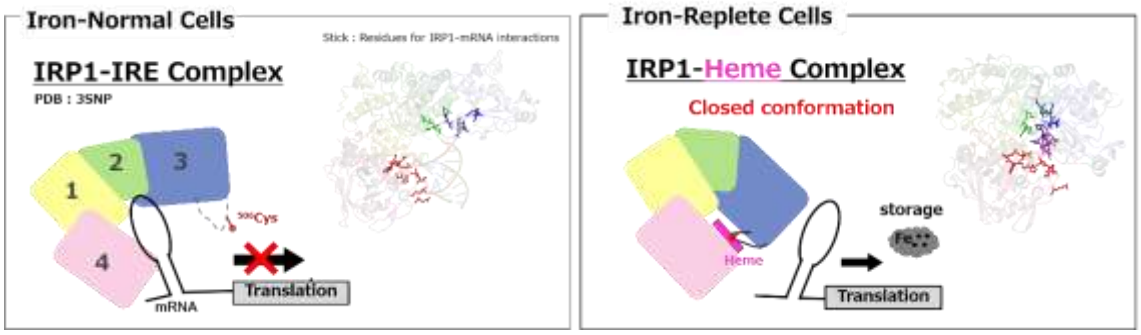

Figure 4.25. The novel mechanism of regulatory processes controlling IRP1 by heme.
In iron-repleate cells, heme binds to ^{506}Cys in the loop region (500-511). Domain 3 is close to domain 2 in comparison to the IRP1-IRE complex. The conformational changes by heme binding to IRP1 inhibits the IRE binding to IRP1.

References.

1. J. Wang, K. Pantopoulos, Regulation of cellular iron metabolism. *Biochem. J.* **434**, 365–381 (2011).
2. W. E. Walden, A. Selezneva, K. Volz, Accommodating variety in iron-responsive elements: Crystal structure of transferrin receptor 1 B IRE bound to iron regulatory protein 1. *FEBS Lett.* **586**, 32–35 (2012).
3. W. E. Walden, A. I. Selezneva, J. Dupuy, A. Volbeda, J. C. Fontecilla-Camps, E. C. Theil, K. Volz, Structure of dual function iron regulatory protein 1 complexed with ferritin IRE-RNA. *Science*. **314**, 1903–1908 (2006).
4. P. Piccinelli, T. Samuelsson, Evolution of the iron-responsive element. *RNA.* **13**, 952–966 (2007).
5. B. Guo, Y. Yu, E. A. Leibold, Iron regulates cytoplasmic levels of a novel iron-responsive element-binding protein without aconitase activity. *J. Biol. Chem.* **269**, 24252–24260 (1994).
6. Y. Ke, J. Wu, E. A. Leibold, W. E. Walden, E. C. Theil, Loops and bulge/loops in iron-responsive element isoforms influence iron regulatory protein binding. Fine-tuning of mRNA regulation? *J. Biol. Chem.* **273**, 23637–23640 (1998).
7. J. B. Goforth, S. A. Anderson, C. P. Nizzi, R. S. Eisenstein, Multiple determinants within iron-responsive elements dictate iron regulatory protein binding and regulatory hierarchy. *RNA.* **16**, 154–169 (2010).
8. A. I. Selezneva *et al.*, Crystallization and preliminary X-ray diffraction analysis of iron regulatory protein 1 in complex with ferritin IRE RNA. *Acta Crystallogr. Sect. F Struct. Biol. Cryst. Commun.* **62**, 249–252 (2006).
9. Z. Otwinowski, W. Minor, Processing of X-ray diffraction data collected in oscillation mode. *Methods Enzymol.* **276**, 307–326 (1997).
10. E. J. Dodson, A Collaborative Computational Project, number 4: Providing Programs for Protein Crystallography. *Univ. York, Heslington, York Y01 5DD, UK.*
11. B.W.Matthews, Solvent content of protein crystals. *J. Mol. Biol.* **33**, 491–497 (1968).
12. P. Emsley, B. Lohkamp, W. G. Scott, K. Cowtan, Features and development of Coot. *Acta Crystallogr. Sect. D Biol. Crystallogr.* **66**, 486–501 (2010).
13. J. Dupuy, A. Volbeda, P. Carpentier, C. Darnault, J.-M. Moulis, J. C. Fontecilla-Camps, Crystal structure of human iron regulatory protein 1 as cytosolic aconitase. *Structure.* **14**, 129–139 (2006).
14. P. V Afonine, R. W. Grosse-Kunstleve, N. Echols, J. J. Headd, N. W. Moriarty, M. Mustyakimov, T. C. Terwilliger, A. Urzhumtsev, P. H. Zwart, P. D. Adams, Towards automated crystallographic structure refinement with phenix.refine. *Acta Crystallogr. D. Biol. Crystallogr.* **68**, 352–367 (2012).
15. S. C. Lovell, I. W. Davis, W. B. Arendall, P. I. W. de Bakker, J. M. Word, M. G. Prisant,

J. S. Richardson, D. C. Richardson, Structure validation by Cα geometry: and Cβ deviation. *Proteins Struct. Funct. Bioinforma.* **50**, 437–450 (2003).

16. J. H. Dawson, L. A. Anderssons, M. Sono, Spectroscopic investigations of ferric cytochrome P-450-cam ligand complexes identification of the ligand trans to cysteinate in the native enzyme. *J. Biol. Chem.* **257** (1982)
17. Crystal structures of CO-, deoxy- and Met-myoglobins at various pH values. *J. Mol. Biol.* **256**, 762–774 (1996).
18. H. Ishikawa, M. Nakagaki, A. Bamba, T. Uchida, H. Hori, M. R. O'brian, K. Iwai, K. Ishimori, Unusual heme binding in the bacterial iron response regulator protein: Spectral characterization of heme binding to the heme regulatory motif. *Biochemistry*. **50**, 1016–1022 (2011).
19. H. Sawai, M. Yamanaka, H. Sugimoto, Y. Shiro, S. Aono, Structural basis for the transcriptional regulation of heme homeostasis in *Lactococcus lactis*. *J. Biol. Chem.* **287**, 30755–30768 (2012).
20. M. C. Kennedy, L. Mende-Mueller, G. A. Blondin, H. Beinert, Purification and characterization of cytosolic aconitase from beef liver and its relationship to the iron-responsive element binding protein. *Proc. Natl. Acad. Sci. U. S. A.* **89**, 11730–11734 (1992).
21. D. J.A.Netz, J. Mascarenhas, O. Stehling, A. J.Pierik, RolandLill, Maturation of cytosolic and nuclear iron–sulfur proteins. *Trends Cell Biol.* **24**, 303–312 (2014).

CHAPTER V

GENERAL CONCLUSIONS

Iron metabolism is tightly regulated for iron homeostasis by IRP1 and IRP2, but the iron regulatory mechanisms by IRPs remain to be established. In mammalian cells, heme-induced oxidation of IRP2 leads to lose the IRE binding activity. The IRE binding activity in IRP1 is also regulated by heme without the heme-induced oxidation, but the ligation of heme for IRP1 had not yet been confirmed. To clarify the mechanism of heme-mediated regulation of iron hemostasis for IRP1, I focused on the interaction to IRP1 with heme and the functional properties.

Redox-Dependent Axial Ligand Replacement and Its Functional Significance in Heme-bound IRPs (Chapter II)

In Chapter II, I clarified that IRP1 specifically binds heme to HRM (Cys-Pro), as observed for IRP2, and the heme environmental structures in IRP1 was close to those of "heme-regulatory" proteins, suggesting that heme binds to IRP1 as the signaling molecule for sensing the intracellular iron concentration status. Furthermore, using pulse radiolysis, I focused on the heme coordination structure of intermediates after reduction of the heme iron, revealing the structural factors differentiating heme binding to HRM in the IDD domain of IRP2 from those of other HRMs located outside of the IDD domain. Considering that the oxidative modification is only observed for heme-bound IRP2, but not IRP1, probably owing to the structural flexibility of IRP2, I proposed that the transient 5-coordinate His-ligated heme is a prerequisite for oxidative modification of heme-bound IRP2, which functionally differentiates heme binding of IRP2 from that of IRP1.

Functional Significance of Heme Binding in Iron Response Element Binding of Iron Regulatory Proteins. (Chapter III)

The typical hemoproteins using heme as the active center tightly bind heme to the protein, while “heme-regulated” proteins have relatively low heme binding affinity. To examine the functional significance of the heme binding in IRP1, I focused on the affinity of heme in IRP1. I found that the heme binding affinity of IRP1 (K_d = 4.7 ×10^{-7} M) was lower about 10^6 than that of hemoglobin, and close to that of HRI (~10^{-10} M). These results suggested that IRP1 binds or dissociates heme in responses to heme concentration in the cells. Furthermore, to further confirm the heme binding as the signaling molecule for the IRE binding in IRP1, I observed that the addition of heme dissociate IRE from the IRP1-IRE complex, suggesting that the heme binding to IRP1 facilitates the dissociation of IRE from the IRP1 complex. However, a large excess amount of heme was required for the dissociation. I supposed that some specific heme carrier or heme chaperone proteins would transfer heme to IRP1.

Structural Characterization of Heme-dependent Regulation Mechanism of Iron Response Eement Binding in Iron Regulatory Protein 1. (Chapter IV)

In Chapter IV, to structurally examine the heme-dependent regulation mechanism for the IRE binding in IRP1, I solved the crystal structure of IRP1 in the complex with heme. The crystal structure clarified that IRP1 binds heme to ^{506}Cys in HRM (Cys-Ile). The IRP1-heme complex was in a “closed” conformation that did not allow access of IRE to the IRE binding site. The conformational change induced by heme binding to IRP1 indicated that IRP1 could not bind to IRE. The heme binding to IRP1 regulated the interaction between IRP1 and IRE without oxidative modification mediated by heme.

Heme-Mediated Regulation between IRP1 and IRE in the Intracellular Iron Metabolism.

While heme binds to HRM (Cys-Pro) in Chapter II, the binding site of heme is HRM (Cys-

Ile) in Chapter IV. The structural environment in HRM (Cys-Ile) is similar with that in HRM (Cys-Pro), suggesting that binding heme to HRM (Cys-Ile) may have the spectral characteristics of heme binding to HRM (Cys-Pro). I propose that heme binds to HRM (Cys-Ile) for signaling molecule, and inhibits the interaction between IRP1 and IRE although it has not yet been clarified whether IRP1 uses two types of HRM as the cellular iron concentration.

To date for IRP2, heme binds to the IDD domain, and IRP2 undergoes proteasomal degradation after the oxidative modification, suggesting that IRP2 binds heme as a signaling molecule for iron metabolism. The oxidative modification near mRNA may cause disease. For example, cytoplasmic RNA oxidation is a prominent feature of vulnerable neurons in the brains of Alzheimer's disease patients (2). The oxidative modification requires the activation of molecular oxygen and this process might be induced some unexpected damages in cells.

On the other hands, the inhibition process with association of IRP1 to IRE only is the conformational change by heme binding, without oxygen. The regulation mechanism I proposed here does not involve the generation of the reactive oxygen species, which would be a more “safe” mechanism in vivo. For IRP2, these conformational changes is a safe manner of dissociation from IRE without oxygen. Together with the results in previous studies, I propose that IRP1 and IRP2 have the common iron control mechanism by heme binding, without oxygen. My studies about the heme-mediated regulation between IRP1 and IRE may contribute to the elucidation of the regulatory mechanism for iron hemostasis in the cells.

The human disorders that are causatively linked to defects in the IRE/IRP system. In previous studies, the IRP2 gene lies within a lung cancer-associated locus, and exhibit increased IRP2 mRNA and protein expression (3). It was speculated that this might contribute to iron accumulation in the lungs. The IRE-binding activity of IRP1 was reported to be increased in Parkinson's disease (4). However, the molecular mechanisms by which IRPs may contribute to pathogenesis of the disorders remain to be established.

A large excess amount of heme was required for the dissociation for IRP1-IRE complex. I propose that some specific heme carrier or heme chaperone proteins would transfer heme to IRP1 although the proteins are unknown. These findings in my thesis may be expected to the understanding the IRP/IRE regulatory system underlies the molecular basis of iron metabolism.

References

1. J.-J. Lin, M. M. Patinot, L. Gaffieldt, W. E. Waldent, A. Smithf, R. E. Thach, Crosslinking of hemin to a specific site on the 90-kDa ferritin repressor protein. **88**, 6068–6071 (1991).

2. M. A. Smith, P. L. Richey Harris, L. M. Sayre, J. S. Beckman, G. Perry, P. Richey, A. Morandi, J. Connolly, P. Gambetti, Widespread peroxynitrite-mediated damage in Alzheimer's disease. *J. Neurosci.* **17**, 2653–2657 (1997).

3. D. L. DeMeo, T. Mariani, S. Bhattacharya, S. Srisuma, C. Lange, A. Litonjua, R. Bueno, S. G. Pillai, D. A. Lomas, D. Sparrow, S. D. Shapiro, G. J. Criner, H. P. Kim, Z. Chen, A. M. K. Choi, J. Reilly, E. K. Silverman, Integration of genomic and genetic approaches implicates IREB2 as a COPD susceptibility gene. *Am. J. Hum. Genet.* **85**, 493–502 (2009).

4. B. A. Faucheux, M.-E. Martin, C. Beaumont, S. Hunot, J.-J. Hauw, Y. Agid, E. C. Hirsch, Lack of up-regulation of ferritin is associated with sustained iron regulatory protein-1 binding activity in the substantia nigra of patients with Parkinson's disease. *J. Neurochem.* **83**, 320–330 (2002).